Homogeneous Charge Compression Ignition Combustion of Dimethyl Ether

Pedersen, Troels Dyhr

Publication date:
2011

Document Version
Publisher's PDF, also known as Version of record

Homogeneous Charge Compression Ignition Combustion of Dimethyl Ether

PhD Thesis

Troels Dyhr Pedersen

DTU Mechanical Engineering
Department of Mechanical Engineering

Table of contents

1 Foreword

The work described in this thesis was initiated in June 2006 and completed in January 2010. It was carried out under supervision of associate professor Jesper Schramm at the Department of Mechanical Engineering, Technical University of Denmark.

I wish to thank Jesper Schramm for offering me the PhD position. I also wish to thank the rest of the Internal Combustion Engine Group. Everyone has been supportive and helpful in many situations.

In 2008 I visited the National Traffic Safety and Environmental Laboratories in Tokyo, Japan, for 5 months. The purpose of the visit was to perform experiments with HCCI combustion on a truck engine test bench. I am grateful for having been given this opportunity to work in a professional environment, and wish to thank the people whom I worked with at NTSEL for their help and kindness.

2 Nomenclature

AC	Alternating Current
ASRT	Automatic Scheme Reduction Tool
ATAC	Active Thermo Atmosphere Combustion
ATDC	After Top Dead Center
BMEP	Brake Mean Effective Pressure
BTDC	Before Top Dead Center
CAI	Controlled Auto Ignition
CCI	Combined Combustion System
CFD	Computational Fluid Dynamics
CI	Compression Ignition
CJ	Chapman Jouget
DFT	Discrete Fourier Transform
DI	Direct Injection
DME	Dimethyl Ether
EGR	Exhaust Gas Recirculation
FIR	Finite Impulse Response
FFT	Fast Fourier Transform
GCI	Gasoline Compression Ignition
HCCI	Homogenous Charge Compression Ignition
HTR	High Temperature Reactions
IIR	Infinite Impulse Response
IMEP	Indicated Mean Effective Pressure
LHV	Lower Heating Value
LTR	Low Temperature Reactions
NTSEL	National Traffic Safety and Environment Laboratories
PCCI	Premixed Charge Compression Ignition
PCI	Premixed Compression Ignition
RMS	Root Mean Square
SI	Spark Ignition
SPL	Sound Pressure Level
TDC	Top Dead Center
ZND	Zel´dovich Neumann Döring

3 Résumé

This thesis is based on experimental and numerical studies on the use of dimethyl ether (DME) in the homogeneous charge compression ignition (HCCI) combustion process.

The first paper in this thesis was published in 2007 and describes HCCI combustion of pure DME in a small diesel engine. The tests were designed to investigate the effect of engine speed, compression ratio and equivalence ratio on the combustion timing and the engine performance. It was found that the required compression ratio depended on the equivalence ratio used. A lower equivalence ratio requires a higher compression ratio before the fuel is burned completely, due to lower in-cylinder temperatures and lower reaction rates. The study provided some insight in the importance of operating at the correct compression ratio, as well as the operational limitations and emission characteristics of HCCI combustion.

HCCI combustion process is governed mainly by chemical kinetics. To understand the combustion process therefore requires detailed knowledge of the dominating reaction paths in lean premixed combustion of DME. The reactions were studied by running simulations of HCCI combustion in CHEMKIN II [1] with a detailed reaction mechanism for DME developed at Lawrence Livermore National Laboratory in 2004 [2]. The dominating reactions paths were then identified and used to create a simple reaction mechanism containing 55 reactions only. It contains just enough reactions to successfully predict ignition as well as low and high temperature reactions with reasonable similarity to the original mechanism. By reducing the mechanism to its essential reactions it becomes more useful to CFD models of HCCI combustion. The number of elementary reactions has a great influence on computational demands and computing time, so the use of a simple mechanism greatly reduces both.

Reaction paths for methanol and methane were included amongst the elementary reactions, since these two fuels are commonly used to control the radical behavior in the initial phase of combustion and hence the combustion phasing of the fuel in an engine, as well as enabling an increase in engine power.

The use of methanol for combustion phasing control was tested successfully in a large diesel engine with common rail, in which the piston bowls were widened to give a compression ratio of 14.5. This compression ratio still allows DI CI operation with DME, but requires a substantial combustion delay in HCCI operation with DME to achieve post TDC combustion. By adding methanol to the inlet port during HCCI combustion of DME, the engine reached 50 percent of its full DI CI load capability without engine knock at 1000 rpm and somewhat less at 1800 rpm. The engine also had EGR capability which was used to demonstrate the effect on HCCI combustion phasing of increasing EGR ratios. The EGR percentage, which is limited to about 30 percent in DI CI operation, could be increased to 70 percent in HCCI operation. The large amount of EGR delayed combustion almost to TDC. These tests were performed in Tokyo in 2008 and are described in the second paper in appendix.

One of the limitations with HCCI combustion is combustion knock which increases with the equivalence ratio. The higher concentration of fuel leads to higher rates of reaction, and as the reaction is not spatially uniform, higher pressure gradients result from the combustion. These pressure gradients cause strong acoustic resonance in the combustion chamber. Part of the energy from this resonance is transferred to the cylinder liner and further through the engine block. The engine vibrates both as a result of direct transmission, as well as having its natural resonance frequencies exited. The sound pressure around the engine caused by the high frequencies can reach levels of more than 110 dB.

The third paper describes the testing of various geometries of piston crowns for their ability to reduce the acoustic resonance in the combustion chamber and hence the noise emitted from the engine. The study showed that minimum exposure of the cylinder liner is critical in reducing the transmitted noise. The effect of splitting the chamber into smaller volumes was tested, by shaping piston crowns with cavities. It was found that piston crowns with cavities embedded in the piston performed much better in terms of noise reduction than those with cavities formed between the piston and the cylinder liner. The most notable result was the difference between two common geometries: the flat piston crown and the DI CI bowl-type crown. The latter provided the largest noise reduction of all tested. The combustion efficiency was however reduced by a very large crevice volume in the bowl-type crown.

The physics behind the initial pressure gradients causing the resonance is largely unknown and hence difficult to include in a model. There is however indications that the large pressure gradients are caused by detonations. In some cases at least, explosions alone can not account for the observed pressures, which oscillate at values above those otherwise possible in a constant volume reaction.

Detonations may develop in the wake of pressure waves that are sent out from local explosions. Even though the detonation may not develop to its steady state condition, it may still create a pressure wave of significant magnitude. While the steady state condition may be calculated, it is of higher interest to see if the detonation will develop at all under given circumstances. This was formed the basis of a CFD study. The objective of this study was to see if detonations would occur in CFD simulations of constant volume combustion with a lean premixed charge of DME in atmospheric air. STAR-CD [3] was used in conjunction with the reduced mechanism for DME combustion developed earlier. Detonation waves are known to be planar (when propagating in tubes) and hence the simulation could be set up in one dimension only, which saves computational time while allowing an excellent resolution in the direction of propagation. The studies revealed that with proper time stepping, spatial discretion and a temperature gradient across the domain, detonations will naturally be initiated and develop in a transient solution. The most important implication of this is perhaps that common CFD models may be used to test if certain conditions are more likely to provoke detonations than others.

4 Resumé (dansk)

Denne afhandling er baseret på eksperimentale såvel som numeriske studier af forbrænding af dimethyl æter i HCCI motorer.

Den første artikel som blev udgivet beskriver HCCI forbrænding af ren DME i en mindre diesel motor. Eksperimentet var designet til at undersøge indflydelsen af motorhastighed, kompressionsforhold og luft/brændstofforhold på forbrændingen. Det blev vist at det nødvendige kompressionsforhold afhænger af blandingsforholdet. Et højere luft/brændstofforhold kræver et højere kompressionsforhold for at opnå ren forbrænding, eftersom temperaturniveauet skal hæves for at opnå samme reaktionshastighed ved en mere mager blanding. Studiet belyste endvidere vigtigheden i at anvende det korrekte kompressionsforhold, såvel som de operationelle grænser og sammensætningen af udstødningen fra HCCI forbrændingen.

HCCI forbrændingsprocessen er styret af hastigheden i de kemiske reaktioner. Det er således nødvendigt at forstå de overordnede reaktionsmønstre i forbrændingen af DME for at få et overblik over de mekanismer der styrer forbrændingens faser. Reaktionerne blev derfor undersøgt gennem simuleringer i CHEMKIN II [1] med en detaljeret reaktionsmekanisme for DME, som er udviklet ved Lawrence Livermore National Laboratory [2]. De dominerende reaktionsveje blev identificeret og opstillet i en simplere mekanisme kun indeholdende 55 reaktioner. Denne mekanisme bibeholder de vigtigste indledende reaktioner såvel som de dominerende reaktioner i hhv. lavtemperatur og højtemperatur forbrændingsfaserne. Ved at reducere mekanismen til det simplest mulige bliver den mere anvendelig i CFD modeller af HCCI forbrænding. Antallet af reaktionsligninger har stor indflydelse på de beregningsmæssige krav og tidsforbruget i en simulering, idet begge kan reduceres betragteligt ved kun at medtage de nødvendige reaktioner.

Reaktioner for metanol og metan blev ligeledes inkluderet i mekanismen, da disse to brændstoffer hyppigt anvendes til at kontrollere koncentrationen af radikaler i forbrændingens lav temperatur fase, samtidig med at motoreffekten kan øges. Brugen af metanol blev testet med succes i en stor dieselmotor udstyret med commonrail indsprøjtning. I denne motor var stemplerne blevet modificeret således at kompressionsforholdet var reduceret til 14.5. Dette kompressionsforhold tillader stadig DI CI drift med DME, men kræver en væsentlig forsinkelse af forbrændingen ved HCCI drift med DME såfremt forbrændingen skal ligge efter TDC i den mest optimale position. Ved at tilføre metanol i motorens indsugningsmanifold under HCCI forbrænding af DME opnåedes omkring 50 % af motorens fulde moment ved 1000 omdr/min uden bankning, og et lidt lavere moment ved 1800 omdr/min hvor der ikke kunne tilføres samme mængde metanol. Motoren var også udstyret med et EGR system og køler, som blev brugt til at demonstrere virkningen af recirkuleret udstødningsgas på forbrændingens timing. EGR procentdelen, som er begrænset til omkring 30 procent ved normal DI CI drift, kunne øges til omkring 70 % hvorved forbrænding kom til at ligge tæt ved TDC. Disse eksperimenter blev udført i Tokyo i 2008 og er beskrevet i den anden artikel.

En af begrænsningerne ved HCCI forbrænding er bankning, som forværres med blandingsforholdet. En højere koncentration af brændstof medfører højere reaktionshastigheder, og da reaktionen ikke forløber jævnt i hele volumenet skaber dette tilsvarende højere tryk gradienter under forbrændingen. Disse tryk gradienter medfører akustisk resonans i forbrændingskammeret. En del af energien i resonansen overføres til cylinder foringen og videre ud i motorblokken, hvilket anslår motorblokkens egenfrekvens. Motoren udstråler derfor støj både ved direkte transmitterede frekvenser såvel som ved motorens egenfrekvens.

Den tredje artikel beskriver afprøvning af forskellige udformninger af stempeltoppe. Disse testes for deres evne til at reducere den akustiske resonans i cylinderen og dermed den udstrålede støj. Studiet viste at det er vigtigt at cylinderforingen bliver dækket mest muligt af under forbrændingen, altså med et stempel som når op til topstykket. Forbrænding i hulrum i stemplet gav langt mindre støj end hvis forbrændingen foregik i et fladt kammer eller på ydersiden af stemplet. Det mest bemærkelsesværdige resultat var forskellen mellem to almindelige stempler: det flade stempel som anvendes i SI motorer og det skålformede som anvendes i CI motorer. Sidstnævnte gav den mest lydløse forbrænding af alle testede stempler. Forbrændingsvirkningsgraden blev dog forringet i det skålformede stempel da dette havde et uforholdsmæssigt stort volumen mellem cylinder og stempel.

Den fysiske forklaring på tryk gradienternes opståen er i store træk ukendt og dermed vanskelige at modellere. Der er dog indikationer på at tryk gradienterne i en vis udstrækning kan opstå som følge af detonationer. I nogle tilfælde er trykstigningerne så voldsomme at de ikke har noget tilfælles med almindelige trykbølger forårsaget af eksplosioner, hvormed de kun kan skyldes detonationer.

Detonationer kan udvikle sig som følge af trykbølger fra eksplosioner, som finder sted lokalt i cylinderen. Selvom en detonation ikke når at udvikle sig fuldt ud til en stationær tilstand vil den stadig kunne danne en kraftig trykbølge i en cylinder, hvor gassen allerede er delvist reageret og har en høj reaktionshastighed som følge af de høje temperaturer. Det er muligt at beregne chokbølgers og detonationers egenskaber med stor nøjagtighed under stationære forhold, men den transiente udvikling er mindre velkendt. Det er derfor af stor interesse at undersøge hvilke betingelser der ligger til grund for udviklingen af detonationer under forbrændingen. Dette blev undersøgt i et CFD studium. Formålet med studiet var at undersøge om detonationer kunne opstå i CFD simuleringer af konstant volumen forbrænding af en mager blanding af DME og atmosfærisk luft. STAR-CD [3] blev anvendt sammen med den simple mekanisme for DME som tidligere var blevet udviklet. Studierne viste at med en tilstrækkelig rumlig og tidsmæssig opløsning kunne detonationsbølger opstå i simuleringerne. Den vigtigste følge heraf er at almindelige CFD modeller vil kunne benyttes til at undersøge hvilke betingelser detonationer opstår under.

5 Introduction

5.1 About HCCI combustion

Homogeneous charge compression ignition, or HCCI, is generally regarded as a promising technology for future power train concepts, since it allows an engine to operate with high thermal efficiency and very low emissions of particulate matter and nitric oxides. There is however some drawbacks that still keep the principle from being used in commercial engines. These include a limited load capability, excessive engine noise caused by knocking combustion and the problem of controlling combustion phasing and heat release rate. These areas are the main focus points of the current research.

Several variations of the original HCCI concept have been developed to overcome the problematic issues. Hence names such as PCCI (premixed charge compression ignition), PCI (premixed compression ignition), CAI (controlled auto ignition) etc. are commonly used to denote specific variations of premixed combustion. A thorough description of the various principles is given in [4]. The common feature of all these concepts is that they are all low temperature combustion processes which result in lower levels of nitric oxides and particulate matter than the SI and DI combustion principles.

Proprietary names are also emerging as the technologies are implemented in commercial vehicles. Volkswagen have the GCI (gasoline controlled ignition) and CCI (combined combustion system), which are implementations of gasoline and diesel HCCI variants. CCI have been demonstrated in their Touran model, but are not ready for production.

General Motors have developed a technology called Ecotec, which is currently tested in the US model Saturn Aura. The engine uses variable valve timing, direct injection and electric cam phasing to achieve proper timing of HCCI combustion with gasoline.

Mercedes have demonstrated an HCCI engine and calls their technology DiesOtto, which is a gasoline engine with the ability to switch to auto ignition combustion mode. The prototype engine, which was presented in 2008, is a very complex HCCI engine with features such as variable compression ratio, variable valve timing and variable geometry turbo charging.

It is obvious that engines with the abovementioned technologies will be quite expensive, so the question is if the benefit in terms of modest fuel savings can really justify the additional cost to the consumer. It may one of the reasons that despite the efforts to commercialize HCCI, development appears to be slow within the automotive industry. It may be that the interests in commercializing the concepts are not yet large enough to justify the efforts. When looking into the potential fuel savings, figures from 15 - 30 % in part load operation are common guesses. Such savings are fully possible with hybrid solutions as well, although these tend to be even more costly and increase the weight and complexity of the vehicle.

Design changes such as downscaling (both engine and vehicle) or improved aerodynamics are also logical means of achieving the same fuel saving with even lower cost to the consumer, assuming that the consumers can accept smaller cars. Reducing the size of the engine is however often connected with extra costs for pressure charging and other means of maintaining (or even increasing) the engine power, so the resulting cost saving from reduced fuel consumption is most likely offset by the higher cost of the vehicle. Downscaled engines is therefore of limited interest to the consumer.

Given that HCCI is not the only candidate technology for obtaining a better fuel economy, it must be competitive in cost to the other solutions, as well as offering other benefits. A good argument for using the HCCI principle is that it can potentially eliminate the need for expensive after-treatment solutions that are otherwise required to remove emissions of particulate matter and nitric oxides. The only problematic emissions from HCCI combustion are unburned hydrocarbons and carbon monoxide. These are however easily removed by an inexpensive oxidizing catalyst. Such catalysts have a high conversion factor even at low exhaust temperatures, meaning that HCCI engines can easily meet current emission requirements.

The direction of future developments based on the HCCI concept is still largely undetermined. The main reason is the degree of freedom allowed in terms of fuels, injection principles and controlling strategies, which require a large amount of research to cover. Each proposed concept has its own benefits and disadvantages, and so far no concept has made any significant breakthrough that makes large scale production of the engines possible. It is however likely that HCCI engines will be ready for commercial use within a few years, simply because increasing fuel costs make such investments both logical and necessary.

5.2 Background of this project

The use of DME as a diesel substitute had been in focus for some years at Department of Mechanical Engineering. The first person to demonstrate DME in an engine was Svend Erik Mikkelsen from Haldor Topsøe A/S, who discovered its potential by using it in a lawn mover and a fork lift. Despite switching of the ignition the engine continued running, thereby demonstrating its diesel ignition properties in an engine with a compression ratio suited for gasoline. These discoveries lead to a project, in which DME was tested in a small diesel engine at DTU [5]. Results were promising, but it was also clear that DME did not have the lubricity required to function with standard diesel high pressure pumps and injectors [6]. A high pressure pump requires a fuel with lubrication, since the surfaces will otherwise make contact and the pump will therefore eventually wear out. Diesel injectors are also to some degree susceptible to wear if the fuel does not have any lubricity.

The troubles with diesel injection equipment lead to the idea of using HCCI combustion of DME instead, since this would not require high pressure injection systems. The author was offered this option for his M.Sc. project. The project successfully demonstrated the concept [7]. Funding for a Ph.D. position was given to continue the research, and the outcome is described in this thesis.

5.3 Scope of investigation

During the initial phase of the project, the basic advantages and disadvantages of HCCI combustion of DME were uncovered by experiments at DTU. The first paper in appendix describes the findings of the DME HCCI combustion on the modified Bukh engine. While it was demonstrated that DME is a suitable fuel for the HCCI process, it was also found that:

- Optimum combustion phasing is critical to obtain a high indicated efficiency
- Combustion phasing may be regulated by changes to the compression ratio
- Changes to the equivalence ratio also changes combustion phasing
- Combustion phasing is less sensitive to engine speed
- The combustion process becomes very noisy at increased engine loads
- Emissions of hydrocarbons and carbon monoxide generally relate to the size of the crevice volume

The initial findings lead to the focus on the two subjects for the rest of the project:

- Can combustion phasing be adequately controlled by manipulating the chemical reactions only?
- Can combustion noise be reduced or avoided?

5.3.1 The study on combustion phasing

In general, controlling the combustion phasing by mechanical means such as variable valve train or variable compression ratio is quite a demanding and expensive solution. From an experimental point of view, such modifications could not be undertaken with the resources available.

An alternative option for controlling the combustion phasing is either to manipulate the fuel ignition properties, or the inlet temperature. DME has a relatively low temperature of auto ignition and a short ignition delay, which effectively limits the compression ratio to about 10. Therefore, to retard the combustion and allow for a higher compression ratio, inlet cooling would be required. While inlet air heating is a common solution used for gasoline and other higher octane fuels when operating in HCCI combustion mode, cooling inlet air far below the ambient temperature is a demanding task with potential complications such as ice formation in the inlet. Therefore the best option left for combustion phasing control is to manipulate the fuel ignition characteristics.

To obtain a certain level of insight into the reactions dominating the combustion process, a reduced scheme for the reaction mechanism was developed. This allowed a better overview of the reaction paths, as well as the role of radicals. It also led to an understanding of the special low temperature reactions that are observed during HCCI combustion of DME. The low temperature reactions appear for a short time during the compression of the charge, but the reactions terminate as temperature increases further. The reason for this self terminating behavior is that OH radicals are consumed in a chain terminating reaction parallel to a chain branching reaction. The balance shifts towards the

chain terminating reaction as the temperature increases, thereby terminating the reactions which depend on the OH radicals. The OH radical concentration may also be reduced by introducing a second fuel that consumes the radicals. Methanol is one of the fuels that have proven to be very efficient in controlling radical behavior.

Dual fuel operation with DME and methanol formed the basis of the experiments carried out at NTSEL in Tokyo in the summer of 2008. The second paper in appendix describes the outcome of these experiments.

5.3.2 The study on combustion noise

The tendency for the combustion to become very noisy at increased loads was experienced early in the project. It was also recognized as the most important limiting factor on engine load. The back ground for HCCI engine knock was however not very well understood. It was suspected that the combustion noise was related to the noise experienced with SI engine knock. This kind of knock can be caused by the development of detonations in the end gas region. Such detonations result in strong pressure waves which can reach very high amplitudes. The pressure waves observed in HCCI combustion resemble such detonation waves under strong knocking conditions. This phenomenon is further treated in this thesis.

Detonations are very well understood and the underlying physics are thoroughly explained in literature. It was therefore decided that a basic model of a stationary detonation should be set up, to create a basic understanding of stationary detonation characteristics. Since detonations in HCCI combustion is a transient event, it was also decided to setup simulation cases in STAR-CD to investigate the requirements for capturing the development of detonations. These cases were successful in showing that detonations can develop in short distances, and therefore also in homogeneous charge combustion engines.

To verify experimentally that detonations occur in lean combustion an experiment was setup, using the Bukh engine. A piston was shaped with a rectangular tunnel in which the detonation could develop. The cylinder pressure recordings showed clear indications of super sonic shock waves with very high amplitudes, which are almost certain indications detonation.

The development of detonations can be limited by reducing the dimensions of the volume in which the detonations develop. A large open volume such as with a flat piston type, which is typical of experimental HCCI engines that are converted from SI operation, is therefore not desirable. It was therefore decided to look into different shapes of piston geometries that could reduce the tendency for detonations to develop, and hence reduce the combustion noise. This could potentially allow for higher engine loads without excessive engine noise. The most successful piston geometry turned out to be a diesel bowl piston type, which reduced the combustion noise to a level similar to diesel combustion in the same engine. The results from the experiments are found in the third paper in appendix.

6 The basics of HCCI combustion

6.1 Combustion principle

The HCCI combustion process concept is based on auto ignition in a lean premixed fuel/air charge. The combustion event is therefore governed mainly by chemical kinetics, which clearly separates it from the diffusion combustion in DI CI engines as well as the flame propagation in SI engines.

The abbreviation HCCI has become a covering term for internal combustion technologies that utilize lean premixed combustion at low temperatures. The temperature region for low temperature combustion starts around 1500 K, which is the minimum temperature required for satisfactory conversion of CO to CO2 in the power stroke. The highest temperature allowed is usually determined by the amplitude of the engine knock. Knocking is a high pitched sound caused by large pressure gradients in the combustion chamber due to very rapid combustion. This limit is reached around 1800-2000 K with DME as fuel, corresponding to an excess air ratio of approx. 2.5. At this temperature level the formation of NO is also increasing notably, thereby reducing one of the important advantages of lean premixed combustion.

6.2 Combustion characteristics

In general, the highly premixed fuel/air charges will burn to completion within a few milliseconds near TDC. The ideal HCCI combustion process is therefore not much different from a constant volume explosion due to the very short duration of the combustion. The term explosion implies that the process is spatially uniform and hence the pressure rise rate is also uniform. Although an explosion is usually connected with destructive events, it does not have any damaging effect on the engine as long as the end pressure is within the design limits of the engine.

With an excess air ratio of 3 or less, the majority of the heat release lies within less than one millisecond in a well mixed charge. This results in a fast pressure rise rate, typically above 10 bar per one tenth of a millisecond or higher. At this rate of combustion it is common that not all of the charge reacts simultaneously, which can be caused by temperature gradients and uneven fuel distribution in the chamber. As a result, large pressure gradients are created in the combustion chamber. This causes the air to oscillate with high amplitude in the chamber. The frequencies of the oscillations are identical to the resonance frequencies, which may be calculated or determined by computer simulations. The oscillations are similar to those observed in SI engine knock. HCCI knock may - like SI engine knock - be harmful to the engine if the load is high enough; otherwise it may run continuously at knocking conditions without any damaging effects to the piston or cylinder walls. Knocking does however shorten the life of cylinder pressure transducers, since the membranes of the transducer are typically loaded beyond their design specifications when they are impacted by pressure waves.

Part of the energy contained in the pressure waves in knocking combustion is transferred to the engine and causes the engine exterior surfaces to emit acoustic noise. As higher

fuel concentrations lead to faster reactions and therefore higher differences in pressure, the acoustic noise is increased with the engine load.

Controlling the rate of combustion is thus a challenge. It is possible to control the low temperature heat release by constraining the development of radicals in the initial phases of the combustion with additives or dual fuel combinations that consume radicals through chain terminating reactions. There is however currently no methods that allow control of the heat release rate in high temperature premixed combustion, which is fully governed by reaction kinetics.

6.3 Combustion phasing parameters

6.3.1 Compression ratio

The most important factor to combustion phasing is the compression ratio. Fuels vary greatly in their auto ignition characteristics. Their individual reaction chemistry gives large differences in ignition delays. Some fuels, such as gasoline and methanol which have high octane ratings, require a high compression ratio and hence temperature to obtain auto ignition. Other fuels, typically those with high cetane rankings such as diesel and DME in particular, have low auto ignition temperatures and low ignition delays. Such fuels require only modest compression ratios to ignite.

6.3.2 Equivalence ratio

The equivalence ratio is also important to combustion phasing. If the equivalence ratio is increased during operation of the engine, the rate of reaction is increased as well due to a higher fuel concentration and a higher temperature increment during combustion. This results in an instantaneous advancement of the combustion phasing. As the temperature of the cylinder liner and piston increase slowly hereafter, the charge reacts even earlier due to increased heat addition. Both the instantaneous and the slower advance of the phasing pose a challenge in terms of maintaining the combustion at an optimum point in the cycle.

6.3.3 Inlet temperature

The timing of the combustion is sensitive to inlet temperature, since the rate of formation of the radicals needed to initiate the combustion is a function of the temperature. The position of the initial part of the heat release may therefore be moved by controlling the inlet temperature. A common approach is to preheat the inlet air. By using a regulated mixture of hot and cold air, the temperature can be regulated on a cycle-to-cycle basis. This approach has been used in a number of studies [8, 9 and 10].

6.3.4 Exhaust gas recirculation

The use of exhaust gas recirculation (EGR) is a well known method for reducing the nitric oxides in engines in part load operation. The exhaust gas returned to the inlet decreases the specific heat ratio, which means that combustion temperatures will be lowered as well. In diesel engines the usual limit is approx. 30 % EGR, as the oxygen concentration eventually decreases to a level which reduces the combustion efficiency. This is because the diffusion flame is incapable of consuming all the available oxygen in

the cylinder. In HCCI combustion however, it is possible to use much higher quantities of EGR since there are no diffusion flames. It is only required that the equivalence ratio is kept below unity.

The purpose of using EGR in HCCI engines is not to reduce the formation of nitric oxides, although it does have that effect as well on the already low level of nitric oxide formation. The primary purpose is to affect the combustion phasing. If hot EGR gases are used, either as an internal residual gas or an external un-cooled recycled gas, it advances combustion phasing. Cold EGR gas will usually retard the combustion phasing.

The trapped residual gas within the cylinder is sometimes referred to as internal EGR. It has a promoting effect on combustion phasing, due both to its temperature as well as a certain level of radicals. It was used in one of the first successful implementations of HCCI in a gasoline powered two-stroke motorcycle engine, which competed in the Paris-Dakar race. The principle was named Active Thermo-Atmosphere Combustion (ATAC) [11].

6.4 Thermal efficiency

The HCCI concept is, for the time being, only considered practically applicable for part load operation, mainly due to the problems associated with combustion knock and engine noise. It is therefore not possible for an HCCI engine to obtain the same thermal efficiency as an SI or DI CI engine in full load operation. The indicated efficiency is however excellent with HCCI combustion, since it is close to being an ideal Otto process.

Compared with an SI engine in part load operation, HCCI combustion at the same compression ratio is much more efficient. The main reason is that the inlet throttling losses greatly reduces the SI engine efficiency at part load.

HCCI combustion may obtain the same efficiency as a diesel engine at part load, provided that the engine compression ratio is equal to a diesel engine. The diesel engine does not have throttling losses other than that produced by the EGR system. Combustion duration is longer for diesel engines, but the combustion efficiency is very high and the heat loss is low. The HCCI engine combustion efficiency is not as high as the diesel, which offsets the advantage of a faster combustion.

6.5 Emission characteristics

One major advantage of the HCCI concept is that the lean and premixed combustion reduces the formation of harmful pollutants, mainly particulate matter and nitric oxides.

Particulate matter is not formed since the combustion is fully premixed with a large excess of oxygen. Formation of particulate matter from the lubricating oil is still taking place, but the amount of PM related to combustion of lubrication oil is hardly measurable.

As for NO formation it is very low, typically in the order of 10-50 ppm. The combustion temperature is below the level where the rate of production for NO becomes significant.

Elevated levels of hydrocarbons from crevice volumes and carbon monoxide are easily dealt with in a simple oxidation catalyst. After treatment systems for HCCI are therefore relatively inexpensive, compared to the cost of particulate filters and catalytic converters.

7 Combustion of DME

7.1 Combustion stoichiometry

The ideal combustion of DME in dry air is described by the reaction:

$$\lambda \cdot 3 \cdot (3.76N_2 + O_2) + CH_3OCH_3 \rightarrow 3H_2O + 2CO_2 + \lambda \cdot 11.28N_2 + 3 \cdot (\lambda - 1) \cdot O_2 + 1329\ kJ/mol$$

The stoichiometric fuel to air ratio (FA ratio) is derived:

$$3\ mole \cdot (3.76 \cdot 28.01\ g/mole + 32.00\ g/mole) + 1\ mole \cdot 46.07\ g/mole = 411.95\ g + 46.07\ g$$

$$FA_{S,DME} = \frac{m_{fuel}}{m_{air}} = \frac{46.07\ g}{411.95\ g} = 0.1118$$

The equivalence ratio is given as the ratio of the actual FA ratio to the stoichiometric FA ratio:

$$\phi = \frac{FA}{FA_S}$$

The typical equivalence ratio in engine experiments with DME is from 0.2 to 0.5.

7.2 Physical and chemical properties of DME

Table 1: Properties of DME

Chemical formula:	CH_3OCH_3.
Chemical weight:	46.07 g/mol.
Melting point:	-141 °C
Boling point at atm. pressure:	-24.4 °C
Vapor pressure at 20 °C:	5.1 bars
Critical pressure:	53.7 bars
Critical temperature:	126.9 °C
Heat of combustion, LHV:	28.84 MJ/kg
Heat of vaporization at -20 °C:	410.2 kJ/kg
Auto ignition temperature:	235 °C
Flash point:	-41 °C
Flammability limit in air	3.4-17 vol. %

The data are supplied by Haldor Topsøe A/S. More information about DME is available at [12]. DME has a cetane rating in the range of 55-60. The cetane ranking means that DME has a shorter delay than diesel fuel, which has a cetane ranking of 40-46 (45-50 for premium diesel).

7.3 Development in the use of dimethyl ether as a fuel

As oil derived fuels are becoming increasingly harder to exploit and hence more expensive, alternative fuels are starting to become both economically and politically attractable. In a future society it is most likely that a variety of sources are used to produce a variety of fuels for engines. The sources will likely be prioritized such that those domestically available will be given a primary role in the supply chain.

A prime example of a nation shifting its focus from oil towards its domestic resources is China, which is undoubtedly the leader within DME production. The wish to avoid dependence on fuel import has led the country to utilize its coal resources for fuel production. Coal is now utilized to produce large quantities methanol, ethanol and DME. As of 2009, the country has capacity to produce more than 7 million tons of DME per year, a capacity which is expected to be near 15 million tones per year in 2010 [13]. The current production is used mainly as a supplement to LPG which has similar properties. The situation in China is therefore that DME is now commonly available in large quantities. There are a small number of buses in Shanghai that has been converted to DME and are operating in the city.

In Japan, a few small scale DME plants have been built so far, and a small fleet of trucks are currently being tested [14, 15 and 16]. The National Traffic Safety and Environmental Laboratories (NTSEL) have been responsible for converting the trucks and engines. The government has taken large steps to the protection of the air quality in Tokyo, by implementing strict regulations for all vehicles. As an example, all diesel trucks operating within the city limits are required to be fitted with particulate filters. It is therefore likely that Japan will increase their efforts towards implementing DME as a diesel substitute in the future. The question remains which resources will be used for the production of DME, given that Japan does not have coal or natural gas, and thus are forced to import the feedstock for the production.

8 Description of experimental engine setup

8.1 Engine

The engine used for the experimental work at DTU is a 0.9 L, 2 cylinder, 4 stroke DI CI engine which is constructed for marine applications. It is a simple construction with pushrod valve operation which makes it easy to dismantle and reassemble. The cylinder head is a flat 2 valve design. It is naturally aspirated and does not have EGR.

The engine used for experiments at NTSEL in Tokyo was an Isuzu 4.6 L 4 cylinder truck engine, which was modified with a common rail system developed for DME. It was equipped with EGR and a high capacity EGR cooler. It was furthermore fitted with an injection system for methanol for the experiment. The engine and the experimental setup are described separately in the second paper in appendix.

8.1.1 Engine setup

The engine is coupled to an eddy current type dynamometer from Zöllner. The dynamometer does not have motoring capability, so one of the two cylinders on the engine was kept in DI CI operation with diesel fuel, in order to maintain the engine speed and heat up the engine.

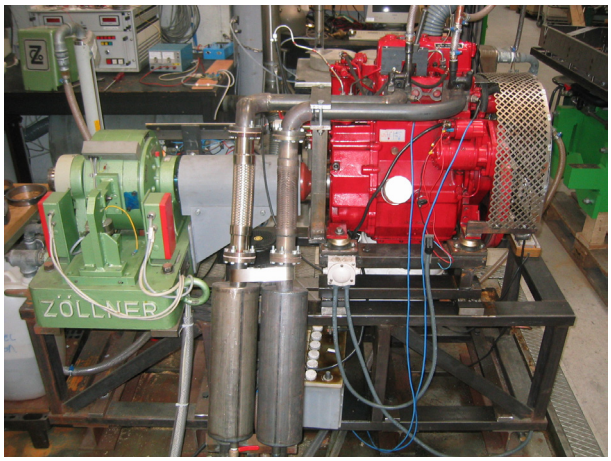

Figure 1: Engine stand

8.1.2 Modifications

The first modification needed to run the engine in HCCI mode was to adapt the compression ratio to suit the fuel ignition properties. Since the compression ratio needed to run on DME was not known initially, a solution which allowed a variable compression volume was installed in the cylinder head. The original diesel injector hole was enlarged to accommodate a steel cylinder, so that a piston could be used to control the compression volume. The arrangement is shown in figures 2 and 3. By adjusting the piston crown height a compression ratio of 14 was made, and with the adjustment piston in bottom position, the compression ratio could be varied from 9 to 14 while the engine was running. This modification has also been used in an HCCI engine at Lund University [17].

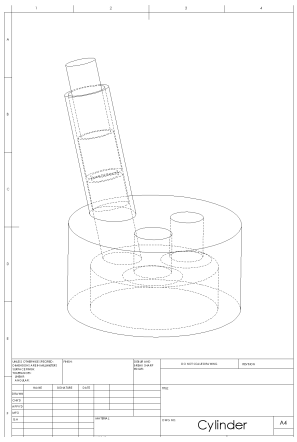

Figure 2: Variable compression volume piston arrangement

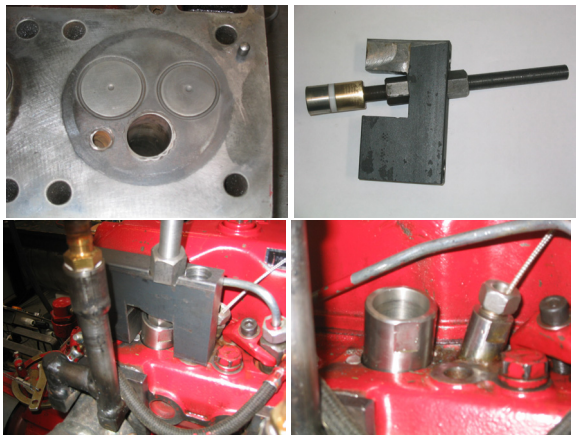

Figure 3: Pictures displaying the insertion of variable piston in cylinder head

It was found that the compression ratio necessary to obtain the optimum combustion timing depends on mainly the engine load. Another factor which affects combustion timing is engine speed, but the effect was shown to be of less significance than the engine load. This may be explained by the fact that heat losses are lower at higher engine speeds and hence the temperature near TDC increases with engine speed.

It was found that high engine loads require the compression ratio to be around 9.5 – 10, while low engine loads require a higher compression ratio of 11 – 13 to complete the combustion. It was however concluded that a fixed compression ratio of 10 was sufficient to cover the load range of practical interest, which is the medium to high load.

In the experiments with combustion acoustics, it was necessary to place pressure transducers around the perimeter of the cylinder liner. Rather than making irreversible changes to the engine block, it was decided to lift the cylinder head and place the transducers in a 10 mm steel plate between the engine block and the cylinder head. This modification is shown in figure 4.

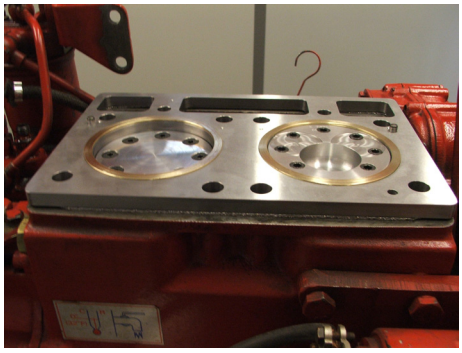

Figure 4: Insertion of steel plate between engine block and cylinder head

8.1.3 Piston modifications

To facilitate the experiments with compression ratios and piston top lands, pistons with changeable heads where constructed from a set of original pistons. The pistons were milled down and 8 holes with 6 mm tread were placed around the perimeter of the piston. Figure 5 shows the assembly of piston and piston crown.

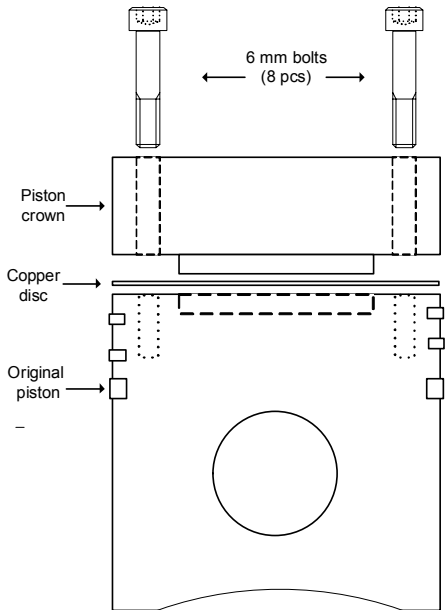

Figure 5: Assembling the piston and piston crowns

The elevation of the cylinder head with 10 mm and an additional head gasket required the pistons to be 11 mm higher. Since the weight of the pistons should be the same, it became necessary to trim material from both pistons and the top pieces produced. If balancing was neglected the engine would suffer from strong vibrations. The engine manual specifies complete weight of the piston and connecting rod to be 1104 grams +/- 10 grams, but this target could not be reached precisely with all piston crowns. Some vibration was encountered when piston crowns were not within the specified weight tolerance.

The fastening of the piston tops onto the piston was made tight to ensure a low contact resistance to heat transfer, so that the piston would not become extremely. An annealed copper disc was used to seal the joint and to ensure optimum heat transfer between the adjoining surfaces. The mounting does not have to be strong to hold the piston top however, as long as the engine speed is moderate. The exact force acting on the piston crown attachment due to acceleration may be determined by taking the second derivative of the expression for piston position and multiplying this with the weight of the piston crown, which weighs approx. 200 grams.

The piston tops used in the acoustic experiments are illustrated and described in paper III.

8.2 Cylinder pressure transducers

The first transducers used were Kistler 6052 CU piezo electric transducers. This transducer is not water cooled, but still maintains a high precision at elevated temperatures. It is not susceptible to thermal shock due to a low diaphragm area and front sealing, which results in a low heat transfer through the pickup. Since it is connected to the combustion chamber through a small diameter bore, combustion is quenched before reaching the transducer.

The piezo electric transducer responds to pressure changes, not absolute pressure. A change in pressure on the diaphragm results in a small charge of electrons. As insulation resistance is never perfect, some of the charge is lost before it reaches the charge amplifier. This causes the amplifier signal to drift, especially when changing the engine load. To fix the signal, a constant leakage current through the charge amplifier is established by coupling a large bleeder resistance to the transducer signal. The discharge current stabilizes the signal at an RMS value around zero, without affecting the magnitude of the signal.

Kistler claims that the transducer is resilient to knocking combustion due to a reinforced diaphragm, but this was clearly not adequate for the kind of knocking experienced in this project. Two of these pickups were used to investigate the acoustic behavior of various combustion chamber geometries. The continued exposure to knocking combustion resulted in one of them to fail completely as the diaphragm collapsed, while the other was partly damaged which resulted in reduced sensitivity.

To replace the broken transducer with a more reasonably priced option, an optical transducer from the US based company Optrand was selected for trial. This type of pickup measures absolute pressure by measuring the deflection of the diaphragm with light. The sensor is connected to an amplifier through a fiber optical cable. The amplifier outputs a voltage from 0.5 to 5 volts, with the lower voltage corresponding to 1 atmosphere. Since drift does not occur with this transducer it is not necessary to calibrate the sensor or correct the signal for drift; it may be used directly after scaling. It was however noted that the signal from the amplifier includes broadband noise, which is likely caused by the amplification stage of the transducer. This means that low pass filtering had to be applied for data that were to be used for the heat release analysis. When the sampling frequency is high the relative error on the pressure change between samples becomes very significant, which necessitates filtering before heat release calculations. For frequency analysis the signal-to-noise ratio is however quite low and filtering is not required.

8.3 Data acquisition

The signals are acquired by a National Instruments USB-6212 data acquisition unit. It has a maximum sample rate of 400 kS/s which is shared between the active channels.

The sample clock for the DAQ is supplied externally by a ScanCon encoder connected to the engine shaft. It delivers 3600 pulses per revolution and a separate pulse to indicate one full revolution. This resolution, 10 samples per CAD, is necessary since the

combustion event is often very fast. Additionally, as a consequence of knocking combustion, there is usually a range of high frequencies present in the combustion chamber. It is therefore required that the sampling frequency is at least twice the highest frequency present in the chamber to avoid aliasing and erroneous measurements. When sampling 10 times per CAD, the sampling frequency becomes 72 kHz at 1200 rpm and the highest frequency that may be detected is therefore 36 kHz. This should be sufficient since the resonance frequencies are usually not higher than 15-20 kHz.

It is necessary to correct the signal for zero level deviation, which can only be done by estimating the cylinder pressure. This is a source of some error in the heat release analysis, where pressure is relatively low in a large part of the cycle. A deviation of +/- 0.1 bar is however insignificant at higher pressures where the heat release is to be calculated, and the IMEP calculation is not affected at all since the error is the same during compression and expansion.

9 Heat release calculations

9.1 The Heat Release analysis

In order to visualize the rate of the combustion it is necessary to perform a heat release analysis. This analysis can provide the crank angle resolved rate of combustion.

The heat release analysis [18] looks as follows:

$$\frac{dQ_{HR}}{d\theta} + \frac{dQ_{wall}}{d\theta} + \frac{d(m\,c_V\,T)}{d\theta} = \frac{\gamma}{\gamma - 1}\,p \cdot \frac{dV}{d\theta} + \frac{1}{\gamma - 1}\,V \cdot \frac{dp}{d\theta}$$

In this expression the terms on the left hand side are the chemical heat release, the wall heat transfer and the energy loss related to mass escaping the process. The mass loss is most often insignificant and is therefore usually not included.

The heat transfer is in the order of +/- 2 Joule per CAD for a 1 liter cylinder. The heat release is in the order of 10-100 Joule per CAD or higher. The magnitude and shape of the heat release rate are therefore not affected much by the heat transfer. In many situations it is therefore irrelevant to improve the accuracy with the additional term for heat transfer. Only if the accumulated heat release and combustion efficiency is of interest should this be required.

9.2 Location of TDC

The mechanical TDC position of the engine is possibly the most critical parameter in the heat release analysis. The impact of a deviation between the estimated and real TDC position on the IMEP with a typical combustion cycle can be seen in table 2.

Table 2: Influence of TDC offset on IMEP calculation

Position offset (CAD)	-2.0	-1.0	-0.5	-0.1	0	+0.1	+0.5	+1.0	+2.0
IMEP	406	446	467	483	487	491	507	527	567
Deviation (%)	-16	-8	-4	-0.8	0	+0.8	+4	+8	+16

It is clear that even a minor deviation from the correct TDC results in a significant error in the IMEP calculation.

The peak pressure may be used as a preliminary indicator of the TDC. This assumption will result in a certain deviation depending on the engine size, as heat losses will reduce the pressure and cause it to peak shortly before TDC. For 4-stroke engines in typical vehicles the peak pressure may appear around 0.5 CAD before TDC, whereas for small two stroke engines the peak pressure may appear as much as 2 CAD before TDC due to relatively high heat losses in such small engines.

It is possible to locate the TDC with reasonable accuracy with the cylinder head removed. Positioning the crank angle encoder so that the z-pulse occurs exactly in this position is

however not possible, since it implies tightening the encoder on the shaft while maintaining an accuracy of $1/10^{th}$ of a degree. It is therefore required that the TDC position is determined through measurements rather than relying on the encoder position to be adequately precise.

One way to determine the TDC is to use a capacitive sensor which is inserted in to cylinder like a pressure transducer. It measures the distance to the piston by electrical capacitance, and due to symmetry in the produced curve it is possible to locate the TDC with very high precision.

There are also several ways to determine the TDC position from the pressure measurements. Five of these methods are tested and evaluated by Nilsson and Eriksson [19]. The most accurate method is based on a comparison of the slopes on the compression and expansion sides of the cylinder pressure curve. It does however require more work than may be justified by its accuracy.

A similar method in the paper has an acceptable accuracy and requires less user programming. This method compares the polytropic coefficients at the pressure infliction points. The infliction points are those where the $2.^{nd}$ derivative of the curve is zero, which is also identified as the point where the curvature steepness switches from increasing to decreasing or inverse. The location of these points is illustrated in figure 6.

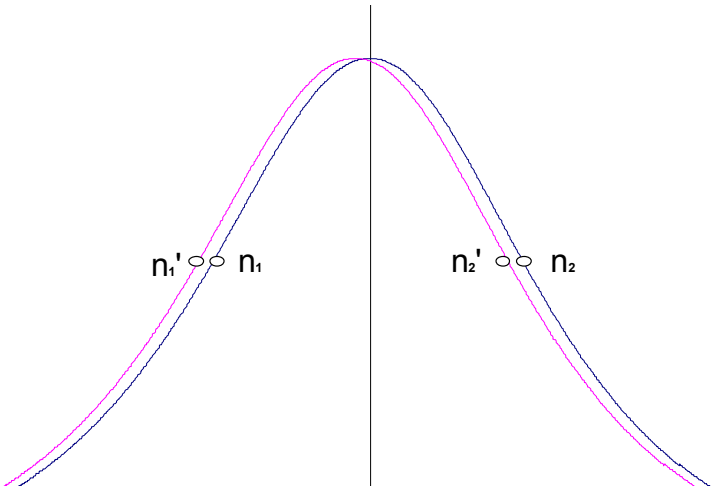

Figure 6: Illustration of infliction points on motored cylinder pressure curve.

The pressure increase per interval CAD is determined directly, and thus it is only a matter of locating the position of the most positive and negative values of pressure change. Then the polytropic coefficients n_1 and n_2 is calculated at these two locations using the relation for polytropic processes:

$$p_1 V_1^{\,n} = p_2 V_2^{\,n} \Leftrightarrow n = \frac{\ln\left(\frac{p_1}{p_2}\right)}{\ln\left(\frac{V_2}{V_1}\right)}$$

To determine the correct location of the TDC, the two polytropic coefficients are first calculated with the pressure curve positioned such that the pressure peaks exactly at TDC. The polytropic coefficients are termed n_1 and n_2. By displacing the pressure curve, another set of coefficients may be calculated. These are termed n_1' and n_2'. The values are used in this expression:

$$R = \frac{n'_2 - n'_1}{n_2 - n_1}$$

Now, to determine the correct position, the curve is displaced until the value of R is between 2.2 and 2.3. At this position the pressure curve will be at TDC.

The inherent weakness of this method is that it is sensible to noise. Noise can cause both the peak pressure and pressure infliction points to be unidentifiable. It was noted that the signal from the optical pressure transducer was too biased with noise for this method to be used accurately, while the noise level on the piezo electric pickup was low enough for an accurate position.

9.3 Specific heat ratio

The accuracy of the heat release estimate depends on the specific heat ratio, which is the ratio of the specific heats:

$$\gamma = \frac{c_p}{c_v}$$

The specific heat ratio decreases with temperature. For pure air, the temperature dependence of the specific heat ratio is often simplified to the relation:

$$\gamma(T) = \gamma_0 - \frac{8}{100}\frac{T}{1000}$$

This correlation is however not very accurate at higher temperatures, and is not suitable for use with gas mixtures either. The composition of unburned and burned mixtures is also of importance, although the mass fraction of changing species is quite small.

A better estimate has been made in EES, by using the internal tables of c_p and c_v to determine the specific heat ratio as a function of temperature. Figure 7 illustrates the temperature dependence of the specific heat ratio for dry air, for a lean unburned mixture

(excess air ratio 3) of air and ethanol, for the corresponding burned mixture and an average of burned and unburned. All components are assumed to be ideal gasses.

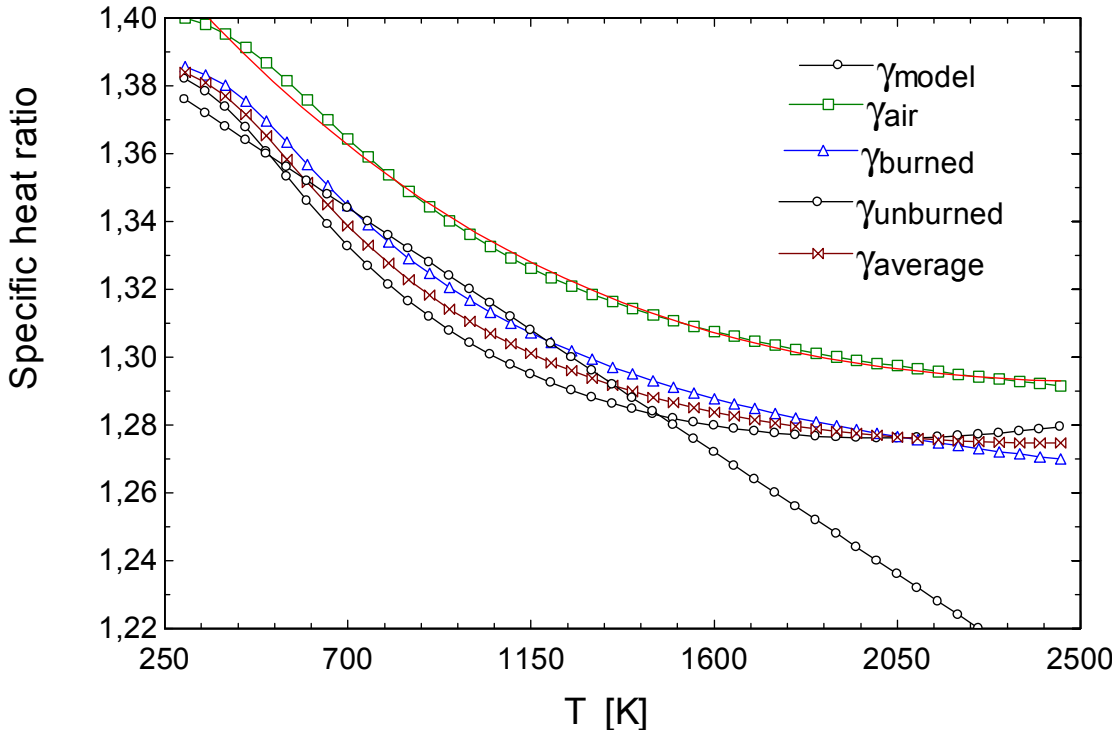

Figure 7: The specific heat ratio calculated for dry air, for a burned and unburned charge and the average of burned and unburned charge. The linear relation is for the model expression.

As can be seen from the figure, simply assuming a linear relationship will result in a great deviation at elevated temperatures, when compared to the values calculated from the tabulated properties.

For motoring conditions with pure air, the curve for pure air will provide a better estimate on the specific heat ratio than the linear expression. For operating conditions, the specific heat ratio is less depending on whether the gas is burned or not, than it is on temperature. The error of using the average value is les than one percent and hence acceptable for calculations of heat release.

The calculation of gamma may be performed with a third order polynomial fit. The equations in table 3 are very close approximations to the curves above, at temperatures higher than 400 K

Table 3: Polynomial fits of specific heat ratios

Air	$\gamma = 1.45 - 1.62 \cdot 10^{-4} T + 5.49 \cdot 10^{-8} T^2 - 1.26 \cdot 10^{-11} T^3$
Unburned	$\gamma = 1.44 - 2.22 \cdot 10^{-4} T + 9.39 \cdot 10^{-8} T^2 - 1.26 \cdot 10^{-11} T^3$
Burned	$\gamma = 1.44 - 1.18 \cdot 10^{-4} T + 6.96 \cdot 10^{-8} T^2 - 9.51 \cdot 10^{-12} T^3$
Average	$\gamma = 1.44 - 2.03 \cdot 10^{-4} T + 8.18 \cdot 10^{-8} T^2 - 1.11 \cdot 10^{-11} T^3$

The calculations do not take into account that the effects of dissociation or presence of other intermediate species. It is however not very important, since the amount of dissociation at 2000 K is insignificant. For HCCI combustion these approximations will therefore be acceptable.

9.4 Temperature estimate

Assuming ideal gas behavior and no mass loss, the temperature may be estimated from the ideal gas law:

$$T = \frac{pV}{mR_{mass}}$$

R_{mass} is the mass based gas constant, 287 J/kg-K. This value is only valid for dry air. The gas constant valid for the unburned and burned charges is calculated as:

$$R_{mass} = \frac{R_{molar}}{M_{mixture}}; \quad M_{mixture} = \sum x_i M_i$$

where R_{molar} is the universal gas constant, $M_{mixture}$ is the molar weight of the mixture, x_i the mass fraction of species i and M_i the molar weight of species i.

Table 4: Molar masses and gas constants calculated for air, burned and unburned charge.

Mixture	Components	Molar mass	Gas constant
Air	N2: 0.78, O2: 0.21, Ar: 0.01	28.97	287.0
Unburned	N2: 0.739, O2: 0.225, DME: 0.036	29.55	281.4
Burned	N2: 0.739, O2: 0.15, CO2: 0.069, H2O: 0.042	29.28	283.9
Average	Based on burned and unburned	29.42	282.6

The change in the mass based gas constant before and after combustion is insignificant. An average value of 283 is sufficient to improve accuracy in the temperature calculation with both burned and unburned mixtures.

Since pressure and volume are known with good precision, the most critical is the determination of the cylinder mass, m. The amount of air entering the engine may be estimated from the volumetric efficiency and the intake conditions which are well known parameters for a diesel engine, while the amount of residual gas may be estimated from the exhaust temperature and cylinder pressure at EVC. A more precise evaluation of the trapped mass may be made by measuring the air flow with a laminar flow meter, if the valve overlap does not result in air flowing through the engine.

9.5 Heat losses

The preferred method of calculating heat transfer is by the Woschni Correlation. The heat transfer between a gas and a surface of area *A* is given by:

$$\frac{dQ}{dt} = h \cdot A \cdot \left(T_{gas} - T_{sur}\right)$$

Where h is the convective heat transfer coefficient with units W/m^2K. Woschni developed an expression for this coefficient, based on the empirical correlations for flow. With HCCI combustion this expression was in need of a revision to account for the difference with lean combustion. Junseok et al [20] made an extensive experimental study on the instantaneous heat transfer in HCCI combustion and proposed a modified expression for the heat transfer coefficient:

$$h = \alpha \cdot L^{-0.2} \cdot p^{0.8} \cdot T_{gas}^{-0.73} \cdot v$$

Here, α is a scaling factor which is adjusted to satisfy the total energy balance. The rest of the left hand terms are instantaneous values. L is the characteristic length, which is changed from being the cylinder bore in the original expression, to the instantaneous chamber height. p and T are the pressure and temperature, respectively. v is the gas velocity, which is divided into two separate terms, with the first being a mean gas velocity and the second a combustion induced velocity:

$$v = C_1 \overline{S_p} + \frac{C_2}{6} \frac{V_d T_r}{p_r V_r} (p - p_{mot})$$

S_p is the average piston speed and V_d is the displacement volume. T_r, p_r and V_r are values of temperature, pressure and volume at a reference location, such as intake valve closing. p is the pressure and p_{mot} is the motored pressure at the same reference location. The modification to this expression is that C_2 is divided by 6, since the combustion induced velocity is much lower with HCCI combustion than with SI combustion.

The constants C_1 and C_2 are engine specific, but may be approximated by the expressions:

$$C_1 = 2.28 + 3.08 \frac{\pi B w_p}{\overline{S_p}}; C_2 = 0.00324$$

Where w_p is the swirl factor, which must be estimated if not provided by the engine manufacturer.

10 The reaction kinetics of DME

10.1 Elementary reaction model

All elementary reactions are modeled using the three parameter form of the Arrhenius expression:

$$k(T) = A \cdot T^{b} e^{\left(\frac{-E_A}{R_U T}\right)}$$

with units

$$T : K$$

$$E_A : \frac{Cal}{mol}$$

$$R_U : \frac{Cal}{mol \cdot K}$$

The unit of A depends on the reaction type.

The parameters needed to calculate the forward reaction rate coefficient are the frequency factor A, the temperature exponent b and the activation energy E_A. These parameters are supplied for both forward and reverse reactions in the reaction mechanism used to model DME combustion.

10.2 The detailed reaction scheme

The reaction kinetics of DME is described in details by a reaction scheme named DME 2000 from Lawrence Livermore National Laboratory. The reaction scheme is based on studies on premixed DME/air flames at atmospheric pressure. Extensive documentation is available for this scheme [21]. Units are in mol, Calories and Kelvin.

Low pressure and Troe fall-off corrections are given for some reactions. The details of these corrections are beyond the scope of this report, but the corrections are included in the simplified scheme for completeness.

10.3 Reducing the mechanism for lean combustion

The full scheme was developed to model both lean and rich flames. Rich flames involve much more complicated reaction paths than lean flames. Reactions leading to the formation of higher hydrocarbons are included, such as ethylene. Since ethylene is believed to be an important precursor to soot, the mechanism can potentially be used to predict soot formation in rich flames. The formation of higher hydrocarbons is however very low at lean and premixed conditions, since the possibility of local rich combustion zones is very limited. Hence there is no need to include these species in the description of lean combustion.

In addition, many reactions which may be relatively important at low temperatures and pressures have insignificant reaction rates when temperature and pressure are elevated.

In order to apply the reaction scheme in CFD models the scheme needs to be simplified without loosing its accuracy. The target was that the reaction mechanism should be reduced considerably without affecting the ignition delay, low temperature reaction paths, heat release rate, sensitivity to radical concentrations and composition of products.

There are some commercial tools available that performs automated reduction of reaction schemes. A software called ASRT (automatic scheme reduction tool) was developed by Yamauchi et al [22] and used specifically for DME. These reduction tools can eliminate elementary reactions from the main paths, which further simplifies the total scheme. The application of such tools was however beyond the scope and purpose of the study, in particular since a major benefit of reducing the scheme is that it creates a fundamental understanding of the reaction paths.

The process of reducing the scheme began by setting up and running a CHEMKIN simulation with the full reaction scheme. CHEMKIN is a program developed for simulation of chemical reactions. The software analyses the mechanism and other data that is supplied by the user and solves the stiff ordinary differential equation system that constitute the problem.

To simplify the detailed reaction scheme, a set of well known operating parameters were chosen from the functional experimental setup. An excess air ratio of 4, a compression ratio of 10 and an engine speed of 1000 rpm were used. The results from this simulation run were used as the basis for reducing the scheme.

The operating parameters are sufficient for obtaining a model that functions well within the operational limits of HCCI combustion. Changes to equivalence ratio are limited due to the narrow temperature interval within which HCCI can be realized. Variation to engine speed should not affect the outcome either due to the short timescale of the reactions compared to the engine speed. Finally, changes to the compression ratio will only affect the temperature history and hence the timing of the combustion process.

The method used to reduce the scheme was to select only the dominating paths from the fuel molecule to complete combustion products. The dominating carbon containing species were picked out initially, and the paths leading to the formation and destruction of these species were identified.

Besides fuel species the scheme has a number of non-carbon radical reactions. These reactions are between the species: O, H, O_2, H_2, OH, H_2O, HO_2 and H_2O_2. The dominating reactions were selected based mainly on the species rate-of-production. Although concentrations of highly reactive species may be low, their rate of production is often very high. By choosing only those reactions with high rates of production, the scheme for non-carbon radicals may be simplified greatly.

The result from this process was a new scheme with 29 species and 55 reactions. Figure 8 was constructed to illustrate the reaction paths in the reduced scheme. The scheme itself is listed in appendix A in the CHEMKIN format. A list of the species names is given in the end of this chapter.

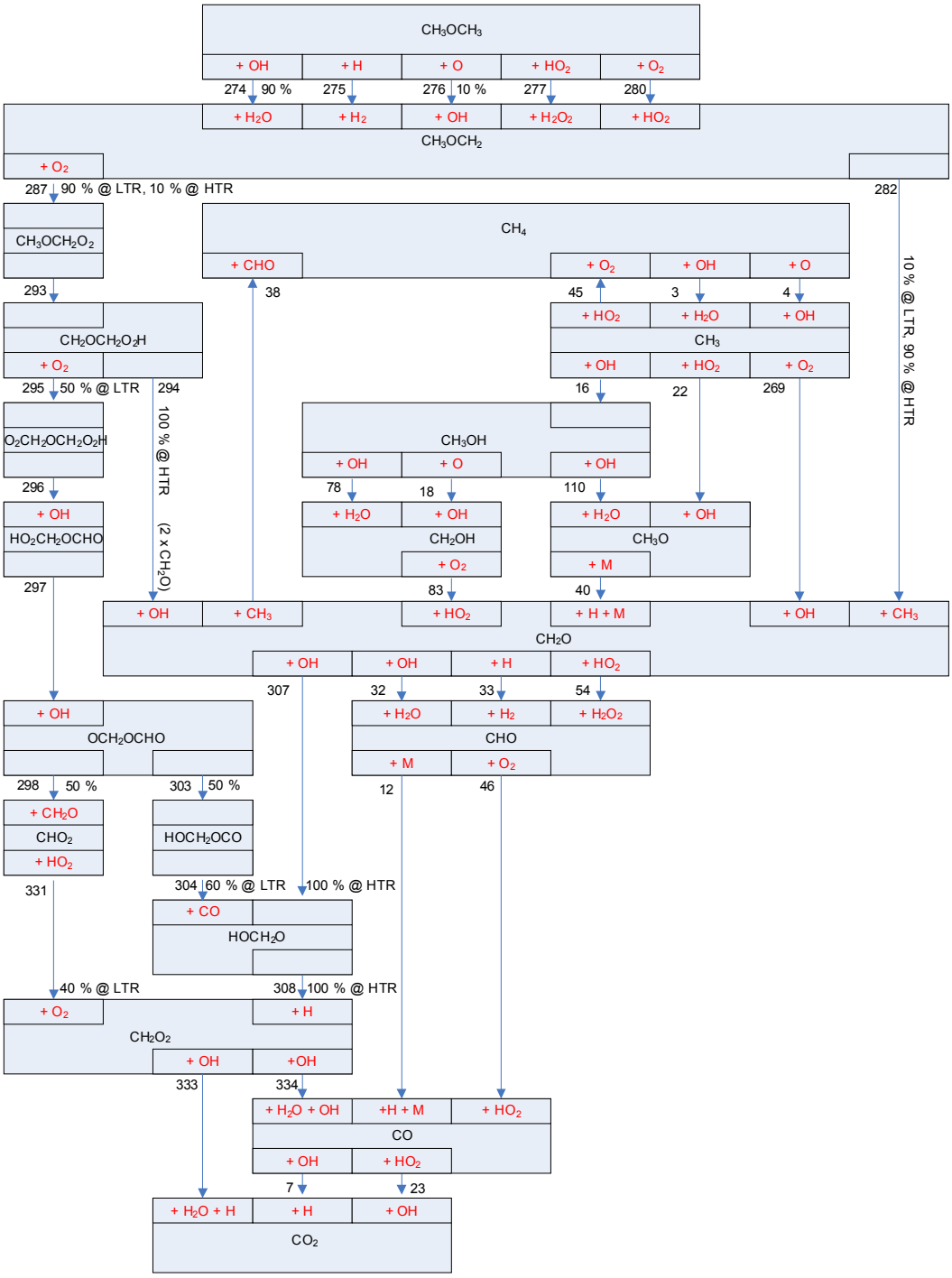

Figure 8: Reduced reaction scheme for lean combustion of DME

Arrows in the scheme indicate the dominating reaction way. Percentage numbers indicate the approximate distribution on the paths.

The radicals that are placed in the small boxes e.g. [+ OH] denotes that this radical reacts with the radical in the larger box in which it resides. If no radical is in the box, the reaction is by decomposition. An M denotes a third body collision.

References to reaction numbers are to the numbers used in the original mechanism. The reason is that this makes it easier to identify the reactions in the original scheme.

10.4 Comparison of the full and the reduced schemes

To evaluate the performance of the reduced scheme against the complete scheme, the two schemes were tested in a CHEMKIN simulation with identical parameters. The heat release and accumulated heat release are plotted in figures 9 and 10.

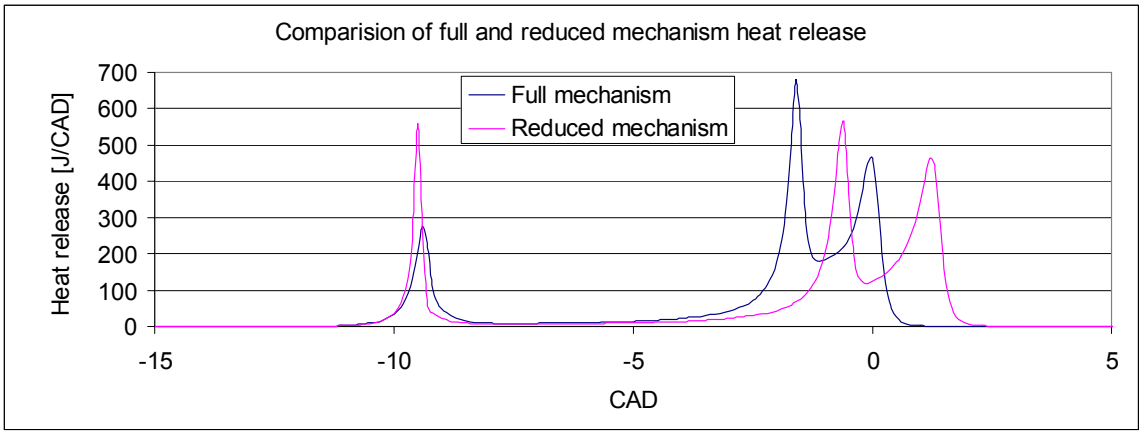

Figure 9: Simulated heat release for the full and reduced mechanisms

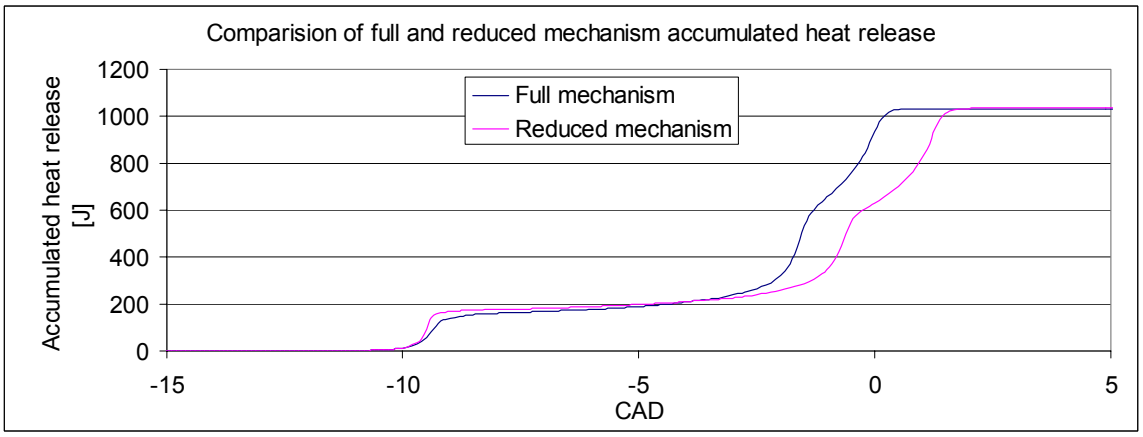

Figure 10: The accumulated heat release of the full and reduced mechanisms

It is noted that the ignition timing is perfectly preserved with the reduced scheme. All initial reactions with DME were included in the reduced scheme to preserve the mechanism behavior in the first stages of combustion.

The reduced scheme however results in minor deviations in the heat release. The LTR heat release is of shorter duration and with a higher peak in the reduced scheme, but as can be seen from the accumulated heat release the total heat released in the LTR reactions is not very different.

The HTR reactions are slightly delayed and with slightly lower peaks in the reduced scheme. The shape of the two stage HTR combustion is however well preserved, and the final accumulated heat release is identical for the two schemes.

It is found that the reduced scheme is adequately accurate for use in simulations. There is however some potential for improving the scheme in order to match observations better. The most notable deviation between simulations and experiments is in the delay from LTR to HTR reactions, which is often significantly shorter in experiments.

10.5 Reaction paths

10.5.1 Initiation and low temperature reaction paths

Figure 11 shows the temperature and heat release plotted together. The low temperature reactions starts approx. 750 K and are terminated at around 900 K.

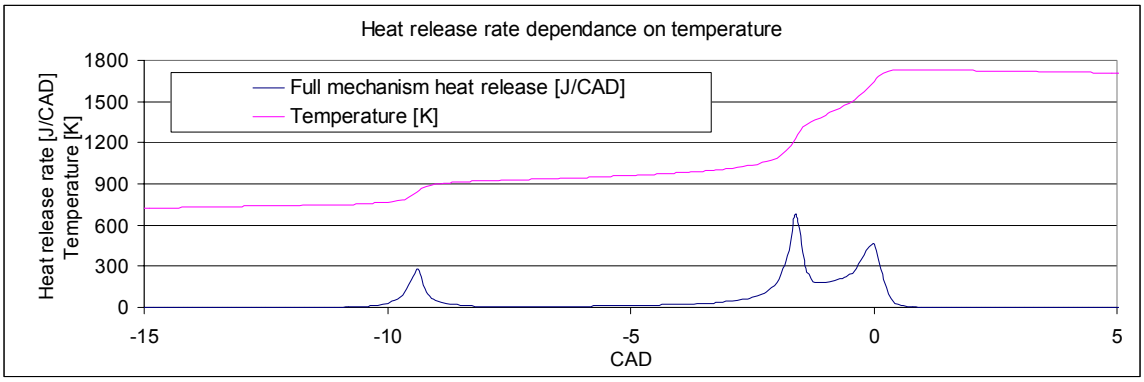

Figure 11: The heat release dependence on temperature

The LTR is self-terminating due to chain-terminating processes becoming dominating as the temperature increases. This gives the characteristic blue flames, which in case of DME releases a substantial part of the total energy in the fuel.

In experiments, the LTR appears in a very consistent manner. There is very little cycle to cycle variation in both CAD position and magnitude. The development of the LTR heat release is always observed to occur with the same magnitude. This is because the heat release from the LTR is not dependant on initial fuel concentration. The concentration of fuel molecules is not rate limiting; it is the concentration of OH radicals that determines the heat release in the LTR combustion stage.

LTR are of high importance to the subsequent release of the remaining chemical energy. The temperature increase of course means that the reactivity of the gas is increased, but the LTR also creates a few stabile radicals such as hydrogen peroxide (H_2O_2),

formaldehyde (CH_2O) and formic acid (HCO_2H), that are ready to proceed to the final oxidation steps to CO and CO_2. Hydrogen peroxide in particular is important, since it becomes unstable as temperature increases, and thereby becomes a source of hydroxyl (OH) radicals.

The initial breakdown of DME occurs by reaction with molecular oxygen. It has a very low conversion rate, but since there are no other active radicals being formed at this temperature it is the only reaction that can produce CH_3OCH_2 initially. Once OH radicals are being produced further down the chain, these radicals are responsible for the major part of the first oxidation step.

There are two major reaction paths from the methoxy-methyl (CH_3OCH_2) radical. The path to the left in the scheme (fig. 8) is the primary at low temperature reactions, while the path to the right is dominating at high temperature reactions.

The first step in the low temperature reaction (LTR) scheme DME combustion is the formation of the methoxy-methyl radical, CH_3OCH_2, which is possible by several reactions. The dominating reaction is 274, but to ensure a good prediction of ignition delay it is necessary to include reaction with molecular oxygen as well. Reactions with three other radicals (H, O and HO_2) are also included in the mechanism since they are relevant at higher temperatures.

$$\#274: CH_3OCH_3 + OH \rightarrow CH_3OCH_2 + H_2O$$
$$\#280: CH_3OCH_3 + O_2 \rightarrow CH_3OCH_2 + HO_2$$

Initially, reaction 280 is the dominating reaction since there are no OH radicals. It produces CH_3OCH_2 at a very low rate, but the later steps produce OH radicals for reaction 274.

The methoxy-methyl radical predominantly combines with molecular oxygen in reaction 287 during the LTR reactions.

$$\#287: CH_3OCH_2 + O_2 \rightarrow CH_3OCH_2O_2$$

Following reaction 287 is reaction 293 in which an H-radical shifts its position in the molecule. This happens almost instantaneously.

$$\#293: CH_3OCH_2O_2 \rightarrow CH_2OCH_2O_2H$$

This molecule may now react in two different ways. The first is dissociation which produces one OH radical and two formaldehyde radicals, while the second is the absorption of molecular oxygen:

$$\#294: CH_2OCH_2O_2H \rightarrow 2\,CH_2O + OH$$
$$\#295: CH_2OCH_2O_2H + O_2 \rightarrow O_2CH_2OCH_2O_2H$$

Initially reaction 295 is dominating. It is followed by reactions 296 and 297:

$$\#296: O_2CH_2OCH_2O_2H \rightarrow HO_2CH_2OCHO + OH$$
$$\#297: HO_2CH_2OCHO \rightarrow OCH_2OCHO + OH$$

This reaction path creates two OH radicals. Since one OH radical was consumed initially in reaction 274, the path creates one surplus OH and is therefore chain branching.

As the temperature increases, reaction 294 begins to take a larger share. It produces two formaldehyde molecules. These react with OH to form two HCO in reaction 32.

$$\#32: CH_2O + OH \rightarrow HCO + H_2O$$

Thus one OH radical is consumed overall in this reaction path, which makes it chain terminating. The self-terminating behavior of the LTR reactions is therefore a direct result of the reaction path shifting from a chain branching to a chain terminating path.

The shift can be seen in figure 12 which illustrates the rate of production of the relevant radicals during the LTR combustion phase. The dissociation reaction (44 in the figure) becomes dominating around 1.93 milliseconds and continues to increase. The formation of the formyl radical which is chain terminating reaction is seen to increase as well, which causes the net production of OH radicals to become negative and eventually leads to OH concentration being reduced to very low levels.

Following reaction 297, the OCH2OCHO radical produced may now react in two different ways at approximately equal rates to produce formic acid (HCO_2H). Reaction 298 is followed by reaction 331, in which also formaldehyde is produced:

$$\#298: OCH_2OCHO \rightarrow HCO_2 + CH_2O$$
$$\#331: HCO_2 + HO_2 \rightarrow HCO_2H + O_2$$

Alternatively by reactions 303, 304 and 308 which also produce CO:

$$\#303: OCH_2OCHO \rightarrow HOCH_2OCO$$
$$\#304: HOCH_2OCO \rightarrow HOCH_2O + CO$$
$$\#308: HOCH_2O \rightarrow HCO_2H + H$$

This branch in the LTR process ends with the formation of formic acid, which reacts slowly at low temperatures. It is therefore accumulated together with other stabile radicals such as hydrogen peroxide and formaldehyde.

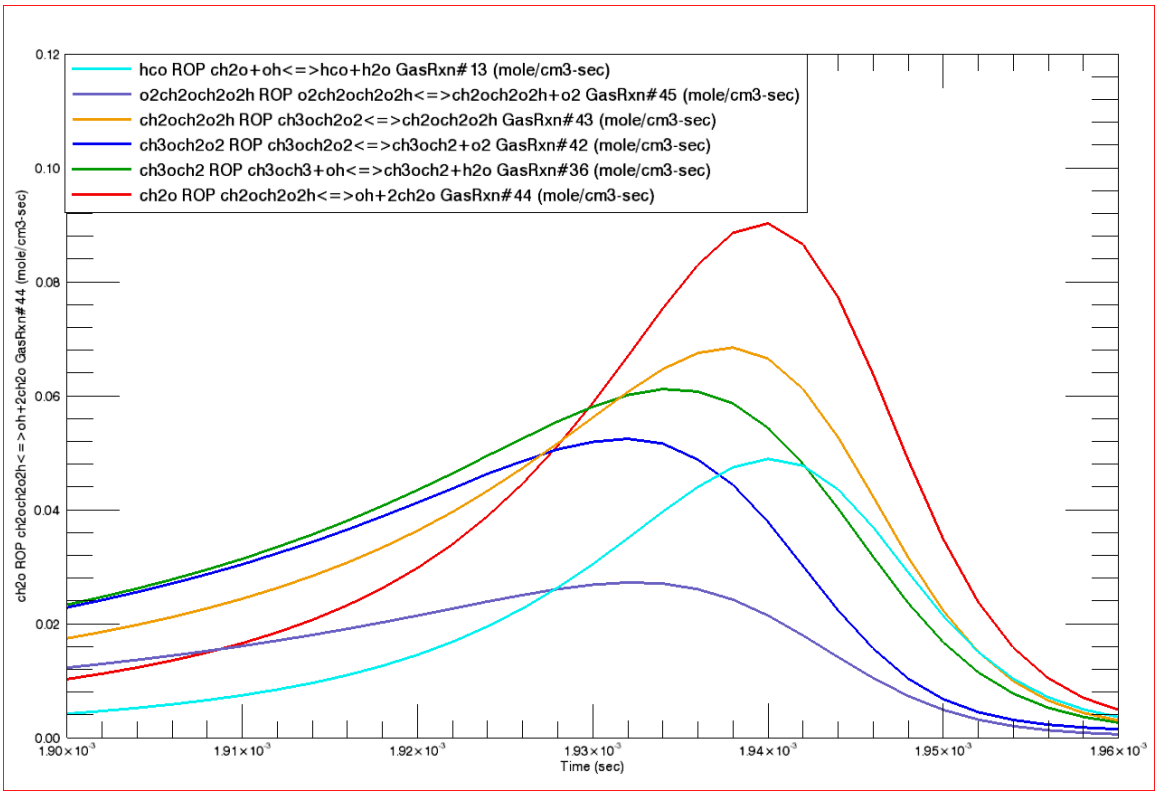

Figure 12: Termination of the low temperature reactions

Formaldehyde is the intermediate radical with the highest concentration in the interval between the LTR and HTR processes. Formaldehyde appears to have a constant concentration, but it is produced and consumed continuously. Production is mainly through dissociation of the methoxy-methyl radical. Consumption is by reaction 32 that produces HCO, which dissociates by reaction 12, to form CO:

$$\#12 : HCO + M \rightarrow CO + H + M$$

The continuous production of CO consumes the majority of the available OH radicals and keeps the other possible reactions at low levels. With a limited amount of OH radicals available, the reaction path consisting of reactions 274, 282, 32 and 12 dominate the interval between the LTR and HTR processes.

The non-carbon radicals interact in a simple way during the LTR process. First the hydrogen produced mainly by reaction 12 combines with O_2 to form HO_2. The HO_2 then combines with itself, H or OH. Roughly half reacts to form H_2O_2 which accumulates. About half of the remaining HO_2 produces new OH radicals, and the rest is used in the chain terminating reaction.

$$\#26: H + O_2 \rightarrow HO_2$$
$$\#50: HO_2 + HO_2 \rightarrow H_2O_2 + O_2$$
$$\#47: HO_2 + H \rightarrow 2OH$$
$$\#49: HO_2 + OH \rightarrow H_2O + O_2$$

As the temperature increases, thermal dissociation of the methoxy-methyl radical (reaction 282) becomes important. The thermal dissociation produces equal quantities of methyl and formaldehyde. The methyl radical mainly reacts with HO_2 to produce CH_3O, which then looses an H in a third body collision and becomes formaldehyde:

$$\#282: CH_3OCH_2 \rightarrow CH_2O + CH_3$$
$$\#22: CH_3 + HO_2 \rightarrow CH_3O + OH$$
$$\#40: CH_3O \rightarrow CH_2O + H$$

Some CH_3 also reacts with the formaldehyde to produce the methane:

$$\#38: CH_3 + CH_2O \rightarrow CH_4 + HCO$$

Methane is accumulated during the LTR process, since the temperature is insufficient for this molecule to be oxidized.

10.5.2 High temperature reactions

The HTR reactions are dominated by thermal cracking of CH_3OCH_2 to CH_3 and CH_2O. The methyl radical may react with the CH_2O to produce CH_4, which is again oxidized in through various reactions to CH_2O.

HTR reactions exhibit a two stage combustion process, where the heat of reaction of the first stage is mostly from the formation of CO and H_2O, while the second stage is the oxidation to CO_2. This produces two peaks in the heat release. The pattern is visible in detailed CHEMKIN simulations, but not in heat release analysis of real combustion.

In the first step all remaining fuel is converted to formic acid, HCO and CO. HCO now reacts mainly with O_2 to produce CO:

$$\#46: HCO + O_2 \rightarrow CO + HO_2$$

The formic acid (HCO_2H) that was produced during the LTR is converted mainly by reaction 333, but also some in 334:

$$\#333: HCO_2H + OH \rightarrow CO_2 + H_2O + H$$
$$\#334: HCO_2H + OH \rightarrow CO + H_2O + OH$$

The non-carbon radical activity utilizes the H atom from reaction 333 to produce new HO_2 and OH radicals, as well as converting the H_2O_2 intermediate that was stored during the LTR reactions:

$$\#26: H + O_2 \rightarrow HO_2$$
$$\#50: 2HO_2 \rightarrow H_2O_2 + O_2$$
$$\#51: H_2O_2 \rightarrow 2OH$$

The second step is the final oxidation of CO to CO_2.

$$\#40: CO + OH \rightarrow CO_2 + H$$

The non-carbon radicals act differently in the second step, since now only OH is in demand. The H from reaction 40 is used by reaction 8 to form OH and O. The O is then used in reaction 10 to produce two more OH. Hence a total of three OH are produced for every H supplied. HO_2, which was produced in reaction 46, combines with roughly a third of the OH in a terminating reaction.

$$\#8: H + O_2 \rightarrow O + OH$$
$$\#10: O + H_2O \rightarrow 2OH$$
$$\#49: HO_2 + OH \rightarrow H_2O + O_2$$

The overproduction of OH radicals ensures that the rate of CO conversion is mainly limited by the temperature. Any CO existing after the combustion will therefore be due to quenching or crevice volumes, or simply a low combustion temperature. Only a very small concentration of CO is produced due to dissociation of CO_2, since the temperature is not high enough for dissociation to be significant.

10.6 Manipulating low temperature reactions

10.6.1 Effect of methanol on low temperature reactions

The main purpose of using methanol is to obtain a higher octane rating of the fuel, obtained mainly by increasing the ignition delay of the fuel. In other cases DME has been used as an ignition improver for methanol or other fuels in DI CI engines.

In an HCCI engine both fuels are premixed with the inlet air. The principal role of the methanol is to function as an inhibitor of the LTR heat release. When methanol constitutes about 30 % of the total fuel mass, the LTR heat release is almost eliminated.

The inhibition of the LTR reactions is due to the consumption of OH radicals by reactions 78 and 110, which are the major paths of oxidation for methanol:

$$\#78: CH_3OH + OH \rightarrow CH_2OH + H_2O$$
$$\#110: CH_3OH + OH \rightarrow CH_3O + H_2O$$

Both of the radicals formed in the reactions above react to form formaldehyde:

$$\#83: CH_2OH + O_2 \rightarrow CH_2O + HO_2$$
$$\#40: CH_3O + M \rightarrow CH_2O + H + M$$

The OH consumption by reactions 78 and 110 means that less DME reacts through reaction 274, and thus the chain propagating reaction is reduced.

The advantage of reducing the LTR is that the HTR is delayed proportionally with the LTR reduction. The amount of methanol can thus be used to control the combustion phasing.

The effect of the dual fuel combination with methanol was demonstrated in cooperation with NTSEL in September 2008. Paper II in the appendix describes the outcome of the experiment. It was found that with about 30 % (mass) methanol added to the intake the combustion could be delayed to shortly after TDC, which improved the indicated efficiency and reduced the pressure rise rate. Furthermore, a change in the combustion towards less knocking could be observed from the engine noise.

10.6.2 Effect of EGR

The use of exhaust gas recirculation (EGR) in diesel engine combustion was introduced to limit the formation of NO by reducing the combustion temperature. By reusing exhaust gas the specific heat capacity of the gas is increased due to the increase in CO_2 and H_2O concentrations. This reduces the temperature rise significantly. The specific heat ratio is however reduced, which reduces the amount of piston work.

There is a limit to how much EGR may be used in diesel combustion, as the oxygen concentration is decreased with increasing EGR. This reduces the rate of reaction in the diffusion flames and hence slows the combustion. A maximum of approx. 30 % vol. of EGR is normally regarded as the limit for diesel engines. Increasing the amount of EGR will result in excess production of particulate matter and inefficient combustion.

In HCCI combustion, EGR may be used to control the heat release. By decreasing the specific heat ratio, the temperature during compression will also be significantly reduced due to the lower specific heat ratio. This results in a delayed LTR reaction, but it does not reduce the amount of heat released or radicals produced. The second effect of the EGR is that the oxygen concentration is reduced. It was demonstrated that the reaction rate during the last part of the HTR phase could be slowed down, when the initial oxygen concentration was near the stoichiometric limit. The benefit of EGR is therefore that it allows late timing of the combustion and a reduction of the LTR combustion. This means that detonation and engine knock may be avoided. It is however on the cost of efficiency, as the IMEP is reduced significantly.

The effect of EGR was demonstrated in at NTSEL in September 2008. Paper II in the appendix describes the outcome of the experiments with EGR.

10.7 List of species

Radicals of hydrogen and oxygen

H	hydrogen atom
O	oxygen atom
H_2	molecular hydrogen
O_2	molecular oxygen
OH	hydroxyl radical
H_2O	water
HO_2	hydroperoxy radical
H_2O_2	hydrogen peroxide

Radicals with one carbon atom

CO	carbon monoxide
CO_2	carbon dioxide
CHO	formyl radical
CHO_2	hydrocarboxyl radical
CH_2O_2	formic acid
CH_2O	formaldehyde
CH_2OH	hydroxymethyl radical
CH_3OH	methanol
CH_3	methyl radical
CH_3O	methoxy radical
CH_4	methane

Radicals with two carbon atoms

CH_3OCH_3	dimethyl ether
CH_3OCH_2	methoxy-methyl
$CH_3OCH_2O_2$	methoxy-methyl peroxide
$CH_2OCH_2O_2H$	[unnamed]
$O_2CH_2OCH_2O_2H$	[unnamed]
HO_2CH_2OCHO	[unnamed]
OCH_2OCHO	[unnamed]
$HOCH_2OCO$	[unnamed]
$HOCH_2O$	[unnamed]

11 Engine acoustics

The third paper in appendix deals with the effect of combustion chamber shape on the combustion noise. Pictures of the piston crowns are found in this paper, as well as the relevant findings. To evaluate the efforts, it was required to measure the sound emitted by the engine accurately, as well as using objective means of evaluating the recorded sound. This section presents the setup used to obtain the data, the data treatment and the evaluation of the data.

11.1 Measurements

The cylinder pressure and the acoustic noise were measured to determine the coherence and evaluate the noise level produced by the engine. This section describes the considerations for these measurements, the data treatment and the presentation of the data.

11.2 Choice of sampling frequency

In general, the highest possible sampling frequency should be applied in any case, to obtain the best possible resolution of the signal and to cover as high a frequency range as possible. If the frequency range is well known, the sampling rate may be set to a value that satisfies the Nyquist criterion of at least two times the highest frequency present.

The cylinder pressure may be sampled based either on an external or an internal sample clock. If the data are collected for a heat release analysis, it required that a crankshaft angle encoder is used as an external sample clock. HCCI combustion is a very fast event and high frequencies are present in the chamber after the combustion. To capture the combustion event and avoid aliasing from the resonant frequencies in the chamber, the sample rate must satisfy the Nyquist criterion. A crankshaft encoder with 3600 pulses per revolution was chosen for this task. The highest detectable frequency then becomes:

$$f_{Nyquist} = \frac{1}{2} f_{sample} = \frac{1}{2} \frac{N[rev/\min] \cdot 3600[samples/rev]}{60[\sec/\min]} = \frac{1}{2} N \cdot 60[samples/\sec]$$

so that at 1200 rpm, the sample rate becomes 72 kHz and the Nyquist frequency becomes 36 kHz. This is considered to be fully satisfactory under normal circumstances, since the frequencies generated are rarely detectable above 20 kHz

Frequencies higher than the Nyquist frequency must however be considered as a potential source of error. When the sampling frequency is inadequate a false frequency is produced in the sampling process, which is called an alias. In cases of strong combustion knock the resonance frequency of the diaphragm of the transducer may become a source of aliasing. The diaphragm resonance frequency is approx. 160 kHz for the Kistler sensor, and 120 kHz for the Optrand sensor. To prevent aliasing an analogue low pass filter must be applied before sampling, to block these resonance frequencies.

If a frequency analysis of the cylinder pressure is to be performed it is advantageous to use a high sample frequency independent of engine speed. This is achieved by using the internal clock of the data acquisition device. This makes the sampling frequency independent of engine speed. A sampling frequency a few times higher than required to satisfy the Nyquist Criterion improves the signal-to-noise ratio considerably, which is advantageous if the high frequency content is to be analyzed. Errors from noise and discrete level sampling that would normally be less significant with a long or infinite sample length are more critical within a finite number of samples. Increasing the sampling rate will therefore reduce the relative significance of such errors.

11.3 Equipment

The acoustic sound was measured with a Bruel & Kjær model 2250 portable sound level meter. The signal from the AC output from the meter was used, since it outputs the instantaneous sound pressure level as measured by the diaphragm. The signal was sampled together with the cylinder pressure. The sound pressure level was measured at a distance of 1 meter in compliance with normal practice.

Figure 13: Position of Sound level meter in test cell

11.4 Handling the confined space acoustic issues

Since reverberation is a major issue in such a small confined and nearly cubic volume as the test cell, a lot of effort was made to reduce the reverberation in the room to an acceptable level. 50 mm sound absorbing plates were positioned on the walls and on the floor to absorb and reduce the reflections of higher frequencies, mainly from 1 kHz and up. Lower frequencies require deeper insulation, but there was no need to reduce these, since they would not be generated by the HCCI combustion and therefore not of relevance to the study.

The microphone was positioned at a distance of approx. 50 centimeters from the wall, with insulation behind it. This should mean that wavelengths shorter than 0.5 m (above

680 Hz) are measured correctly, since they are not reflected behind the microphone, and there is no stagnation pressure due to the microphone being 1 wavelength from the wall.

11.5 Post sample digital filtering

The procedure of converting the collected data into meaningful results requires that undesired frequency content is separated by filtering. Since the data are now discrete, the filtering process must be conducted discretely as well. The main advantage of filtering sample data is that the filter may be adapted to suit the application, and the influence of different filters may be evaluated on the same signal.

11.5.1 Filter methodology

There are two distinct methods of filtering discretely sampled data. One is the Infinite Impulse Response (IIR) which is usually a digital implementation of an analogue filter. The other is the Finite Impulse Response (FIR) which is a purely digital technique. LabView has been the primary tool in this thesis for signal analysis, since it is equipped with a large variety of IIR and FIR filters.

The IIR filter has the same advantages and disadvantages as its analog counterpart. They are designed as analogue filters such as Butterworth, Bessel etc. It is also possible to define the filter order to define the steepness of the filter up to any order. The disadvantage of the filter is that the filter phase response is non-linear, meaning that the various frequencies appearing in the signal will be delayed differently. This will also affect the heat release analysis and particularly any calculation depending on precise knowledge of the pressure such as IMEP.

The FIR filter is a technique that uses a finite amount of input values to calculate the output, rather than specifying a low pass frequency. In short, the filter operates as a moving average on the values. The average is based on the number of samples selected by the user. A sufficient number of samples need to available before the filter is effective, with more samples required for blocking of lower frequencies. The main advantage of FIR filtering is that the phase response is linear, which means that the signal is better preserved after filtering. The filter does however delay the entire signal after filtering.

11.5.2 Filtering of pressure data for heat release analysis

The cylinder pressure data must be low pass filtered to avoid pressure oscillations from distorting the heat release analysis. The best way to find the separating frequency is to compare the unfiltered and the filtered signal and then select a frequency that preserves the pressure gradient from combustion while eliminating the subsequent oscillations.

The heat release analysis is dependant on a linear phase response, since the steep gradient during the heat release will otherwise become less steep. Therefore a FIR filter is preferable. An alternative method to counter the non-linear phase response in the IIR filters is to invert the signal after filtering and then apply the same filter again. This inverts the phase delay as well, and the resulting signal is of a much higher quality than what is obtainable with a standard digital IIR filter. The filter order and type must be identical for the filters. The total filter order is twice the order of the individual filter.

11.5.3 Filtering of sample data for frequency analysis

In the frequency analysis, the frequency content originating from the compression and combustion in the cylinder are not of interest. Neither are the lower frequencies of the acoustic noise. These low frequencies must be blocked so that only the higher frequencies are left. The analysis of frequency content by discrete Fourier transformation (DFT) is however not sensitive to phase delays, so IIR filters are suitable for this purpose.

The high pass frequency for cylinder pressure must be below the lowest resonant mode in the chamber. This frequency is easily identified in a DFT of the unfiltered signal.

The high pass frequency for the acoustic noise can be selected as preferred, but with necessary consideration to the sound field in the room. The acoustic property of a closed test cell generally means that low frequencies cannot be attenuated properly. The frequencies are furthermore not of interest since they are generated by intake and exhaust pulsations as well as engine oscillation. It is therefore necessary to eliminate the frequency content below a certain limit in order to evaluate the sound pressure generated by the engine as a direct consequence of the combustion event. A high pass frequency of 1 kHz was considered appropriate for the current study.

11.6 Representation of acoustic measurements

11.6.1 Sound pressure

The sound pressure is the instant difference between the stationary (atmospheric) pressure and that measured by the deflection of a diaphragm. The unit is Pa or uPa depending on the amplitude of the signal.

11.6.2 Sound pressure level

The sound pressure level (SPL) is measured in decibel. It is a quantity defined by a logarithmic scale.

$$SPL = 20\log\left(\frac{p_{rms}}{p_{ref}}\right) \quad [dB]$$

p_{rms} is the root mean square (RMS) of the sound pressure. The RMS value must be obtained in a short term interval for transient noise. p_{ref} is the reference sound pressure at the threshold of human hearing, 20 μPa. The reference value for acoustic measurements is the threshold of hearing for a normal person.

The handheld device was calibrated with a piston calibrator that accurately produces 1 kHz with a sound pressure of 1 Pa, corresponding to 94 dB. The sensitivity was then determined by measuring the rms value of the AC output signal. The unit for sensitivity is V/Pa.

In many applications, weighting of the frequency content is applied, usually a -weighting, which accounts for the sensitivity of the human hearing. This weighting was

not applied in the analysis, since the noise was in a limited frequency range where the sensitivity of the ear is almost linear.

To compare the measurements of engine noise and the cylinder pressure oscillations, it was decided to apply the definition of SPL to the cylinder pressure as well. The reference for the cylinder pressure SPL was set to 1 Pa, since this gave comparable figures of cylinder SPL and acoustic SPL. The ratio between the reference values corresponds to 94 dB.

11.6.3 Time domain representation

The time domain representation is a simple way to illustrate the amplitude of the noise level in time. In figure 14, the white line (top) illustrates the high pass filtered cylinder pressure oscillations measured with the pressure transducer. The red line (middle) is the acceleration of the engine measured with an accelerometer mounted near the top of the cylinder. The green line (bottom) is the acoustic signal recorded with a microphone 1 meter from the engine. The acoustic signal is advanced in the figure below as correction for the delay caused by the distance between engine and microphone. HCCI combustion occurs at 5 CAD BTDC, after which the pressure oscillations set in.

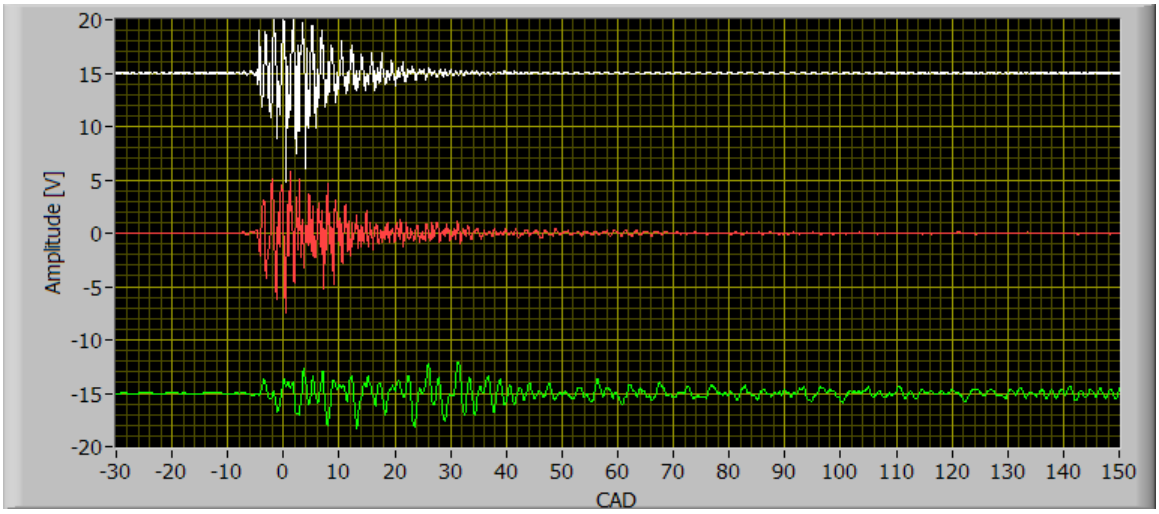

Figure 14: Time domain representation of the cylinder pressure, engine acceleration and acoustic sound pressure

From figure 14 it is seen that the energy from the cylinder pressure oscillations is directly transmitted to the engine structure. The vibration of the engine cause noise with frequencies identical to that of the pressure oscillations to be emitted from the engine, but the majority of the acoustic noise is caused by the engines resonance frequencies which are also excited. The resonance frequencies are however not measured by the accelerometer due to its position near the corner of the engine block, at which point the engine resonance frequencies are weak. The position is however well suited for measuring the directly transmitted frequencies, which is also evident from DFT analysis in the next section.

The SPL of the cylinder pressure, the acceleration level and the acoustic SPL can be calculated in short intervals and presented as in figure 15:

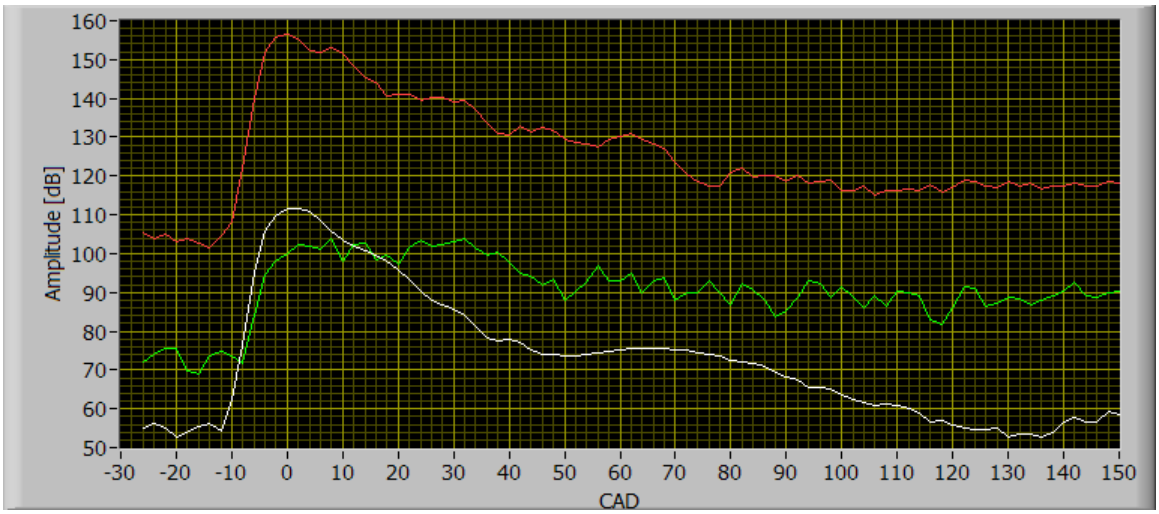

Figure 15: Time domain representation of the SPL of the cylinder pressure, the engine acceleration level and the acoustic sound pressure level

Here the SPL is expressed in dB. The red line represents the cylinder SPL which is seen to increase by more than 50 dB after combustion. The acceleration level (white line) increase by a similar dB value and is generally coherent with the cylinder pressure SPL. The acoustic signal (green line) also increases but remains at a higher level. As mentioned, the acoustic signal originates from the cylinder block resonance which is not properly measured by the accelerometer, and these vibrations are present much longer than the higher frequencies which tend do be attenuated fast.

The time domain representation is useful to show the signal amplitude in time and how it is attenuated. It is however not possible to determine which frequencies are present in the signal. This may instead be visualized in with the frequency domain representation.

11.6.4 Frequency domain representation

To evaluate the frequency content in a discretely sampled signal, a DFT algorithm is used. The specific algorithm commonly applied is called Fast Fourier Transform (FFT).

In the analysis, the frequency range from 0 Hz to the Nyquist frequency is split up into a number of equally spaced intervals. The number of intervals is equal to the sampling frequency divided by the number of samples, so that the frequency resolution becomes:

$$\Delta f = \frac{f_s}{N_s}$$

Usually the number of samples N_s is required to be a power of two (2, 4, 8, 16 etc). It is desired to have a short sample length in which the signal can be considered stationary. The sampling frequency is however very high, which implies that a large number of samples is also required to obtain an acceptable frequency resolution. To limit the sample

time interval while maintaining a high frequency resolution, a short length of samples can be extended with a tail of zero values. This is referred to as zero padding. The zero values do not affect the analysis, so this approach is very useful when a limited sample length must be analyzed.

The FFT algorithm calculates the amplitude of the frequencies in the signal, given by the frequency resolution Δf. The output from the analysis consists of the frequencies and their respective amplitudes, as well as phasing information. A graphic representation is then used to identify the dominating frequencies.

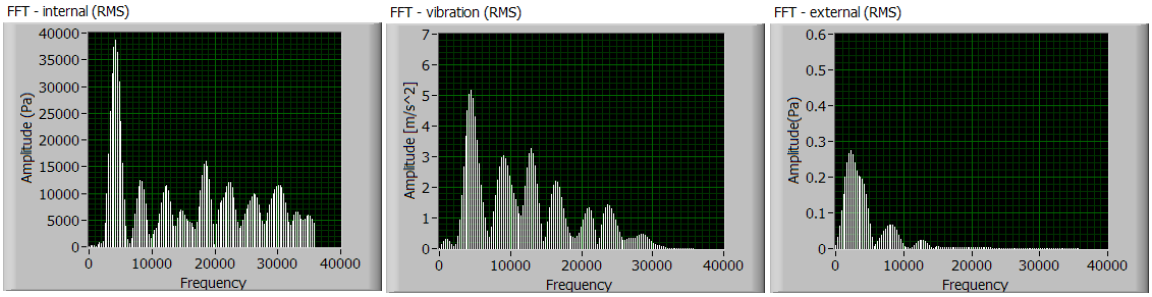

Figure 16: FFT representation of cylinder pressure, engine acceleration and acoustic noise

The particular set of data used in figure 16 illustrates that although a range of high frequencies are dominating the cylinder pressure signal as well as the accelerometer signal, the majority of the sound pressure is caused by frequencies from 1-3 kHz, which is the engine resonance frequencies.

The disadvantage of the frequency domain representation is that the frequency content changes in time. The graphs can therefore represent either a small time step of the time domain accurately, or a larger time step less accurately, based on an average value. The only way to represent the development in frequency content is to use a frequency spectrum analysis.

11.6.5 Frequency spectrum analysis in the time domain

A frequency spectrum chart is suitable for studying the frequencies in the time domain. The frequencies can be displayed in the time domain by splitting up the signal into small overlapping intervals and apply the FFT procedure on each interval. The output of the analysis is an intensity chart with three dimensions: time on the x-axis, frequency on the y-axis and amplitude on the z-axis. The plot can be made in three dimensions, but the z-values are here defined by a color scale to make the plot two-dimensional. To create these charts, a 256 sample length windowed section of the high pass filtered signal is analyzed by FFT. This is done in an interval progressing one CAD with each iteration.

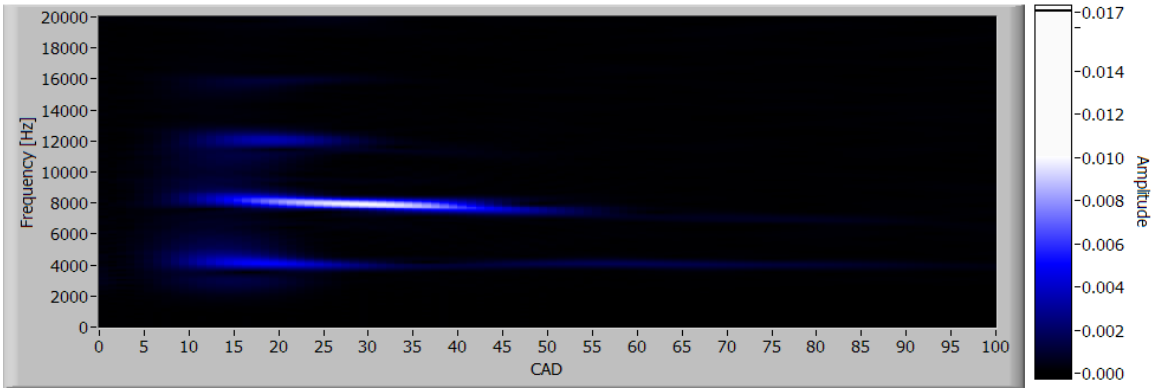

Figure 17: Intensity chart for cylinder pressure oscillation

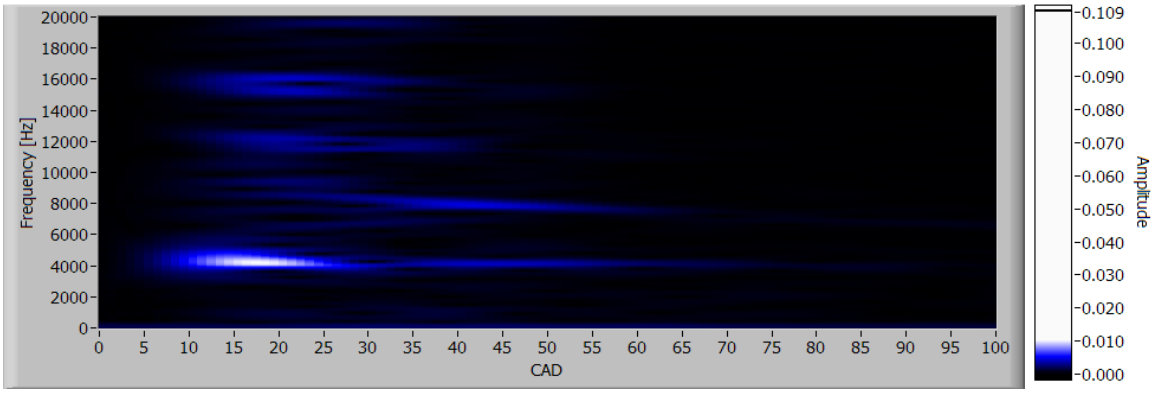

Figure 18: Intensity chart for engine acceleration

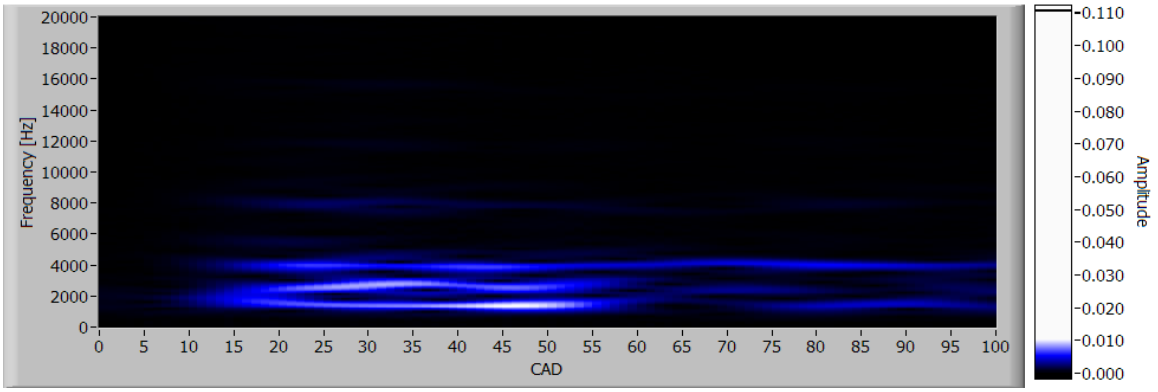

Figure 19: Intensity chart for engine acoustic noise

The intensity spectrograms (fig. 17-19) are created from data collected with the ring shaped chamber geometry. The plots reveal that the same frequencies are present in the cylinder and the surface. The acoustic noise show some indications of the strong 8 kHz tone in the cylinder, but the 4 kHz tone appears to be transmitted better. The frequencies below 4 kHz in the acoustic noise are the engine resonance frequencies. These are seen to be quite strong compared to the directly transmitted frequencies.

11.7 Theory of cylinder acoustics

Cylinder pressure oscillations are initiated by the strong pressure gradients formed when the combustion proceeds unevenly in the chamber. The pressure gradient may be created by a confined explosion in the charge due to spatial variation in fuel or temperature distribution, or a developing detonation, which are discussed in the next chapter.

Once a pressure difference is introduced, the pressure will drive the gas towards the low pressure area. The momentum of the gas means that the gas will continue into the low pressure region even after pressure equalization, thereby increasing the pressure to that of the former high pressure region. The pressure distribution is now reversed and the gas will be forced back to its origin. This behavior is known as resonance.

Established resonance modes in the cylindrical geometry fall in to three categories: circumferential modes, radial modes and axial modes. These are explained in the following subsections. The modes may appear simultaneously by the principle of superposition as shown in table 5.

11.7.1 Circumferential modes

If the charge is pushed from one side of the cylinder wall it will oscillate across the chamber in a transverse motion. This situation is equivalent to pushing a glass of water, which forces the water into moving from side to side. The first mode has one node which runs through the diameter of the cylinder. All of the fluid moves from the low pressure to the high pressure zone across the chamber. This mode is therefore the most powerful in terms of momentum transport.

The second mode has two nodes that are orthogonal and hence two high pressure zones that must be opposite. The gas does not move across the two symmetry lines. The gas movement takes places from the sides of the high pressure zones to the sides of the low pressure zones. In this case the gas movement is split into four directions. This means that less energy is transported across the chamber and hence less energy is transferred to the walls by momentum and heat transfer. So, despite being measurable in the chamber, this mode is less important in terms of energy losses and transmitted sound.

11.7.2 Radial modes

If the pressure rises in the center (or throughout the entire perimeter simultaneously) it will create a radial wave moving from the center towards the cylinder liner. This corresponds to the familiar rings that form when a drop of water hits the surface of a water pool. Like in a glass of water, the wave is reflected back towards the center.

The first mode of vibration has a high and low pressure zone and a circular node. The higher nodes that may be formed have more pressure zones in the same ring pattern. As with the transverse waves, only the lowest mode carries enough momentum to be important.

11.7.3 Axial modes

Axial waves are planar waves that move in the axial direction They may be calculated with normal wave theory. They are however not relevant since the axial space is usually very limited and pressure gradients are therefore not likely to occur.

11.8 Calculation of resonance frequencies

The natural frequencies of a cylindrical chamber can be calculated as [23]:

$$f_{m,n,p} = c\left[\left(\frac{\alpha_{m,n}}{B}\right)^2 + \left(\frac{p}{2L}\right)^2\right]^{1/2}$$

The modes of vibration are the circumferential (m), radial (n) and axial (p), which are natural numbers. C is the local speed of sound, B is the bore of the engine and L is the axial distance. Since the axial distance at TDC is very small for most engines the axial modes are not relevant, since the frequencies are too high to be excited. Therefore only the circumferential and axial modes are of interest. Thus, the equation simply becomes

$$f_{m,n} = c\frac{\alpha_{m,n}}{B}$$

Where

$$c = \sqrt{R\,T\,\gamma(T)}$$

The term $\alpha_{m,n}$ denotes the solutions to the Bessel function of the first kind. These solutions are given in table 5 for the cylindrical case. The speed of sound c is dependant on temperature and specific heat ratio. The specific heat ratio γ is determined by the gas composition and temperature.

Table 5: Mode shapes and factors for the cylindrical chamber

Mode	1,0 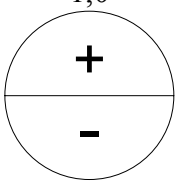	2,0 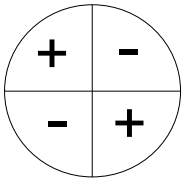	0,1 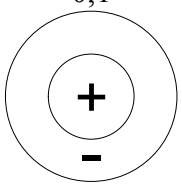	3,0 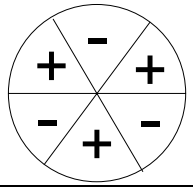	1,1 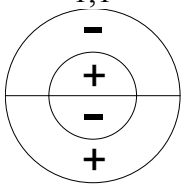
$\pi * \alpha$	1.84	3.054	3.832	4.201	5.332

11.9 COMSOL calculations of cylinder acoustic resonance

The simulation software COMSOL is capable of calculating resonance frequencies in any given cavity. This allows the resonance frequencies of irregular combustion chambers to be determined. To perform this calculation for a given chamber, the only information necessary is the temperature and the gas composition. Using air as gas at a temperature of approx. 1800 K will provide a good approximation for HCCI combustion.

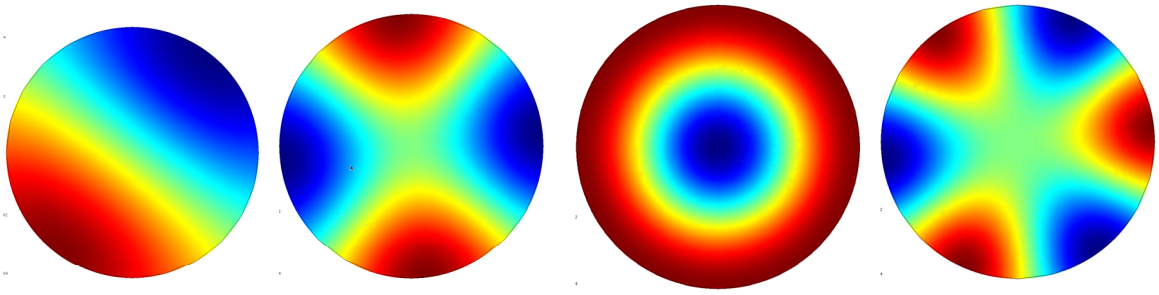

Figure 20: The first four resonance modes in a disc shaped geometry

In figure 20, the four resonance modes with the lowest frequencies are shown. From left, he first circumferential mode (1,0), the second circumferential mode (2,0), the first radial mode and the third circumferential mode.

Figure 21 shows an example of calculated resonance frequencies in the ring shaped geometry, with the piston in the TDC position. This calculation was used to verify that the frequencies measured with this particular geometry were in fact caused by resonance, as well as identifying the modes.

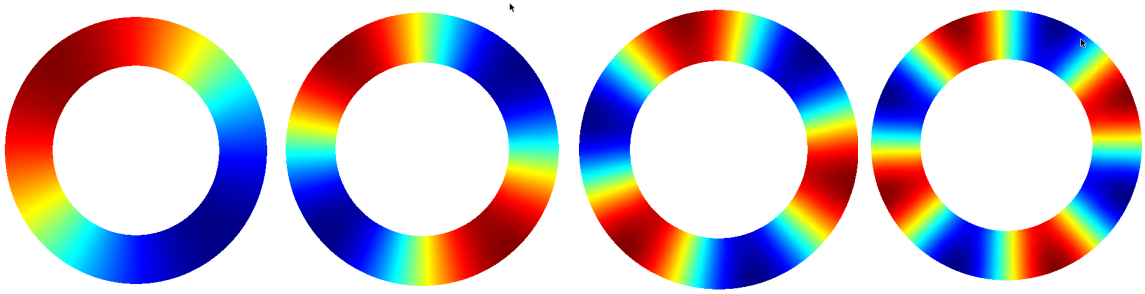

Figure 21: The first four circumferential resonance modes in a ring shaped geometry.

The frequencies of the modes in fig. 21 are (from left to right): 3.9 kHz, 7.8 kHz, 11.7 kHz and 15.5 kHz. The higher frequencies are overtones (multiples) of the first mode, as a consequence of the similarity with resonance in a tube. The first four circumferential resonance modes were all found to be present in the measurements, and higher predicted modes with frequencies of approx. 20 kHz and 24 kHz were also present at detectable amplitudes. The first radial and axial modes should have frequencies of approx. 28 kHz, but this frequency was hardly distinguishable from the noise level in the FFT analysis.

A case was set up to make a brief study on the piston crown with 7 hemispherical sub chambers (fig. 22). It is important to note that it was required to have a distance of 1 mm to the cylinder head, in order to avoid interference with the valves. This distance is likely of great importance, since eliminating it would result in completely separate chambers at TDC which would make resonance impossible. With the 1 mm gap it was however expected that resonance would occur across the chamber. This was also confirmed in the experiments.

Figure 22: Piston crown with 7 hemispherical chambers

The result from the COMSOL analysis (fig. 23) was that the resonance modes are quite different from the cylindrical case. The lowest resonance frequency is at 3.7 kHz, and the next two modes are in a narrow frequency range around 6 kHz as well as the first radial mode. The next circumferential mode displayed is however at 18 kHz and is therefore not likely to become exited.

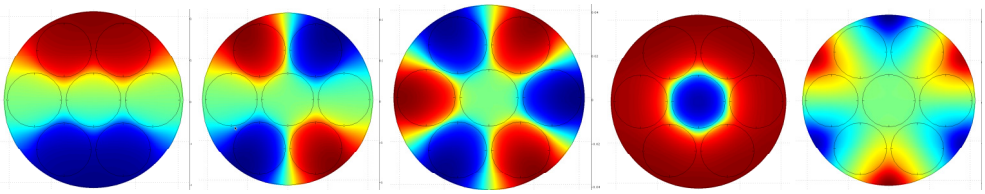

Figure 23: Resonance modes of 3.7 kHz, 5.6 kHz, 6.5 kHz, 6.9 kHz and 18 kHz

It was found that the gas will oscillate between the chambers when these are connected by a small gap. This behavior is known as Helmholtz resonance. The cross section area of the gap connecting the volumes restricts the flow of gas between the chambers, thereby reducing the frequency of the oscillation at TDC. With the piston some distance away from TDC the oscillation modes and frequencies will change to look more like the cylindrical case, as the restriction becomes less significant and the geometry changes towards a normal cylinder.

12 Simulation of detonation phenomena

This chapter deals with the physical phenomena called detonation, which can cause strong pressure pulsations in HCCI combustion.

The first section contains a theoretical description of detonations, which is implemented in a model that can predict stationary detonation wave properties.

The second section deals with a study that was setup to investigate if a CFD model is capable of capturing the detonation event.

The last section describes an experiment that was setup to study detonation waves in HCCI combustion. The presence of strong shock waves was shown, which indicate the presence of detonation waves as well.

12.1 Background

The HCCI engine is operated with a nearly homogeneous charge. Therefore, an ideal HCCI combustion should progress as a control volume explosion. This would result in a relatively high pressure rise rate, but pressure gradients should not occur during combustion. When HCCI combustion is intiated in an engine at lean conditions, it is usually observed that combustion does indeed take place without introducing large pressure gradients, which are indicated by pulsating pressure. The reason is that piston and valves are cold, and hence the charge is not subjected to hot surfaces that may introduce temperature gradients. When the piston and valves are heated up the combustion changes and combustion knock increases. This is due to the temporal and spatial variation in reaction rate, which causes high amplitude pressure waves to propagate inside the cylinder. In the more extreme cases these pressure waves may develop into detonations similar to those that cause SI engine knock.

It is important to note that flame propagation cannot be the cause of these pressure oscillations, since normal flame propagation does not create pressure waves. Besides, flame propagation is very slow at lean conditions and will not be able to consume the charge in the short time span typical of HCCI combustion.

Explosions may be responsible for amplification of pressure waves, as will be argued in the following. The nature of such waves is that they will be acoustic of nature, meaning a limited pressure gradient and amplitude.

Detonations, although only in a partly developed stage, are characterized by supersonic propagation of a steep pressure wave of large amplitude. These may be the explanation of some cases of HCCI engine knock, in particular when the amplitude of the pressure oscillations is large. The best indication of a detonation is the measurement of a pressure increase so fast that it is not consistent with normal acoustic waves created by explosions. An acoustic wave will appear as a slow harmonic increase in pressure, while a detonation wave will appear as an instantaneous pressure increase, likely within to data samples.

The way explosions and detonations may result in pressure osciallations is described in the following sections.

12.2 Explosions

12.2.1 Uniform explosion

An explosion is defined as a fast, uniformly progressing chemical reaction in a perfectly stirred volume of reactants. The rate of reaction is thus governed solely by chemical kinetics. An explosion in a confined space with no volume change is referred to as a constant volume explosion, whereas an explosion in unconfined space which do not lead to a pressure increase is called a constant pressure explosion. In HCCI combustion, only constant volume reactions are relevant since the volume change is very limited during combustion.

An ideal constant volume explosion creates a spatially uniform pressure increase without gradients in pressure or temperature. Real explosions however are rarely ideal, so some spatial and temporal variation usually occurs in the reacting volume, but the overall picture is still that the volume has exploded.

12.2.2 Non uniform explosions and pressure wave amplification

Under some circumstances, such a locally elevated temperature or higher fuel concentration, the explosion will develop faster and thus become a local event in the reacting volume some time before the remaining volume reaches the same rate of reaction. This will result in the exploding volume expanding, and the partly reacted volume being compressed adiabatically. The subsequent reaction in the compressed volume will then be progressing faster, but not necessarily fast enough to complete while the pressure is high.

If the remaining charge explodes while pressure is high it will result in a compression wave with a higher peak pressure than that created in a uniform explosion. This could be an explanation to some situations with large pressure oscillations [24].

It should be noted that the lowest frequency of a standing wave is approximately 5 kHz in a chamber 85 mm across, as given by acoustic theory in the previous chapter. Hence the major part of the heat release must occur within less than 0.2 ms in order to amplify the incoming wave, and ideally peak during the stagnation of the pressure wave. This is a very short time span given the circumstances. Therefore, increasing the time where the pressure is high will also increase the chances of the heat release amplifying the pressure wave properly.

During the tests with piston crowns it was found that the piston crown with 4 chambers formed between piston and cylinder liner gave very large pressure oscillations. This chamber has a resonance frequency of 3.5 -4 kHz due to its Helmholz resonance characteristic. It is plausible that the lower resonance frequency with this piston crown

provided more ideal conditions for amplification of compression waves going from a chamber with explosion to the other chambers with a less progressed reaction.

12.3 Detonations

12.3.1 Introduction

Detonation experiments are usually carried out with gas mixtures at atmospheric conditions in long tubes. These conditions are clearly different from those within combustion engines, in which initial conditions are a high pressure, temperature and a partially reacted gas. Another important difference between detonations in laboratory and combustion engines is that while the first requires a distance measured in meters to form a detonation, the avaliable distance is less than ten centimeters in a normal sized engine.

In an SI engine, the compressed charge is burnt at a temperature considerably higher than its auto ignition temperature. Reactions therefore progress at a very high rate once enough radicals are produced. If the combustion timing of the engine is too early, the temperature in the unburned region will become too high for the fuel to resist auto ignition. This leads to engine knock, which is the common name for detonation. A typical outcome of engine detonation is critical engine failure, such as melting of the piston.

The conditions in SI combustion engines therefore seem to be ideally suited for development of detonations. It is however less certain if HCCI combustion can result in the development of a detonation as well. It may be that detonations develop slower in HCCI combustion and therefore are not as easily recognized as SI engine detonations.

Whether detonations are possible or not in HCCI combustion cannot be determined theoretically. Apart from very well controlled experiments, the best way to get a better understanding of detonations is to make simulations. Here, CFD has been chosen to model constant volume combustion with variations to the intial conditions, with the purpose of seeing if detonations will develop in the simulation.

Before the CFD approach is described, the basic theory for detonations is explained. The equations and theory in the following sections are developed from thermodynamic considerations only, by several researchers in the past century. Perhaps the most fascinating fact about detonations is that the properties, such a propagation speed and pressure increase, can be predicted with very high accuracy. In essence, the conservation equations for a control volume and a chemical equilibrium is all that is required to determine the exact speed of a detonation wave.

The main source used here is the book “Combustion” by Irvin Glassman [25]. Only the essentials for understanding the phenomena has been included, since many derivations are required to reach the usable equations. Sources focused on shock tube experiments include those by John Bradley [26] as well as Edward Greene and J. Toennies [27] .

Another useful source aimed towards computational modelling of detonation phenomena are some articles by Browne, Ziegler, Shepherd and Kao [28 , 29]. These describe a numerical approach to detailed modelling of detonation waves.

The last part of the chapter includes some observations of the cylinder pressure under knocking conditions. These are analyzed in order to determine if the cylinder pressure variations are caused by detonation

12.3.2 Detonation waves

A detonation is composed of a shock wave closely followed by a reaction wave. The shock wave and the reaction wave are dependant on each other. The shock wave cannot sustain its velocity and sharp pressure gradient without the energy from the reaction wave. The reaction wave can only exist in the wake of the shock wave due to the highly elevated temperature which comes from the adaibatic compression.

The concept of a shock wave is in itself a complicated subject. The theory of shockwaves is given in the following section in a way that allows for detonation theory to be added subsequently.

12.3.3 Shock wave

A shock wave is a compression wave that propagates at supersonic velocity. An example of such a wave is the one which is created by airplanes that move at supersonic velocity. The acoustic waves that are normally propagating ahead of the plane are intercepted when the air plane reaches sonic velocity. The waves are super positioned into a high amplitude shock wave, which is characterized by a very steep pressure increase. As the airplane increases its velocity to supersonic, the shock wave also becomes supersonic.

The same principle applies in gaseous and solid matter detonations; the difference being that the driving force is not an object but a chemical reaction behind the wave, which sends pressure waves towards the shock front.

12.3.4 Reference for velocitities

The first step is to establish a reference frame for the conservation equations. Figure 24 illustrates how velocities are defined relative to the shock front and the upstream gas, respectively.

When the shock wave is considered stationary, gas is streaming into the front at the velocity $-u_1$ and out at $-u_2$. The velocities are negative since they are opposite to the direction of the travelling wave.

When using the stationary gas as reference, the wave is seen as moving into a gas which is quiescent before the wave arrives. By adding the wave velocity u_1 to the stationary wave reference velocities, the velocity u_1 now represent the wave propagation velocity into the gas, and the difference $u_1 - u_2$ is the velocity of the gas exiting the wave. Since u_1 is greater than u_2 this difference is positive, meaning that the velocity of the gas is

positive in the x- direction. As the gas follows the shock wave this keeps the pressure and density high after the shock.

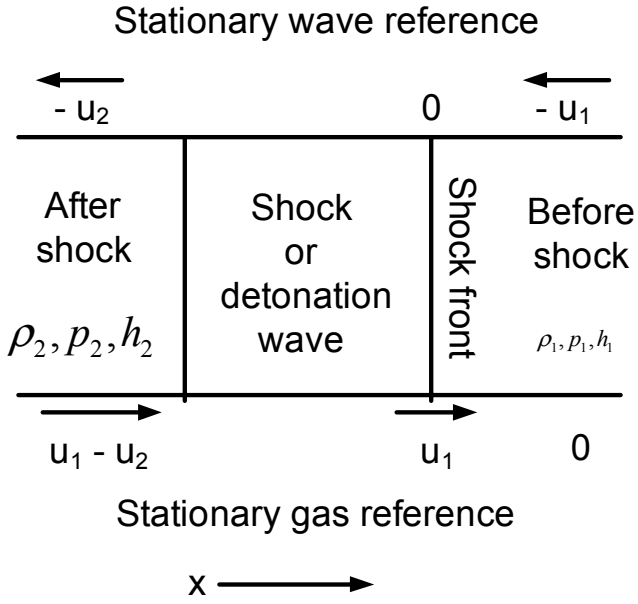

Figure 24: The reference frames for velocities in shock waves

A sketch of the pressure and temperature distribution in a shock wave is given in figure 25. The pressure rise at the front of the wave is very discontinuous, whereas the following expansion is continuous as an acoustic wave. In the figure the pressure decreases back to its original value since there is no chemical heating of the gas. In a detonation wave, the reactions behind the wave will however increase the pressure and temperature behind the wave.

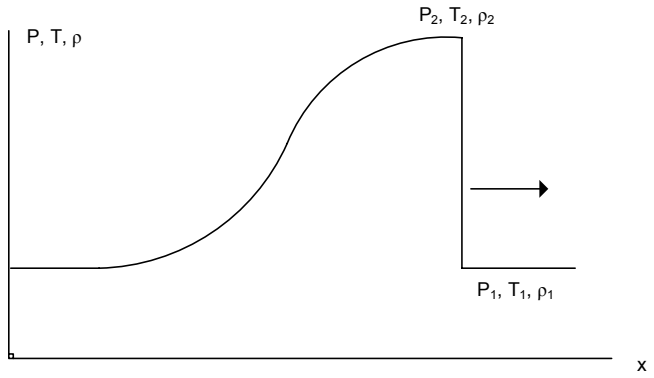

Figure 25: Pressure in a shock wave

Density, pressure and enthalpy are given before the shock and may be determined after the shock. In the following, density and specific volume are used as appropriate to get the simplest expressions.

12.3.5 Conservation equations

In the theoretical treatment of the wave it is regarded as a control volume. What happens in the shock or detonation wave is not of interest in the theoretical treatment, only the states before and after.

The shock wave is now regarded as being stationary within a control volume as defined by figure 24. The conservation laws for the control volume are as follows:

Conservation of mass:

$$(1) \quad \rho_1 u_1 = \rho_2 u_2$$

Conservation of momentum:

$$(2) \quad P_1 + \rho_1 u_1^{\,2} = P_2 + \rho_2 u_2^{\,2}$$

Conservation of energy:

$$(3) \quad h_1 + \tfrac{1}{2} u_1^{\,2} = h_2 + \tfrac{1}{2} u_2^{\,2}$$

The enthalpy is defined as:

$$(4) \quad h \equiv c_P T + h^\circ$$

where h° is the standard enthalpy of formation. In case of changes in the chemical composition due to chemical reactions the heat release is defined as:

$$(5) \quad q = h_1^\circ - h_2^\circ$$

q is zero in a shock wave without heat release or dissociation, which means that the enthalpy can be calculated from temperature alone.

12.3.6 The Rayleigh relation

By combining the equations for mass and momentum a relation for P_2 as function of the specific volume v_2 is formed:

$$(6) \quad p_2 = p_1 - \rho_1^{\,2} u_1^{\,2} (v_2 - v_1)$$

This relation is called the Rayleigh relation. It is universally applicable to both reacting and non-reacting flows since the equations do not hold any term for energy. Given a set of initial conditions (P_1, v_1 and u_1) the relation can be plotted as a straight line in a p-v plot as in figure 26.

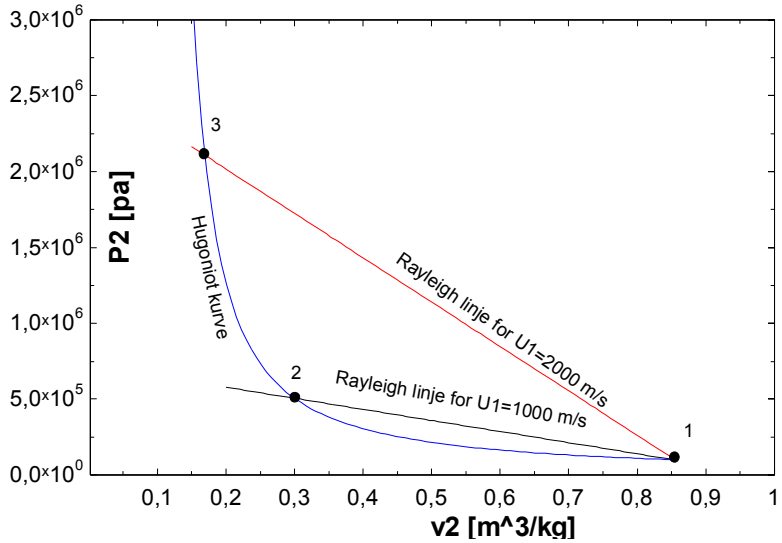

Figure 26: Rayleigh lines for shock waves at 1000 and 2000 m/s intersecting the Hugoniot line

The slope of the line also indicates the speed of the wave, since it may be written as:

$$(7) \quad \frac{p_2 - p_1}{v_2 - v_1} = -\left(\frac{u_1}{v_1}\right)^2 = -\left(\frac{u_2}{v_2}\right)^2$$

12.3.7 The Hugoniot relation

The third conservation requirement may be rewritten to include the pressure:

$$(8) \quad h_2 - h_1 = (p_2 - p_1)\frac{(v_2 + v_1)}{2}$$

This expression is called the Hugoniot relation. It includes the change in enthalpy, which in case of heat release determines the vertical position of the plot in the *p-v* diagram. In non-reacting shock waves with no change in standard enthalpy the relation is referred to as the *Shock adiabat.*

A solution to the Hugoniot relation has been plotted in figure 26, using the same reference point (1) as the Rayleigh lines. The intersections between the Rayleigh lines and the Hugoniot curve mark the specific solutions to the two velocities. It is noted that a shock velocity of 1000 m/s results in a pressure increase five times the original pressure, whereas 2000 m/s results in a pressure increase 20 times the original pressure.

Figure 27 illustrates the Rayleigh and Hugoniot relations as well as the various solution regions I - V. The plot has been constructed in EES using typical conditions for HCCI.

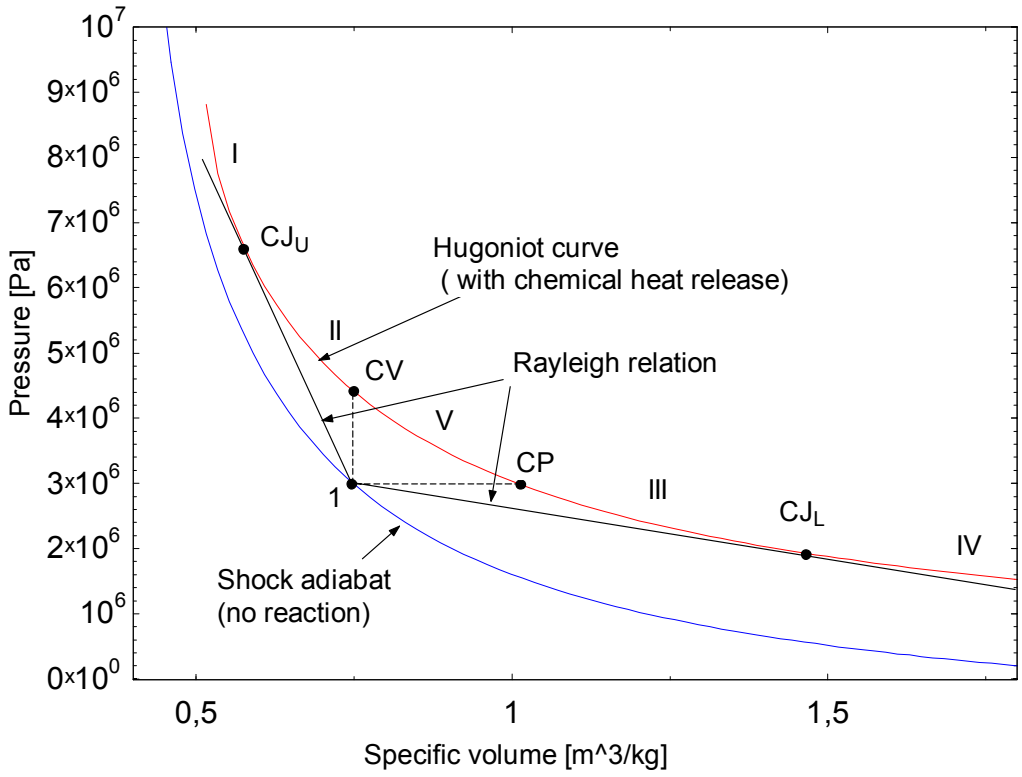

Figure 27: The various solutions to the Rayleigh and Hugoniot relations

Point 1 is the initial condition, here set at a pressure of 30 bars and with a specific volume of 0.75 [m^3/kg]. The straight lines extending from point 1 are selected Rayleigh lines. These lines intersect the Hugoniot curve at the locations CJ_U (upper Chapman Jouget condition), CV (constant volume explosion), CP (constant pressure explosion) and CJ_L (lower Chapman Jouget condition).

The shock adiabat is the range of solutions that satisfy the Hugoniot relation when the enthalpy of formation does not change. Both compression waves and expansion waves are possible, but only compression waves are relevant to detonations.

Solutions in regions I and II are termed weak and strong detonations respectively. It can be shown that solutions in region I are possible but unstable, since the wave speed is sub sonic with respect to the post shock condition. Solutions in region II are not possible, since the solutions in region I are reached first. The only stable solution possible for detonations is therefore the upper Chapman Jouget point, CJ_U. At this point the wave speed is exactly sonic with respect to the post shock condition. The wave speed is termed the Chapman Jouget velocity.

Solutions III and IV are termed weak and strong deflagrations respectively, which is flame propagation at subsonic speed. Deflagrations are not of interest and will therefore not be discussed. Finally, solutions in region V are not possible, as the Rayleigh line can not pass through this section.

A detailed drawing of the pressure and temperature distribution inside a detonation wave is given by the ZND (Zeldovich, Neumann and Döring) model. Typical ratios of the properties in a stoichiometric detonation at atmospheric conditions are illustrated.

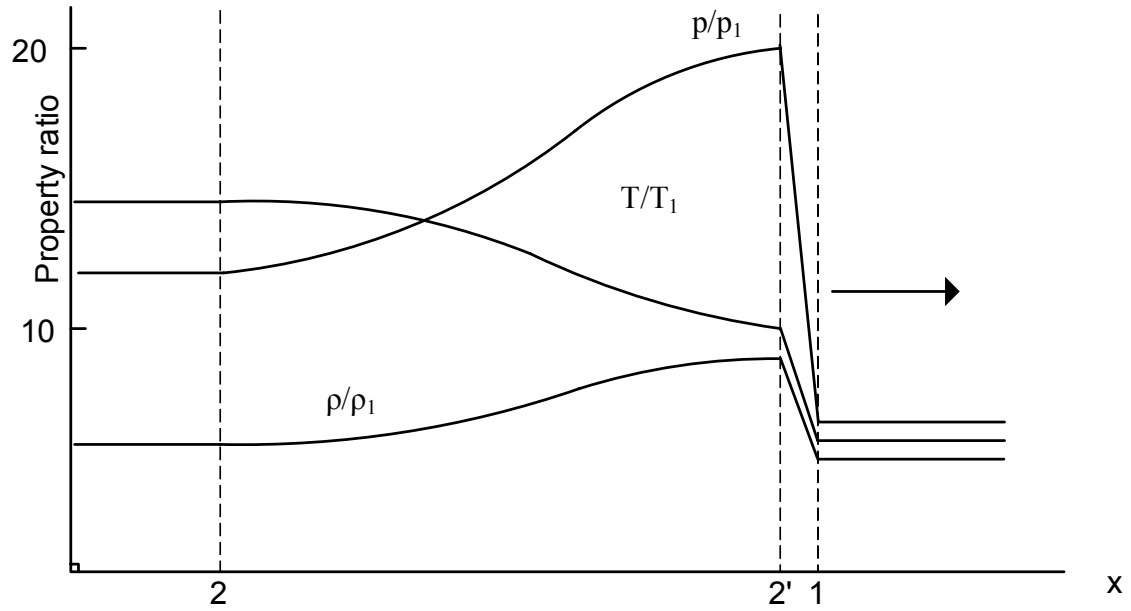

Figure 28: The pressure, temperature and density distribution in a detonation wave

In figure 28, position 1 represents the front of the shock wave, which goes into an undisturbed quiescent gas.

Position 2' is the pressure peak of the shock wave for which the properties are determined by the simultaneous solution of equation 6 and 8, with no chemical energy release.

Position 2 is the conditions after shock and detonation wave, which correspond to the upper Chapman Jouget point. The properties are determined by the simultaneous solution of equation 6 and 8, this time with the chemical energy release.

The decrease in pressure and density after the shock is a result of the decompression following the wave. The decompression is however not to the same pressure as before the wave, since chemical reactions now increase the temperature and therefore also the pressure. The density also increases slightly.

It should be noted that the decompression (rarefaction) of the wave continues after point 2. Since energy must be conserved for the reacted volume, the higher pressure and temperature in and near the wave must therefore result in a pressure and temperature lower than that of a constant volume explosion some distance behind the wave. The material in [] describes the procedure for calculating the properties of the rarefaction wave.

12.3.8 Determination of the Chapman Jouget velocity

The derivations leading to the expressions in this section are too extensive to be explained, so the expressions are given as final results of these derivations. Please refer to Glassman [25] for explanations and derivations.

Due to the convenience of built in functions for determination of all properties required (internal energy, density and specific heats) as well as being a numerical solver, EES was considered an ideal tool for this problem. The following equations constitute the basis for solving the detonation problem. The entire set of equations implemented in the EES model is found in appendix.

The initial conditions required are the pressure, temperature, density and internal energy of the gas:

$$p_1 = 2400000 \quad [Pa]$$

$$T_1 = 726 \quad [K]$$

$$(9) \quad \rho_1 = \left(\sum x_i \rho_i\right) MW_1 \quad \left[kg/m^3\right]$$

$$(10) \quad e_1 = \frac{\sum x_i e_i}{MW_1} \quad [kJ/kg]$$

x_i is the mole fraction of the individual species with density ρ_i (kmol/m^3) in the unburned gas. MW_1 is the average molar weight of the gas. Hence ρ_1 is the average density, and e_1 is the average internal energy.

The model is setup assuming a non-reacted gas. The initial conditions may however change if the gas is partly reacted. In that case the mole fractions must be set according to the composition assumed, and the temperature and pressure adjusted as well. EES does not have the capability to look up internal energies for radicals, so if the gas composition has a large amount of radicals then other means of determining the internal energy must be used.

The post detonation conditions require simultaneous solution of the average internal energy e_2 in the burned gas and the temperature T_2, since these depend on each other. The two equations required are 11 and 12. The specific heat ratio after the detonation is also required and is calculated in eq. 13:

$$(11) \quad e_2 - e_1 = ½ \frac{R \cdot T_2}{\gamma_2 \cdot MW_2} \quad [kJ/kg]$$

$$(12) \quad e_2 = \frac{\sum x_i e_i}{MW_2} \quad [kJ/kg]$$

$$(13) \quad \gamma_2 = \frac{\sum x_i cp_i}{\sum x_i cv_i}$$

In the expressions above, e_2 is the internal energy, R is the universal gas constant, 8314 J/kmol-K, T_2 is the temperature, γ_2 is the specific heat ratio, MW_2 the average molar mass, c_p is the heat capacity at constant pressure and c_v is the heat capacity at constant volume. Subscript 2 refers to post detonation conditions.

The internal energy e_2 depends on the chemical composition of the combustion products. A first guess on chemical composition can be made by finding the chemical equilibrium for a constant volume explosion in CHEMKIN.

The CHEMKIN reactor is initialized with conditions that match the conditions in the cylinder at a compression ratio of 10. An adiabatic compression results in a pressure of 24 MPa and a temperature of 726 K. The initial gas composition is calculated from an equivalence ratio of 0.33.

The resulting temperature from the CHEMKIN run is around 1800 K and the pressure around 6 MPa. This temperature results in negligible dissociation, hence complete combustion products are assumed. For higher combustion temperatures dissociation will however be more significant, and the full range of equilibrium products must be included in the calculations of internal energy.

With proper guess on the mass fractions of species (in this case complete combustion products) after the detonation, the internal energy and specific heat ratio may be determined. The temperature T_2 is now found by iteration in EES. It is required that the guess for T_2 is close to the final value for the solution to converge. It was found that the best way to find the correct temperature was to insert a temporary error variable in equation (5) and then find its minimum through parametric variation of T_2.

T_2 is found to be approx. 1989 K. The pressure is then determined from the following expression:

$$(14) \quad p_2 = \mu \frac{MW_1}{MW_2} \frac{T_2}{T_1} p_1 \quad [Pa]$$

The constant μ is defined as:

$$(15) \quad \mu = \frac{\gamma_2 + 1}{\gamma_2}$$

γ_2 was found previously. μ has a value close to 1.8 if the detonation takes place in air.

Solving equation 14 gives a pressure of approx. 12 MPa.

It is required to evaluate the chemical composition once again at the new temperature and pressure, since dissociation may have become significant. The new equilibrium calculation is performed as a constant volume reaction in CHEMKIN. The reactor is initialized with the new temperature T_2, pressure p_2 and the complete combustion products. At equivalence ratio of 0.33 it is found that it still reasonable to neglect

dissociation and hence assume complete combustion product composition. This keeps the subsequent calculations simple.

At this stage the post detonation conditions have been determined. What remains is the detonation velocity. It is found from equation 16:

$$(16) \quad u_1^{\,2} = \mu^2 \cdot \frac{\gamma_2 \cdot R \cdot T_2}{MW_2} \quad \left[\left(\frac{m}{s}\right)^2\right]$$

u_1 is the velocity of the wave relative to the (stationary) reactants. The square is used to avoid numerical issues in the solver, since the velocity is negative. To determine the velocity of the products relative to the wave, equation (1) is used. The density after combustion is calculated as:

$$(17) \quad \rho_2 = \sum x_i \rho_i MW_2 \quad \left[kg/m^3\right]$$

hence the velocity may be determined as:

$$(18) \quad u_2 = \frac{\rho_1}{\rho_2} u_1 \quad \left[(m/s)\right]$$

An important property of the post detonation speed is that its mach number should be very close to unity. The velocity of the burned gas is exactly sonic at the CJ point, but subsonic between the shock front and the CJ point. This means that the pressure increase from the combustion shortly after the wave may propagate towards and reach the shock front, thereby reinforcing it by superposition. The pressure waves can not pass the shock front however, since the wave is moving at supersonic speed into the upstream gas. This means that conditions upstream are not affected by the approaching shock.

The speed of sound of the wave is calculated for the reactant state, and the speed of sound after the wave is calculated for the reacted state:

$$(19) \quad c_1 = \sqrt{\frac{R}{MW_1}\gamma_1 T_1} \quad \left[(m/s)\right]$$

$$(20) \quad c_2 = \sqrt{\frac{R}{MW_2}\gamma_2 T_2} \quad \left[(m/s)\right]$$

The mach numbers are then calculated:

$$(21) \quad M_1 = \frac{u_1}{c_1}$$

$$(22) \quad M_2 = \frac{u_2}{c_2}$$

The mach number of the combustion products serves as a useful check of the model validity. If all calculations are correct, M_2 should be quite close to unity. M_1 depends strongly on the gas composition, but should be between 2 and 3.5 in atmospheric air.

12.3.9 Results for the stationary solution

The problem was solved in EES with initial conditions corresponding to adiabatic compression at a compression ratio of 10. An equivalence ratio of 0.33 was used, since this usually results in extensive knocking. The properties of ethanol were used for DME in the calculation, since the properties of DME are not available in EES. The heating values are comparable and the chemical composition identical.

The most important results from the calculation are listed in table 6 and 7.

Table 6: Comparison of properties after an explosion and a detonation

State	Initial conditions	Constant pressure explosion (CHEMKIN)	After detonation (EES calculation)
Temperature	726 K	1800 K	1989 K
Pressure	2.4 MPa	6 MPa	12 MPa
Specific volume	0.086 m^3/kg	0.086 m^3/kg	0.048 m^3/kg

Table 7: Calculated velocities and Mach numbers in a detonation

Velocities	
Wave velocity, relative to chamber	1533 m/s
Mach number of wave, relative to chamber	2.92
Burned gas velocity, relative to wave	860 m/s
Mach number of burned gas, relative to wave	1.0004

The mach number of the burned gas is 1.0004 which is quite close to the desired value of exactly 1. It is a very acceptable result which indicates that the equations are correctly implemented.

The post detonation conditions indicate that the pressure wave should be clearly discernible from an explosion. The highest pressure that may be developed by an explosion is 60 Bar, whereas the pressure after a detonation will be twice that. Not calculated here is the peak pressure of the shock front, which will be even higher than the post shock pressure.

12.4 Detonation study in CFD

In the preceeding theoretical detonation model, the problem of initiation and development of a detonation was not considered. The fact that detonation studies take place in tubes of several meters of length makes it relevant to question whether a detonation can develop at all within less than 10 centimeters.

For SI engines it is however a well established fact that detonations occur in the end gas region, which has an extension of a few centimeters only. The detonations can be of such magnitude that the piston melts or breaks. The question is if lean HCCI combustion is capable of developing into a detonations as well, since less chemical energy is available in lean combustion.

These questions are hard to answer from engine experiments due to the lack of control in critical parameters as well as no real means of local measurements , so it was decided to experiment with simple CFD models in order to see if detonations would appear in the simulations.

12.4.1 Problem setup in STAR-CD

It was considered for some time to make a steady state solution to the detonation problem. This would show if the numerical solution was comparable to the theoretical model. Solving the problem as steady state with the wave being fixed in the solution domain was however found to be quite complicated. It required that the flow was initiated as supersonic with the pressure gradient of the shock wave predefined in the volume, in order to start the chemical reactions that support the shock wave. It was considered possible, but most likely very difficult to set up a model for such a flow.

A transient solution in a closed volume allows the detonation wave to develop given certain initial conditions. It makes it possible to visualize the detonation, as well as the wave reflection back into the reacted fluid can be observed. If the volume is extended, the detonation may furthermore be allowed to develop into a stationary form which makes it possible to evaluate the state before and after detonation. Then this information can be compared to the theoretical solution.

Dimension
Ideal detonation waves in tubes are planar. The problem can therefore be solved with a minimum of computational effort by assuming a one dimensional flow field. The domain can then be composed of a stacked layer of single cells with the flow in the x direction only.

The length of the domain is set to 100 mm, since the purpose is to see if detonations can develop within the cylinder of a normal sized engine.

The cell size necessary to avoid convergence issues in STAR-CD is determined mainly by the Courant number, which should preferably be less than unity, for reasons of numerical stability. The Courant number v is defined as:

$$(25) \quad v = u \cdot \frac{\Delta t}{\Delta x}$$

where u is the speed of the gas, Δt is the time step and Δx is the cell size. Since u is the velocity of the combustion products in the lab frame, the relevant speed is $u_1 - u_2$. From table 7 this speed is found to be the difference between 1533 m/s and 860 m/s, so it is 673 m/s). It cannot be expected that the speed reaches the theoretical limit in the simulation but it may be used initially.

The internal solver used for the coupled complex chemistry in STAR-CD has a time step of 1E-5 as default, but this is insufficient given the timescale of the chemical kinetics at high temperatures and must be reduced to 1E-6 by setting constant 154 in the STAR-GUIde to this value.

The time steps of the main solver are required to be small enough to allow the reaction front to keep up with the wave front. If the steps are too large, a long distance is covered by the gas between iterations. Hence the reactions will be separated from the wave by that distance, which does not correspond to the real situation.

The time step size necessary to ensure convergence in the solver was found to be in the order of 1E-4 to 1E-5 before the low temperature reactions begin, since the gas does not move much initially. It must then be reduced to 1E-6 to ensure convergence during the low temperature reactions. If the warning DIVODE (DIVerging Ordinary Differential Equation) appear repeatedly between iterations, the time step size can be reduced further.

Assuming a time step of 1E-6 seconds, a gas speed of 673 m/s and a Courant number of 1, the cell size becomes:

$$\Delta x = u \cdot \frac{\Delta t}{v} = 673\, m/s \cdot \frac{1 \cdot 10^{-6}\, s}{1} = 0.000673\, m$$

A cell thickness of minimum 0.5 mm is thus appropriate to satisfy the Courant number criterion. It was however considered too large for a proper resolution of the wave, so a cell size of 0.1 mm was chosen instead and the time steps reduced correspondingly. It is also possible to set a target for the Courant number in the solver, which will then adjust the time step to keep this target value.

Boundary conditions
The end walls in the domain are solid. The side walls are set to symmetry. Wall friction is negligible since the driving force provided by the pressure gradients are very large, and heat transfer is likewise negligible due to the short time span.

Chemical reaction mechanism implementation
STAR-CD offers two choices of solvers for version 4.10: The "coupled complex chemistry" solver and DARS-CFD. While DARS-CFD would be the preferred option, licenses were not available and could not be acquired in time for this investigation.

The coupled complex chemistry solver allows up the 30 species in a mechanism. These species are defined as scalars in the software. The reaction mechanism is implemented as a list of forward reactions. Reverse reactions are calculated by STAR assuming chemical equilibrium. The reduced mechanism for DME combustion developed earlier includes only 27 species and is thus applicable to the solver.

Formatting of the input file is critical and must be done according to the rules dictated by the manual. These are slightly different from the format used by CHEMKIN. It should be mentioned that it is absolutely critical to check the contents of the cpl.inp01-echo file created by STAR, which holds the information that STAR-CD uses. It was found that minor deviations from the required procedure in making the input file resulted in severe misinterpretations by STAR, such as several orders of magnitude in reaction parameters.

The transport properties are defined in the file *tran.dat* which is identical to the one used by CHEMKIN.

12.4.2 Simulation results

Although a number of variations were made to the setup of the test case, not much difference was found in the transient solution in those cases that successfully resulted in detonations. The general tendency for development in temperature, pressure and gas velocity is shown in figures 29-31. Each figure is composed of 10 frames recorded at 5 microsecond intervals, with the first frame at top. The scale for temperature is Kelvin, for pressure it is Pascal and for gas velocity it is m/s.

To create a disturbance that will ultimately trigger the detonation, a small section at the end of the volume was subjected to an elevated temperature of 1500 K. This establishes a flame front (left of the pictures) as well as inducing a small pressure wave that travels through the volume. This method is widely used to trigger detonation in experiments as well, typically by igniting the mixture with a spark plug.

While the flame is travelling it is accelerated into the unburned mixture by the expansion of the gas in the burned fraction behind the flame. This movement compresses the mixture ahead, which is also starting to react. At some point, typically when that flame front has moved less than a centimetre through the volume, a minor section of the mixture auto ignites some distance ahead of the flame. When this happens, the rapid expansion triggers the development of the detonation.

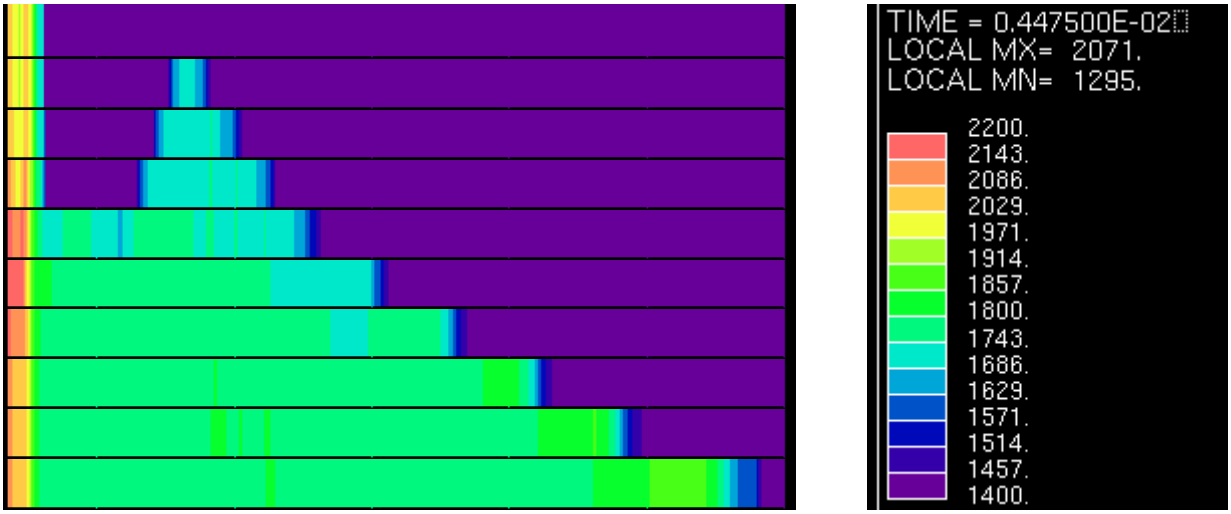

Figure 29: Development in temperature during the development of a detonation

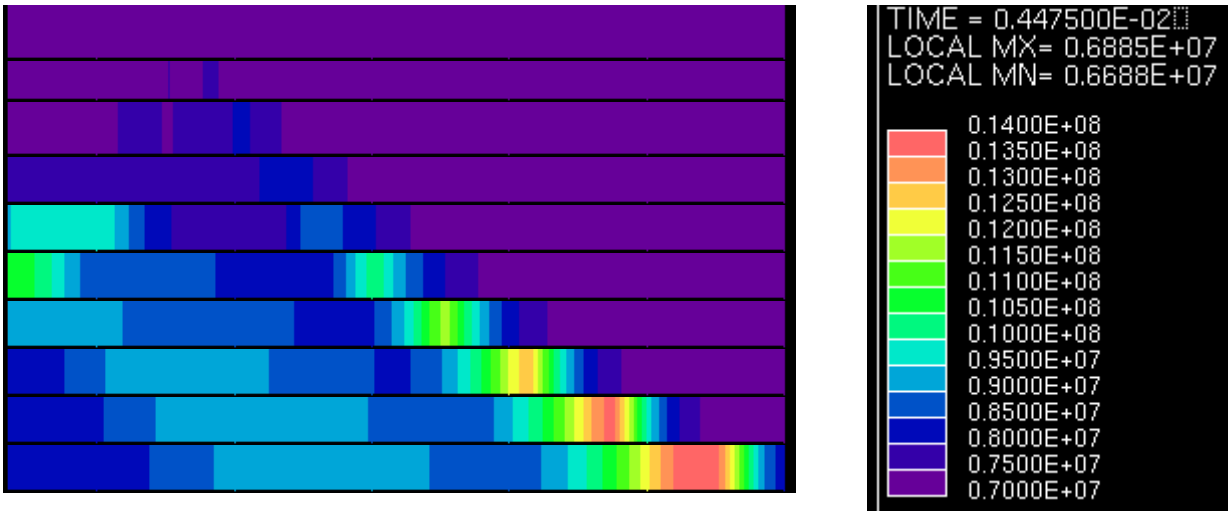

Figure 30: Development in pressure during the development of a detonation

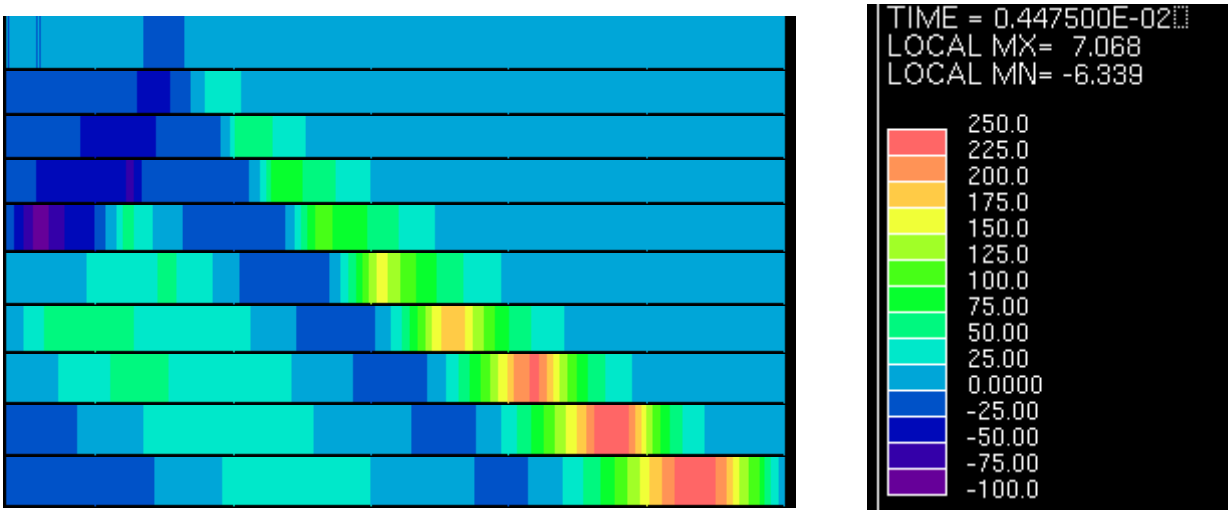

Figure 31: Development in gas velocity during the development of a detonation

The developing detonation, which starts to develop at the second frame, is clearly defined by its sharp temperature gradient initially. The burned temperature is approx. 1900 K, which is not consistent with the calculations, but

The pressure is initially not very high, but as the shock wave progresses it increases in magnitude. The wave progresses to the right, while the unburned mixture to the left auto ignites between to frames. It is seen that the pressure disturbance moves at supersonic velocity, since the gas ahead of the pressure front is unaffected. The wave moves at approximately 1500 m/s.

The gas velocity as shown by figure 31, indicates velocities around 250 m/s. It is below the velocity at stationary conditions, but very high considering that the velocity is induced in such a short time in a limited space.

12.5 Observations of detonation in HCCI combustion

The previous section dealt with determination of steady state properties of a detonation. The studied establish a reference for the velocities and pressure differences that may be expected to arise in detonations. By inspecting the pressure fluctuation under knocking conditions, it may be possible to see if a detonation is the cause. Even a partly developed detonation wave, which has not reached its full speed and amplitude, will be clearly discernible from an unevenly progressing explosion by its large amplitude and discontinuous pressure increase.

12.5.1 Experimental setup

An experiment was made to study detonation waves in HCCI combustion. Since it was desired to obtain planar detonation waves, the combustion chamber was made rectangular by designing a piston crown with a rectangular channel. The idea was that a planar one-dimensional detonation wave would be more likely to occur than a radial detonation wave, as well as easier to detect since it would travel in one direction only. The piston crown is illustrated in figure 32.

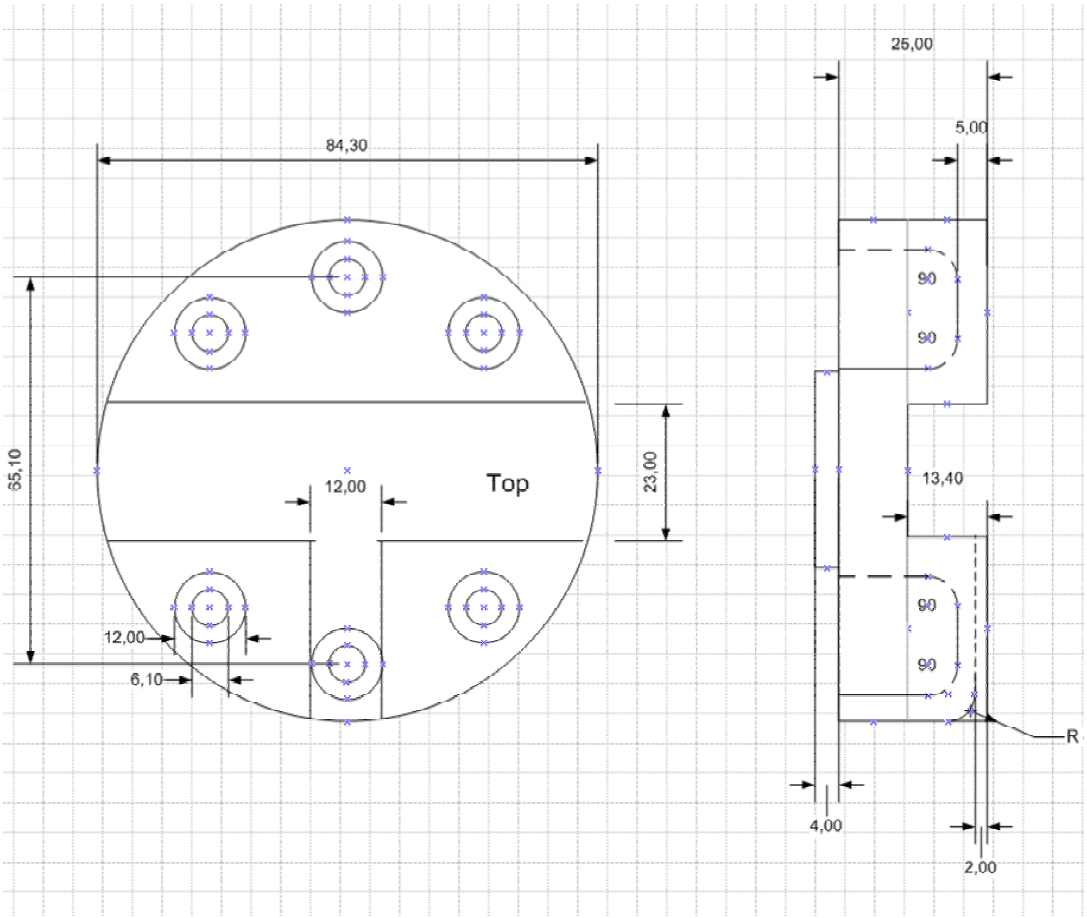

Figure 32: Piston crown with rectangular cut-out

Figure 32 shows the main combustion chamber positioned horisontally across the diameter of the piston. The 2 mm deep channel at the botttom was made to measure the pressure in the middle of the section if normal acoustic waves were to be measured. The pressure transducer recording the detonation wave was mounted at one end of the rectangular section. The details of the transducer mounting is described in the chapter "Experimental setup".

It was considered whether the pressure wave would be recorded properly. At a wave speed of 1000 m/s and a sample rate of 133 kHz (internal sample clock), the distance covered by the wave between samples would be:

$$s = \frac{1000\ m/s}{133000\ s^{-1}} = 0.0075\ m$$

Since the wave front should be less than one millimeter thick, it should thus appear as an instantaneous pressure increase between two measurements. After being reflected a number of lower readings should follow before the wave returns after being reflected from the opposite wall. An indication of a detonation would thus be that the measured peak pressure is obtained between two samples. If the pressure instead rises more slowly, this would indicate a pressure wave non-uniform explosion.

The wave should sustain its discontinuous shape for some time while being reflected several times in the chamber, before being attenuated by friction and degraded into an acoustic wave. Hence the pressure peaks should be observable several times after the combustion and the wave velocity are calculated from the intervals between the peaks, given that the distance covered between pressure peaks is approximately twice the cylinder diameter.

12.5.2 Pressure trace

Figure 33 displays the pressure trace of a knocking cycle. The pressure trace is taken from a series of 20 knocking cycles with varying amplitudes of knock. The observed tendency for very sharp pressure increments and high peaks is dominating in all cases. Combustion takes place approx. 15 CAD BTDC due to the compression ratio being 14:1.

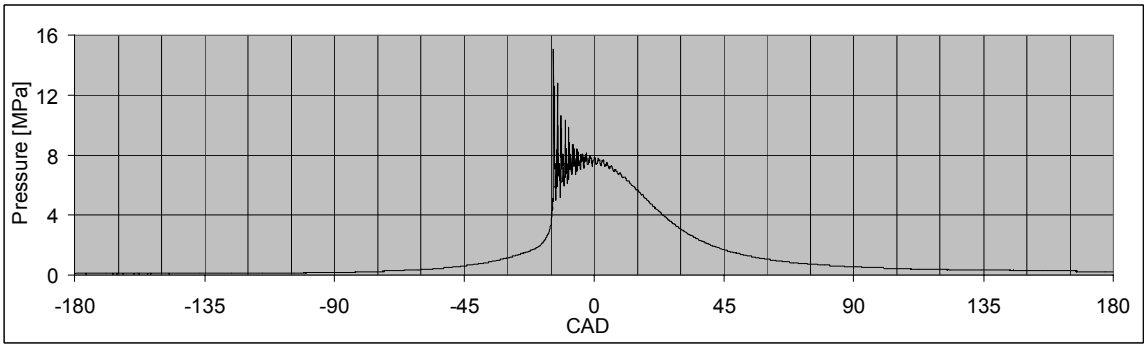

Figure 33: Pressure trace from an HCCI cycle with strong knock

On figure 34, the individual samples are shown in the knocking part of the cycle.

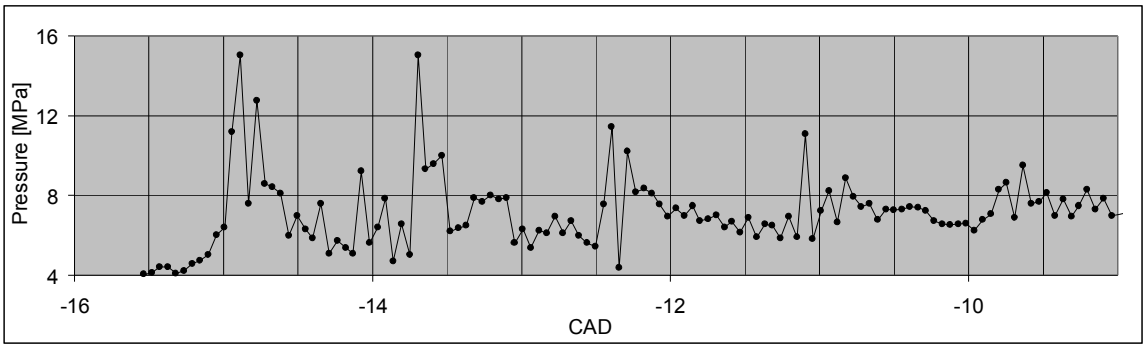

Figure 34: Zoom on pressure trace in knocking combustion

First of all it is noted that the oscillation is very far from being harmonic. The pressure increases are rapid, as expected with a shock wave. The strong oscillation following the peaks is most likely due to resonance in either the transducer or the hole connecting it to the cylinder, which is exited by the impact of the shock wave.

The first two peaks appear with a spacing of 22 samples and the following with a spacing of 24 samples. A spacing of 22 samples is also found in many of the other cycles in the test. Assuming that the peaks are due to the reflection of a single shock wave in the chamber, the velocity of the shock wave may be calculated:

$$v = 2 \cdot 0.084m \cdot \frac{133000 samples / s}{22 samples} = 1015\, m / s$$

This velocity must be compared to the sonic velocity of the chamber. According to acoustic theory, the lowest resonant frequency of a closed rectangular box may be calculated in a similar way as:

$$f = \frac{v}{2 \cdot L}$$

with L being the length of the box, here approx. 84 mm. By making an FFT analysis of the oscillation around TDC where the shock wave appears to have degraded to a harmonic wave, it is found that the frequency is approx. 5 kHz. This corresponds to a velocity of 840 m/s, which is the speed of sound. The temperature corresponding to this speed is approx 1950 K. The difference in temperature between 14 CAD BTDC and TDC is approx. 100 K with adiabatic compression. At 1850 K the speed of sound is 820 m/s. The mach number of the shock wave is therefore approx. 1.24.

13 Summary and conclusion

The focus of the project was within the following subjects:

- **Manipulation of combustion phasing by use of dual fuel and EGR**
- **Reduction of HCCI combustion noise**

Control of combustion phasing was investigated first by a theoretical study on the reaction kinetics of DME in combination with methanol. This study was made with CHEMKIN II, using primarily the homogeneous batch reactor model to model the HCCI engine. The comprehensive detailed mechanism for combustion of DME developed by Lawrence Livermore was reduced to a simple scheme, which is valid only for lean combustion of DME. The reduced scheme also includes reaction paths for methanol and methane, which are both commonly used in combination with DME to moderate the combustion phasing. The simple reaction mechanism for DME combustion was first developed to obtain a fundamental understanding of the combustion process. The conclusion obtained from this study was:

- **The low temperature reactions are self terminating due to a shift in balance between chain branching and chain terminating reaction paths**
- **The low temperature reactions of DME are inhibited when methanol is added, due to methanol consuming OH radicals in chain terminating reactions**
- **The timing of the main heat release is delayed when the low temperature reactions are inhibited by addition of methanol**
- **It is possible to operate at higher compression ratios as well as higher equivalence ratios, when methanol is added to the combustion**

An experimental study on combustion of DME and methanol was carried out as well, on a 4.6 L, 4 cylinder engine at NTSEL in Tokyo. The engine had a compression ratio of 14.5, which enabled both normal DI CI operation and HCCI operation. DME was injected directly with a custom common rail system at an equivalence ratio of 0.25, while methanol was injected at the inlet port. The engine was furthermore equipped with an EGR system capable of recycling and cooling a large fraction of the exhaust gas. This capability was used in another experiment, were EGR gas was used to obtain a delay in combustion phasing. The experiments demonstrated the following:

- **A DI CI engine with a low compression ratio can be operated in both DI CI and HCCI modes without need for further modifications**
- **Combustion phasing can be retarded with a modest amount of methanol added to the inlet air**

- **The engine load obtained in the experiment corresponded to approximately 50 percent of the full load capability for the same engine in DI CI operation at the original compression ratio**
- **The brake specific fuel consumption was comparable to the same engine in DI CI operation**
- **EGR has a retarding effect on combustion phasing. The equivalence ratio can be brought close to stoichiometric without compromising combustion efficiency**
- **EGR decreases the specific heat ratio and therefore also the combustion pressure, which counteracts the efficiency gain from improved combustion phasing**

The second subject was the reduction of HCCI combustion noise. The theoretical approach to this was to investigate the detonation phenomena, since it is suspected that detonations are responsible for the knocking combustion. A stationary detonation of lean DME combustion was modeled to determine the properties of a stationary detonation wave, in order to compare these with observations. A CFD study was setup to investigate if detonations can be created in simulations as well. The reduced mechanism developed earlier was used in the CFD study to reduce computational time. The observations from this study were:

- Detonations are possible in premixed combustion of DME at an equivalence ratio of 0.25. The stationary detonation wave has a pressure peak of 120 bar, and a velocity of approx. two times the local speed of sound
- CFD simulations of HCCI combustion can be used to study detonations when the spatial and temporal resolutions are adequately high
- Detonations appeared in the CFD simulations both when temperature gradients were introduced in the solution domain, and as a consequence of flame propagation following a local ignition event

Detonations develop in short distances in the combustion chamber. It was therefore decided to experiment with piston designs that could reduce the development of detonations, by dividing the combustion chamber into smaller separate volumes. This was done by shaping the top of the pistons. The pistons were tested and the cylinder pressure oscillations as well as the acoustic sound pressure were measured. The tests conducted revealed that:

- **The cylinder pressure oscillations can be reduced by using multiple smaller chambers in the piston**
- **The largest reduction in noise was however obtained with a bowl type piston, similar to a diesel piston. The noise created with this piston was at a lower level than DI CI combustion noise in the same engine**
- **Heat losses were increased due to the increase in piston surface area**
- **Crevice volumes were very large with some pistons due to improper design. The losses due to crevice volumes were partly responsible for the reduction in IMEP with these pistons**

14 References

1. CHEMKIN II: www.reactiondesign.com

2. DME mechanism: https://www-pls.llnl.gov/?url=science_and_technology-chemistry-combustion-dme

3. STAR-CD: www.cd-adapco.com

4. Fuquan Zhao, Thomas W. Asmus, Dennis N. Assanis, John E. Dec, James A. Eng, Paul M. Najt : Homogenous Charge Compression Ignition (HCCI) Engines, key Research and Development Issues. 2003. ISBN 0-7680-1123

5. Rasmus Christensen, S.C. Sorenson, Michael G. Jensen, Ken Friis Hansen: Engine operated on Dimethyl Ether in a Naturally Aspirated, DI Diesel Engine. SAE 971665. 1997

6. Spencer C. Sorenson, M. Glensvig, Duane L. Abata : Dimethyl Ether in Diesel Fuel Injection Systems. SAE paper 981159. 1998

7. Troels Dyhr Pedersen: Homogeneous Charge Compression Ignition Combustion of Dimethyl Ether. Master Thesis. 2006

8. Göran Haraldssson: Closed Loop Control of a Multi Cylinder HCCI Engine using variable Compression Ratio and Fast Thermal Management. Doctoral Thesis. 2005

9. R.E: herold, R. Augusta, D. Foster, J. Ghandi: The Effects of Intake Charge Preheating in a gasoline Fuelled HCCI Engine. SAE 2005-01-3742. 2005

10. Joel Martinez-Friaz, Salvadore M. Aceves, Daniel Flowers, J. Ray Smith, Robert Dibble: HCCI Engine Control by Thermal Management. SAE 2000-01-2869

11. Shigeru Onishi, Souk Hong Jo, Katsuji Shoda, Pan Do Jo, Satoshsi Kato: Active Thermo-Atmosphere Combustion (ATAC) – A New Combustion Process for Internal Combustion Engines. SAE 790501

12. Japan DME Forum : The DME Handbook. 2007

13. Procedings of 3.rd International DME Conference & 5.th Asian DME Conference. 2008

14. Sato, Yoshio; Nozaki, Shinya; Noda, Toshifumi: The Performance of a Diesel Engine for Light Duty Truck Using a Jerk Type In-Line DME Injection System. SAE paper 2004-01-1862. 2004

15. Takayugi Tsuchiya, Yoshio Sato: Development of DME Engine for Heavy-duty Truck. SAE paper 2006-01-0052. 2006

16. Byeong-il An, Yoshio Sato, Seang-Wock Lee, Toshmitsu Takayanagi: Effects of injection pressure on Combustion of a Heavy Duty Diesel Engine With Common Rail DME Injection Equipment. SAE 2004-01-1864. 2004

17. Magnus Christensen, Anders Hultquist, Bengt Johansson: Demonstrating the Multi Fuel Capability of a Homogeneous Charge Compression Ignition Engine with Variable Compression Ratio. SAE 1999-01-3679. 1999.

18. J.A. Gatowski, E.N. Balles, K.M. Chun, F.E. Nelseon, J.A. Ekchian, J.B. Heywood: Heat Release Analysis of Engine Pressure Data. SAE paper 841359. 1984.

19. Ylva Nillson, Lars Eriksson: Determining TDC Position Using Symmetry and Other Methods. SAE 2004-01-1458

20. Junseok Chang, Orgun Güralp, Zoran Filipi, Dennis Assanis, Tang-Wei Kuo, Paul Najt, Rod Rask: New Heat Transfer Correlation for an HCCI Engine Derived from Measurements of Instantaneous Surface Heat Flux. 2004-01-2996.

21. H.J. Curran, .J. Pitz, C.K. Westbrook, P. Dagaut, J-C Boettner, M. Cathonnet: A Wide Range Modeling Study of Dimethyl Ether Oxidation. International Journal of Chemical Kinetics. No. 30 pp 229-241. 1998

22. Toyosei Yamauchi, Atsutaka Matsumoto, Yogo Takada, Tomoyuki Wakisaka: Reduction of Detailed Elementary Reaction Schemes by Newly-developed Automatic Scheme Reduction Tool “ASRT”. SAE 2007-01-1879

23. David scholl, Craig Davis, Stephen Russ, Terry Barash: The Volume Acoustic Modes of Spark Ignited Internal Combustion Chambers. SAE 980893

24. D. Bradley, C. Morley, X. J. Gu, D. R. Emerson: Amplified Pressure Waves During Autoignition: Relevance to CAI Engines. SAE 2002-01-2868.

25. Irvin Glassman: Combustion, Third edition 1996. ISBN 0-12-285852-2

26. John. N. Bradley: Shock Waves in Chemistry and Physics. ISBN 0416488501. 1962

27. Edward Greene, J. Toennies: Chemical Reactions in Shock Waves. LCCN 64023684. 1964

28. S. Browne, J. Ziegler, J.E. Shepherd: Numerical Solution Methods for Shock and Detonation Jump Conditions. California Institute of Technology. GALCIT Report FM 2006.006. 2004

29. S. Kao, J.E. Shepherd: Numerical Solution Methods for Control Volume Explosions and ZND detonation Structure. GALCIT Report FM 2006.007. 2004

15 Appendix A: Reduced scheme for lean premixed DME combustion

NOTE: A units are in mole-cm-sec-K; E units are in cal/mole

Non-carbon radical reactions

	A	b	E
8. $H+O_2=O+OH$	1.97E+14	0.01	6540.0
9. $O+H_2=H+OH$	5.08E+04	2.7	6292.0
10. $O+H_2O=OH+OH$	2.97E+06	2.0	13400.0
11. $OH+H_2=H+H_2O$	2.16E+08	1.5	3430.0
13. $H_2O_2+OH=H_2O+HO_2$	1.00E+12	0.0	0.0
Declared duplicate reaction...			
26. $H+O_2$ (+m) $=HO_2$ (+m)	1.48E+12	0.6	0.0
Low pressure limit: 0.35000E+17 -0.41000E+00 -0.11160E+04			
TROE centering: 0.50000E+00 0.10000E-29 0.10000E+31			
H_2 Enhanced by 2.500E+00			
H_2O Enhanced by 1.200E+01			
CO Enhanced by 1.900E+00			
CO_2 Enhanced by 3.800E+00			
42. $HO_2+O=OH+O_2$	3.25E+13	0.0	0.0
47. $HO_2+H=OH+OH$	7.08E+13	0.0	300.0
48. $HO_2+H=H_2+O_2$	1.66E+13	0.0	820.0
49. $HO_2+OH=H_2O+O_2$	2.89E+13	0.0	-500.0
50. $HO_2+HO_2=H_2O_2+O_2$	4.20E+14	0.0	11980.0
Declared duplicate reaction...			
51. $H_2O_2=OH+OH$	1.29E+33	-4.9	53300.0
52. $H_2O_2+H=H_2O+OH$	2.41E+13	0.0	3970.0
86. $H_2O_2+O=OH+HO_2$	9.55E+06	2.0	3970.0
167. $H_2O_2+H=H_2+HO_2$	4.82E+13	0.0	7950.0
187. $HO_2+HO_2=H_2O_2+O_2$	1.30E+11	0.0	-1629.0
Declared duplicate reaction...			
188. $H_2O_2+OH=H_2O+HO_2$	5.80E+14	0.0	9560.0
Declared duplicate reaction...			

Continued on next page!

Carbon containing radical reactions

3. $CH_4+OH=CH_3+H_2O$	1.93E+05	2.4	2106.0
7. CO+OH=CO2+H	1.40E+05	1.9	-1347.0
12. HCO + m=H + CO + m	1.86E+17	-1.0	17000.0
Reverse Arrhenius coefficients:	6.47E+13	0.0	-442.0
H_2 Enhanced by 2.500E+00			
H_2O Enhanced by 1.200E+01			
CO Enhanced by 1.900E+00			
CO_2 Enhanced by 3.800E+00			
18. $CH_3OH+HO_2=CH_2OH+H_2O_2$	3.98E+13	0.0	19400.0
22. $CH_3+HO_2=CH_3O+OH$	1.10E+13	0.0	0.0
23. $CO+HO_2=CO_2+OH$	3.01E+13	0.0	23000.0
32. $CH_2O+OH=HCO+H_2O$	3.43E+09	1.2	-447.0
33. $CH_2O+H=HCO+H_2$	9.33E+08	1.5	2976.0
38. $CH_2O+CH_3=HCO+CH_4$	3.64E-06	5.4	998.0
40. CH_3O (+m) $=CH_2O+H$(+m)	5.45E+13	0.0	13500.0
Low pressure limit: 0.23440E+26 -0.27000E+01 0.30600E+05			
45. $CH_3+HO_2=CH_4+O_2$	3.00E+12	0.0	0.0
46. $HCO+O_2=CO+HO_2$	7.58E+12	0.0	410.0
53. $CH_3+H_2O_2=CH_4+HO_2$	3.36E+10	-0.3	2502.0
54. $CH_2O+HO_2=HCO+H_2O_2$	5.82E-03	4.5	6557.0
78. $CH_3OH+OH=CH_2OH+H_2O$	7.10E+06	1.8	-596.0
83. $CH_2OH+O_2=CH_2O+HO_2$	3.81E+06	2.0	1641.0
110. $CH_3O+H_2O=CH_3OH+OH$	8.98E+06	2.1	17380.0
269. $CH_3+O_2=CH_2O+OH$	7.47E+11	0.0	14250.0
274. $CH_3OCH_3+OH=CH_3OCH_2+H_2O$	9.35E+05	2.3	-780.0
275. $CH_3OCH_3+H=CH_3OCH_2+H_2$	7.72E+06	2.1	3384.0
276. $CH_3OCH_3+O=CH_3OCH_2+OH$	1.86E-03	5.3	-109.0
277. $CH_3OCH_3+HO_2=CH_3OCH_2+H_2O_2$	1.68E+13	0.0	17690.0
280. $CH_3OCH_2+HO_2=CH_3OCH_3+O_2$	1.90E+11	0.0	-3659.0
282. $CH_3OCH_2=CH_2O+CH_3$	1.27E+14	-0.2	25500.0
287. $CH_3OCH_2+O_2=CH_3OCH_2O_2$	2.00E+12	0.0	0.0
293. $CH_3OCH_2O_2=CH_2OCH_2O_2H$	6.00E+10	0.0	21580.0
294. $CH_2OCH_2O_2H=OH+CH_2O+CH_2O$	1.50E+13	0.0	20760.0
295. $CH_2OCH_2O_2H+O_2=O_2CH_2OCH_2O_2H$	7.00E+11	0.0	0.0
296. $O_2CH_2OCH_2O_2H=HO_2CH_2OCHO+OH$	4.00E+10	0.0	18580.0
297. $HO_2CH_2OCHO=OCH_2OCHO+OH$	2.00E+16	0.0	40500.0
298. $OCH_2OCHO=CH_2O+HCO_2$	5.96E+16	-1.5	19620.0
303. $OCH_2OCHO=HOCH_2OCO$	1.00E+11	0.0	14000.0
304. $HOCH_2OCO=HOCH_2O+CO$	2.18E+16	-2.7	17200.0
308. $HOCH_2O=HCO_2H+H$	1.00E+14	0.0	14900.0
331. $HCO_2+HO_2=HCO_2H+O_2$	3.50E+10	0.0	-3275.0
333. $HCO_2H+OH=H_2O+CO_2+H$	2.62E+06	2.1	916.0
334. $HCO_2H+OH=H_2O+CO+OH$	1.85E+07	1.5	-962.0
338. $HCO_2H+HO_2=H_2O_2+CO+OH$	1.00E+12	0.0	11920.0

16 Appendix B: Detonation model in EES

$$P_1 = 2{,}4 \times 10^6$$

$$T_1 = 726$$

$$\rho_1 = \left[x_{1;N2} \cdot \rho_{N2;1} + x_{1;O2} \cdot \rho_{O2;1} + x_{1;DME} \cdot \rho_{C2H5OH;1}\right] \cdot MW_1$$

$$v_1 = \frac{1}{\rho_1}$$

$$\lambda = 3$$

$$StCoef = 3$$

$$e_1 = \frac{x_{1;N2} \cdot u_{N2;1} + x_{1;O2} \cdot u_{O2;1} + x_{1;DME} \cdot u_{C2H5OH;1}}{MW_1}$$

$$x_{1;N2} = 3{,}76 \cdot StCoef \cdot \left[\frac{\lambda}{3{,}76 \cdot StCoef \cdot \lambda + StCoef \cdot \lambda + 1}\right]$$

$$x_{1;O2} = StCoef \cdot \left[\frac{\lambda}{3{,}76 \cdot StCoef \cdot \lambda + StCoef \cdot \lambda + 1}\right]$$

$$x_{1;DME} = \frac{1}{3{,}76 \cdot StCoef \cdot \lambda + StCoef \cdot \lambda + 1}$$

$$MW_1 = x_{1;N2} \cdot 28 + x_{1;O2} \cdot 32 + x_{1;DME} \cdot 46$$

$$\gamma_1 = \frac{cp_1}{cv_1}$$

$$cp_1 = \frac{x_{1;N2} \cdot \mathbf{Cp}('N2'; T = T_1) + x_{1;O2} \cdot \mathbf{Cp}('O2'; T = T_1) + x_{1;DME} \cdot \mathbf{Cp}('C2H5OH'; T = T_1)}{MW_1}$$

$$cv_1 = \frac{x_{1;N2} \cdot \mathbf{Cv}('N2'; T = T_1) + x_{1;O2} \cdot \mathbf{Cv}('O2'; T = T_1) + x_{1;DME} \cdot \mathbf{Cv}('C2H5OH'; T = T_1)}{MW_1}$$

$$P_2 = \mu \cdot \frac{MW_1}{MW_2} \cdot \frac{T_2}{T_1} \cdot P_1$$

$$e_2 - e_1 = \frac{R_a}{MW_2} \cdot \frac{T_2}{2 \cdot \gamma_2}$$

$$R_a = 8{,}314$$

$$\rho_2 = \left[x_{2;N2} \cdot \rho_{N2;2} + x_{2;O2} \cdot \rho_{N2;2} + x_{2;H2O} \cdot \rho_{H2O;2} + x_{2;CO2} \cdot \rho_{CO2;2}\right] \cdot MW_2$$

$$v_2 = \frac{1}{\rho_2}$$

$$e_2 = \frac{x_{2;N2} \cdot u_{N2;2} + x_{2;O2} \cdot u_{O2;2} + x_{2;H2O} \cdot u_{H2O;2} + x_{2;CO2} \cdot u_{CO2;2}}{MW_2}$$

$$x_{2;N2} = 0{,}7546$$

$$x_{2;O2} = 0{,}1337$$

$$x_{2;H2O} = 0{,}0667$$

$$x_{2;CO2} = 0{,}0446$$

$$MW_2 = x_{2;N2} \cdot 28 + x_{2;O2} \cdot 32 + x_{2;H2O} \cdot 18 + x_{2;CO2} \cdot 44$$

$$\gamma_2 = \frac{cp_2}{cv_2}$$

$$cp_2 = \frac{x_{2;N2} \cdot \mathbf{Cp}('N2'; T = T_2) + x_{2;O2} \cdot \mathbf{Cp}('O2'; T = T_2) + x_{2;H2O} \cdot \mathbf{Cp}('H2O'; T = T_2) + x_{2;CO2} \cdot \mathbf{Cp}('CO2'; T = T_2)}{MW_2}$$

$$cv_2 = \frac{x_{2;N2} \cdot \mathbf{Cv}('N2'; T = T_2) + x_{2;O2} \cdot \mathbf{Cv}('O2'; T = T_2) + x_{2;H2O} \cdot \mathbf{Cv}('H2O'; T = T_2) + x_{2;CO2} \cdot \mathbf{Cv}('CO2'; T = T_2)}{MW_2}$$

$$\mu = \frac{\gamma_2 + 1}{\gamma_2}$$

$$u_1^2 = \mu^2 \cdot \gamma_2 \cdot R_b \cdot \frac{T_2}{MW_2}$$

$$R_b = 8314$$

$$\rho_1 \cdot u_1 = \rho_2 \cdot u_2$$

$$u_3 = \left[\frac{R_b}{MW_1} \cdot \gamma_1 \cdot T_1\right]^{0,5}$$

$$u_4 = \left[\frac{R_b}{MW_2} \cdot \gamma_2 \cdot T_2\right]^{0,5}$$

$$M_1 = \frac{u_1}{u_3}$$

$$M_2 = \frac{u_2}{u_4}$$

$$\rho_{N2;1} = \rho('N2'; T = T_1; P = P_1)$$

$$\rho_{O2;1} = \rho('O2'; T = T_1; P = P_1)$$

$$\rho_{C2H5OH;1} = \rho('C2H5OH'; T = T_1; P = P_1)$$

$$\rho_{N2;2} = \rho('N2'; T = T_2; P = P_2)$$

$$\rho_{O2;2} = \rho('O2'; T = T_2; P = P_2)$$

$$\rho_{H2O;2} = \rho('H2O'; T = T_2; P = P_2)$$

$$\rho_{CO2;2} = \rho('CO2'; T = T_2; P = P_2)$$

$$u_{N2;1} = \mathbf{u}('N2'; T = T_1)$$

$$u_{O2;1} = \mathbf{u}('O2'; T = T_1)$$

$$u_{C2H5OH;1} = \mathbf{u}('C2H5OH'; T = T_1)$$

$$u_{N2;2} = \mathbf{u}('N2'; T = T_2)$$

$$u_{O2;2} = \mathbf{u}('O2'; T = T_2)$$

$$u_{H2O;2} = \mathbf{u}('H2O'; T = T_2)$$

$$u_{CO2;2} = \mathbf{u}('CO2'; T = T_2)$$

17 Paper I: The Effect of Compression Ratio, Equivalence Ratio and Engine Speed on HCCI Combustion of Dimethyl Ether

18 Paper II: Controlling the heat release of DME HCCI Combustion with methanol and EGR

19 Paper III: Reducing HCCI Combustion Noise through Piston Design

JSAE 20077134
SAE 2007-01-1860

A study on the effects of compression ratio, engine speed and equivalence ratio on HCCI combustion of DME

Troels Dyhr Pedersen, Jesper Schramm
Technical University of Denmark

ABSTRACT

An experimental study has been carried out on the homogeneous charge compression ignition (HCCI) combustion of Dimethyl Ether (DME). The study was performed as a parameter variation of engine speed and compression ratio on excess air ratios of approximately 2.5, 3 and 4. The compression ratio was adjusted in steps to find suitable regions of operation, and the effect of engine speed was studied at 1000, 2000 and 3000 RPM. It was found that leaner excess air ratios require higher compression ratios to achieve satisfactory combustion. Engine speed also affects operation significantly.

INTRODUCTION

The HCCI combustion process is known to produce little or no particulate matter and low levels of NO, while having the potential of a high indicated efficiency at part load operation. In the recent years, the use of DME in the HCCI combustion process has caught the attention of automotive engineers. DME is an interesting fuel for the HCCI process, as it has auto ignition properties superior to normal diesel fuel, thereby ensuring ignition at moderate compression ratios without the need for preheating. Exhaust emissions of unburned DME and lower hydrocarbons as well as CO may be treated in a simple catalytic conversion.

Studies on the application of DME in the HCCI combustion process may be divided into three categories with respect to the supplementary fuel or additive usage. These are studies on combustion of pure DME, studies on additive effects and studies of dual fuel combustion.

Combustion of pure DME has previously been studied by Zheng et al [1] at a compression ratio of 17 and engine speeds from 1400 -2000 RPM. Highest IMEP achieved with pure DME was 3.1 Bar. Another study by Shenghua et al [2] used a lower compression ratio of 10.7 and engine speeds of 1800 and 2000. A BMEP of 3.2 bar was achieved in this study. In both of these cases it was concluded that DME is only suitable for part load operation, as higher engine loads causes unacceptable pressure rise rates and knock. Shenghua et al [3] made a later study were three different compression ratios (8, 10.7 and 14) were used with variation of speed and fuel input. A BMEP of 3.5 Bar at a compression ratio of 8 was demonstrated in this study.

Hamada et al [4] have investigated the ignition timing through a study of the formation of OH and HCHO radicals in the low temperature reactions, using a spectroscopic method. A large interval of compression ratios at constant speed (1400 RPM) was used. Useful data on the duration and onset of low temperature reactions were presented here.

The most common finding is that HCCI combustion of DME results in a very limited operability, and that timing of heat release is difficult. The use of EGR is now commonly regarded as a promising strategy to control HCCI combustion of pure DME [5, 6], whereas other strategies are concerned with the use of DME in combination with other fuels.

Studies of additive effects include those of Yamada et al [7] who studied the reaction suppression effect of methanol and the reaction enhancing effect of ozone. Ogawa et al [8] studied the effect of direct injection of water and methanol in a premixed DME HCCI engine. Studies of dual fuel operation include those of Zheng et al, who have made an extensive theoretical and experimental research on dual fuel combustion of DME with natural gas, methane and methanol [9, 10]. Sato et al [11] also studied the use of DME and hydrogen in combination with methane. Other studies of dual fuel operation include those of Shudo et al [12], who used a DME-reformed gas as supplement to combustion of pure DME. It was found that control of ignition timing was enabled by varying the amount of reformed DME to pure DME.

The combustion of pure DME in HCCI combustion mode is however still of interest, as information on the combustion of pure DME helps to clarify the need of additional fuel or additives. If the right operating strategy is used it may be argued that the benefits of this engine principle compensates for its shortcomings.

DESCRIPTION OF THE EXPERIMENT

OBJECTIVE

The goal of this study was to determine the influence of compression ratio (CR) and engine speed on HCCI combustion of DME at selected excess air ratios.

MOTIVATION

The primary motive for investigating HCCI combustion of DME is that of avoiding high-pressure pumps and injectors. As DME has a very low lubricity, pumps and injectors are susceptible to rapid wear. If DME can be introduced with a low pressure nozzle instead, these problems are avoided.

Prior experiments have shown that the combustion of pure DME in the HCCI process necessitates a careful choice of CR to achieve the best possible result, e.g. a high IMEP and indicated efficiency. It is also of interest to investigate the influence of engine speed on the combustion process. Higher engine speeds may improve the characteristics of the combustion, which may be of interest in smaller engines.

EXPERIMENTAL OUTLINE

Excess air ratios

From earlier experiments it was found that the richest mixture that could be used without excessive knock would be an excess air ratio (lambda) of 2.5. It was also found that compression ignition of mixtures leaner than the excess air ratio of 4 required a high compression ratio of about 12-14, and that such lean mixtures cannot produce sufficient torque to keep an engine running except for idle conditions.

Three different excess air ratios were chosen to represent the rich limit (lambda 2.5), the lean limit (lambda 4) and a value in between (lambda 3). As keeping an equivalence ratio constant can be a challenge when air flow changes, three constant values of fuel mass per cycle were used instead. The three values are however referred to as lambda 2.5, 3 or 4 in the text and figures.

Variation of engine speed

The HCCI combustion is a premixed and homogeneous combustion which is mainly governed by chemical kinetics. The reactions therefore occur very fast compared to DI CI engines and SI engines, but may still be affected by engine speed.

It is well known that higher engine speeds lead to a more adiabatic compression of the mixture, but also increases the heat flux from the combustion chamber and therefore results in higher in-cylinder temperatures.

To investigate the possible effects of engine speed on the combustion event and engine performance, an interval of engine speed comparable to that of a medium duty engine has been chosen. To avoid excessive amounts of data, the fixed engine speeds used were 1000, 2000 and 3000 RPM.

Variation of compression ratio

The CR has been varied from 8.8 to 12.8 in steps of 0.2. The purpose was to accurately determine the range of CR necessary to achieve satisfactory engine performance within the desired range of excess air ratios and engine speeds.

Determining the usable interval of compression ratio at different engine speeds and equivalence ratios

In this study, the lowest acceptable compression ratio is found at the point where the engine is capable of self-sustaining combustion. It was necessary to preheat the inlet air at the lowest compression ratios to initiate HCCI combustion, but if combustion did not proceed after preheating was removed, the operating point was not considered valid.

With lambda 4 it was however difficult to determine whether HCCI combustion was completed while the CR was in the lower end. To determine if combustion was satisfactory, the amounts of CO_2 and CO were monitored to determine if the combustion efficiency was satisfactory. It turned out that the combustion resulted in higher amounts of CO than CO_2 until the CR was raised enough to complete the final CO oxidation. A figure displaying emissions of CO and CO_2 is found in the results section.

At the higher engine speeds it was more difficult to initiate HCCI combustion of the leaner mixtures lambda 3 and 4. As preheating the air could not effectively solve this problem, preheating was done by running the engine with the rich mixture for a short time before shifting to the leaner mixture. If the compression ratio was adequate the combustion would continue and stabilize; otherwise it would only continue for a short while before entering a mode of partial combustion.

The highest acceptable compression ratio is found at the point at which no further improvement in performance is achieved. While it is difficult to determine this limit during the experiment, it is clear from the results that IMEP as well as indicated efficiency peaks at the optimum compression ratio and then decreases as compression is further increased. This happens fast with lambda 2.5, while lambda 4 benefits from a higher compression ratio than the lowest acceptable.

While the intensity of knock or pressure rise rate is sometimes used as a subjective limit of operation, this limit is not used in this study as it is desired to show the amplitude of engine knock when operating limits are exceeded.

Interpretation of DME heat release curves

The process of HCCI combustion of DME takes place in two distinctive stages, which may be observed in the heat release curves in the results section. The first stage is commonly termed cool flames or low temperature reactions (LTR).

The LTR occurs when pressure reaches 15-16 Bar. The reactions are highly temperature dependant and are therefore seen to occur at the same pressure and hence roughly the same temperature. A simplified mechanism for these is described by Yamada et al [7], which include a set of chain branching reactions (1) and a chain terminating reaction (2):

$$CH_3OCH_3 + OH \rightarrow \alpha OH + \beta HCHO + other \quad (1)$$

$$HCHO + OH \rightarrow CHO + H_2O \quad (2)$$

This set of reactions shows that DME reacts with OH to produce HCHO and reproduce OH in some quantity. The role of HCHO is that it accumulates and reacts with OH without reproduction of OH, thereby terminating the process. This explains the behavior of LTR heat release which is always found to decrease and terminate before the next stage of combustion takes place. The LTR is therefore of high importance to the subsequent combustion process, as it provides heat and radicals to initiate the subsequent combustion.

The major part of the thermal heat release is found in the high temperature reaction (HTR). Yao et al [13] has described the combustion process in detail. The HTR is governed by the normal combustion reactions that ultimately lead to the production of CO. The most critical reaction is the final oxidation of CO, as this reaction requires a temperature above 1400 K to initiate. Due to wall quenching at low combustion temperatures, large amounts of CO do not reach this temperature in a lean combustion process, hence leading to high levels of CO in the exhaust.

The HTR reactions are fast and cause heat release rates to become very high. Therefore, controlling this reaction is the key to successful operation of HCCI with any fuel.

EXPERIMENTAL SETUP

Engine

The study was carried out using a 4-stroke, 2-cylinder DI diesel engine from BUKH (Danish engine manufacturer), model DV24. The specifications for this engine are given in table 1.

One cylinder was operated with diesel fuel in its original DI CI combustion mode in order to keep the engine running and also to keep the engine heated. The operation of this cylinder would otherwise not influence the operation of the cylinder operating in the HCCI mode.

The other cylinder was modified for HCCI operation with DME as described in the following section.

Table 1 Specifications of BUKH DV24

Bore	85 mm
Stroke	85 mm
Connecting rod length	160 mm
Compression ratio	18.5
Inlet valve opens	32 BTDC
Inlet valve closes	64 ABDC
Exhaust valve opens	64 BBDC
Exhaust valve closes	32 ATDC

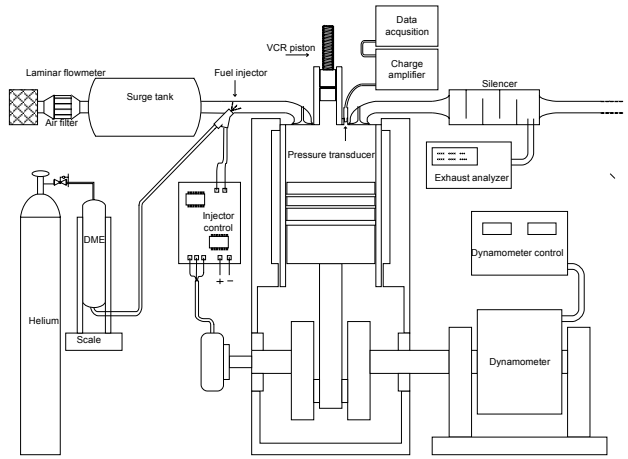

Figure 1: Experimental setup

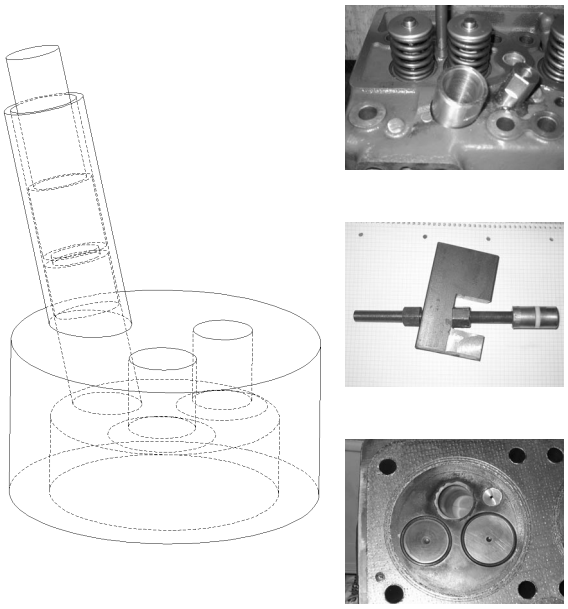

Figure 2 Coupling of regulating cylinder and cylinder head. Left: position of regulating cylinder in cylinder head. Right top: regulating cylinder is inserted through the cylinder head. Right center: Regulating piston is fixed with nuts on either side of rigid bracket. Right bottom: Regulating cylinder intersects compression volume.

Engine modification

To obtain a lower CR than the original, the piston top was lowered to give a geometric CR of 14.3. This CR is empirically high enough to ensure ignition and complete combustion of very lean charges with DME. To enable further adjustment of the CR, a cylinder with an internal diameter of 25 mm and an external diameter of 30 mm was inserted through the cylinder head to connect with the compression volume. The volume of the regulating cylinder could then be used to adjust the compression volume by the adjustment of a piston. To allow space for this arrangement, the existing passage for the fuel injection valve was expanded and used for the regulating cylinder. Figure 2 illustrates the arrangement.

With the regulating cylinder and piston arrangement, the compression volume is adjustable from 14.3 to 8.8 by extracting the piston up to 50 mm out of the regulating cylinder.

As both cylinder liner and regulating cylinder are subjected to the engine cooling water it is assumed that thermal conditions are approximately equal in both volumes. Combustion should therefore occur simultaneously in both volumes.

Fuel injection system

The DME was injected in pulses into the intake manifold of the modified cylinder by means of a standard gasoline injector with a free flow capacity of 190 g/min. The arrangement is seen in figure 1.

The fuel supply tank was pressurized at 8 bars in order to avoid formation of vapor bubbles in the fuel supply line and near the injector. The amount of fuel per injection was calibrated using a precision scale with a resolution of 0.1 gram intervals to determine fuel consumption in 500 injections.

Injection timing and duration was controlled using a programmable microcontroller. The signal from a quadratic encoder on the engine shaft was used as reference for the injection. In this study, the amount of fuel is kept constant for all speeds for each of the three target values of lambda. Volumetric efficiency is however not constant. For the three target values of lambda, the actual values are therefore slightly different, as shown in table 3.

Table 3: Target and actual excess air ratios

RPM	1000			2000 & 3000		
Target λ	2.50	3.0	4.0	2.5	3.0	4.0
Fuel [mg]	25	20	15	25	20	15
Inject. [ms]	4.7	3.6	2.5	4.7	3.6	2.5
Vol. eff.	0.96			0.88		
Actual λ	2.45	3.06	4.08	2.25	2.81	3.74

The variation in actual lambda is considered to be of less importance, as the concentration of fuel is limiting the rate in lean combustion and not the concentration of oxygen, which is abundant.

Cylinder pressure data acquisition

The cylinder pressure was measured using a Kistler 6052A pressure transducer. A Kistler 5001 charge amplifier was used for amplification of the signal from the transducer. The acquisition of the pressure was made using a computer with a data acquisition card. The clock and trigger signals for the acquisition was supplied by an encoder with 3600 pulses per revolution. TDC alignment was made by software correction.

The setup used for acquiring the cylinder pressure was designed to provide a high resolution of the cylinder pressure, as the combustion durations were expected to be from 5 - 10 CAD. Thus, using a lower resolution such as 1 sample per CAD would be insufficient, as samples would not provide much information about the event. In addition, a sampling frequency at least 2.5 times higher than the highest frequency expected should be used to avoid aliasing.

Emissions

It is a common observation that the HCCI process with gaseous fuels does not produce soot, and that the emission of NO is very low due to the low peak temperatures of HCCI combustion. Those emissions are thus not the primary concern with this combustion principle and have therefore not been measured either.

The emissions of CO_2, CO and THC were measured with a Bosch ETT 8.55 portable exhaust analyzer. The emissions were monitored with the purpose of identifying the quality of the combustion, which was used to determine when satisfactory combustion occurred, and also when combustion was stabilized. It is easily seen from the values of hydrocarbons, CO and CO_2 if the combustion process is at steady state or in transition.

DATA TREATMENT

Cylinder pressure data treatment

Due to the nature of the HCCI combustion, one or more shockwaves of some amplitude always follows the combustion. The shockwave causes a resonating wave in the combustion chamber which is similar to that caused by knocking combustion. This phenomenon has been studied in detail by Vressner et al [14]. Apart from the noise emitted from the engine, knocking combustion is believed to enhance the heat transfer to the combustion chamber walls [15]. This is another good reason why engine knock must be limited.

The frequency of the shockwaves observed is in the region of 4500 – 6000 Hz, with higher engine speeds and in-cylinder temperatures leading to higher frequencies. Wavelengths were determined by close examination of the oscillating parts of the pressure curves. The heat release analysis is heavily biased by these pressure pulsations, as these are interpreted as heat release as well as the

pressure rise from the combustion. This is particularly the case when the pressure pulsations have a frequency and amplitude that produce pressure rise rates in the same order of magnitude as the heat release itself.

To ensure that the heat release analysis is only applied to the pressure rise from the combustion, the pressure curve has been smoothed out by applying the method of moving average to remove the pulsations. In this method, the mean of a specific number of pressure values on both sides of the desired value is determined. To eliminate the observed oscillations, the number of pressure values found in one wavelength of the lowest unwanted frequency is the number of points that are averaged. For 1000 RPM this meant that averaging was made across 12 pressure values, whereas for 2000 RPM 20 pressure values were used and for 3000 RPM 30 pressure values were used.

Heat release analysis

The cylinder pressure data is used in the heat release analysis. In this study, a simple analysis is performed point-by-point by means of the equation:

$$\frac{dQ}{d\theta} = \frac{\gamma}{\gamma - 1} p \frac{dV}{d\theta} + \frac{1}{\gamma - 1} V \frac{dp}{d\theta}$$

Where Q is the equivalent heat release [J], θ is the crank angle degree (CAD), γ is the specific heat ratio, p is the pressure in Pascal and V is the volume in cubic meters.

The heat release calculations were carried out using the averaged cylinder pressure data. Given that the heat release curves should not be used to measure quantitatively the amount of heat released, the specific heat ratio was set to 1.3 for convenience.

Calculation of IMEP

The indicated work from start of compression to end of expansion (3600 cylinder pressure values) was calculated on the basis of the averaged cylinder data as:

$$W_i = \sum_{i=1}^{3600} \left(\frac{p_i + p_{i+1}}{2} \right) \left(V_i + V_{i+1} \right) \text{ [J]}$$

where p_i and p_{i+1} are values of cylinder pressure [Pa] and V_i and V_{i+1} are values of cylinder volume [m^3]

The net indicated mean effective pressure in figures 28-30 was calculated as:

$$IMEP = \frac{W_i}{V_D} \quad \text{[Pa]}$$

where V_D is the displacement volume [m^3].

Pressure rise rates

The pressure rise rate was calculated as:

$$\frac{dp_{i+5}}{d\theta} = 100000 \cdot \left(p_{i+10} - p_i \right) \quad \text{[Bar/CAD]}$$

where θ is the CAD. The values of the averaged cylinder pressure data points are thus compared 1 CAD apart. The highest value found this way is the maximum pressure rise rate.

Indicated efficiencies

The indicated efficiencies stated in figures 31-33 are calculated using the lower heating value of the fuel and the indicated work:

$$\eta_{in} = \frac{W_i}{m_{fuel} \cdot LHV}$$

where m_{fuel} is the injected mass of fuel per cycle [kg] and LHV is the lower heating value of the fuel

Knock amplitude

The knock amplitude was determined as the largest pressure drop during one half-width of a pressure pulsation in each cycle. The width used was 7 data points for 1000 RPM, 11 data points for 2000 RPM and 15 data points for 3000 RPM. The pressure drop was used instead of pressure increase, as the algorithm used to find the peak amplitude could otherwise identify the pressure rise from combustion as knock. The amplitude given in the figures 7, 15 and 23 are mean values of the peak values found for 10 consecutive cycles. This correlates reasonably well with the amplitude that was observed by visual inspection of the unfiltered pressure curves.

CA50

The point at which an estimated 50 % of the fuel energy has been converted to thermal energy is termed CA50. As the LTR reactions consume some 10 percent or more of the total energy, CA50 will in most cases be found within 1 CAD before the peak of heat release. Thus CA50 is an excellent measure of combustion timing, provided combustion efficiency is satisfactory. Estimates of CA50 are given in figures 11, 19 and 27.

RESULTS

On the following three pages, illustrative examples of cylinder pressure curves and the corresponding heat release curves are given. On the bottom of the page is a summary of knock amplitude and CA50. It should be noted that curves have been chosen to illustrate combustion taking place after, near and before TDC. This was however not possible in a few cases where combustion was advanced in all operating points.

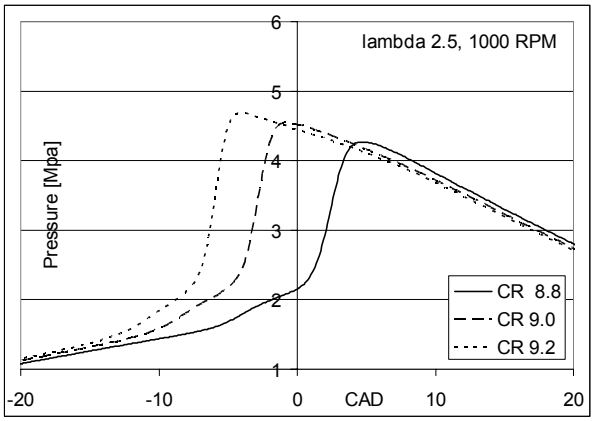

Figure 4: Cylinder pressure curves for CR 8.8, 9.0 and 9.2

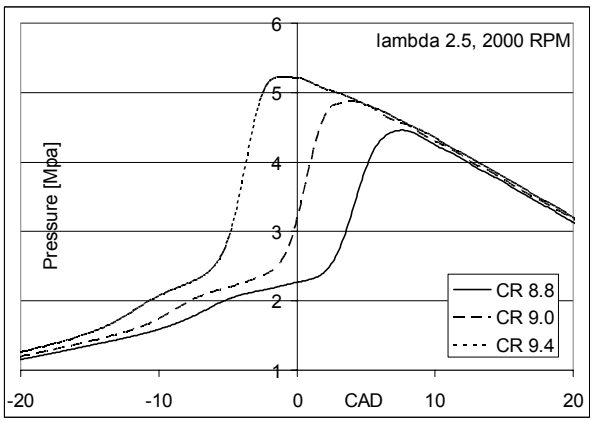

Figure 5: Cylinder pressure curves for CR 8.8, 9.0 and 9.4

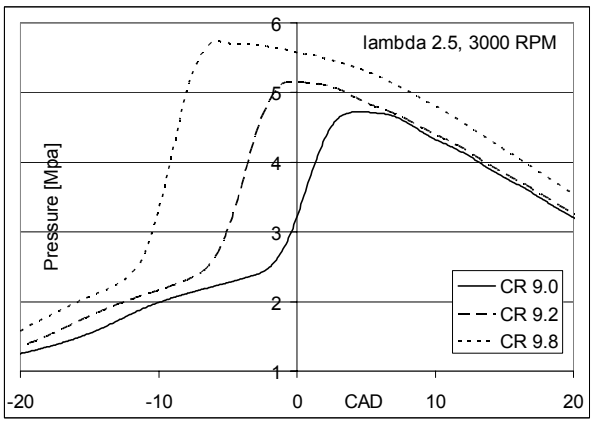

Figure 6: Cylinder pressure curves for CR 9.0, 9.2 and 9.8

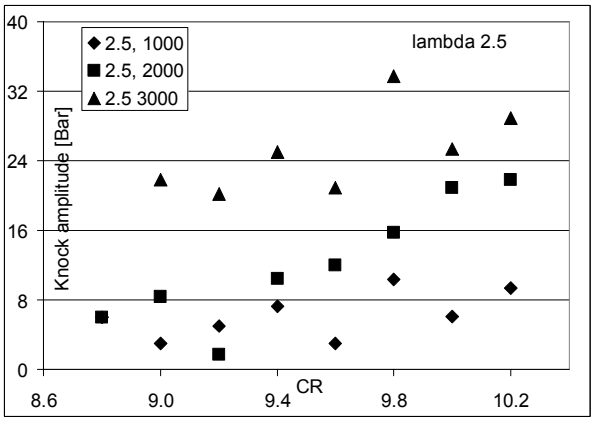

Figure 7: Knock amplitude for lambda 2.5

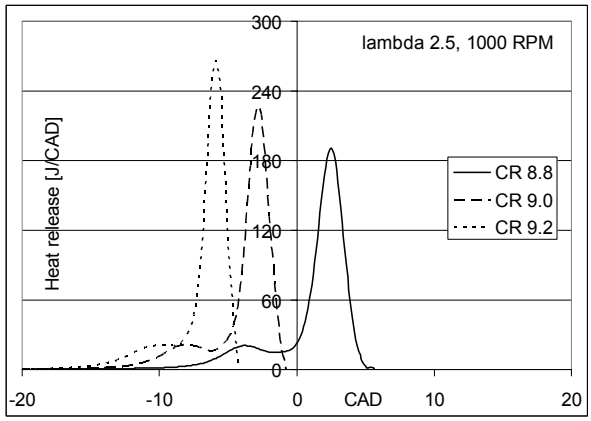

Figure 8: Equivalent heat release for CR 8.8, 9.0 and 9.2

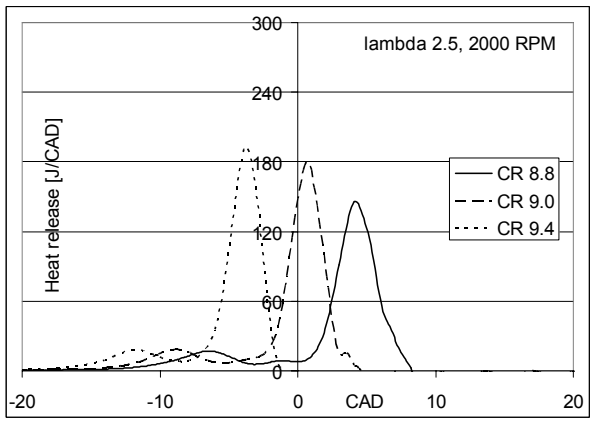

Figure 9: Equivalent heat release for CR 8.8, 9.0 and 9.4

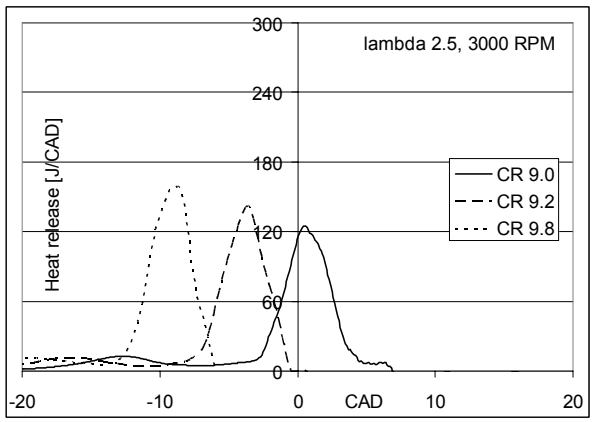

Figure 10: Equivalent heat release for CR 9.0, 9.2 and 9.8

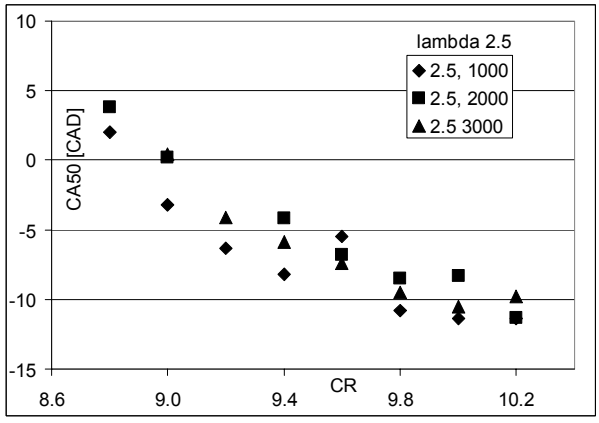

Figure 11: CA50 for lambda 2.5

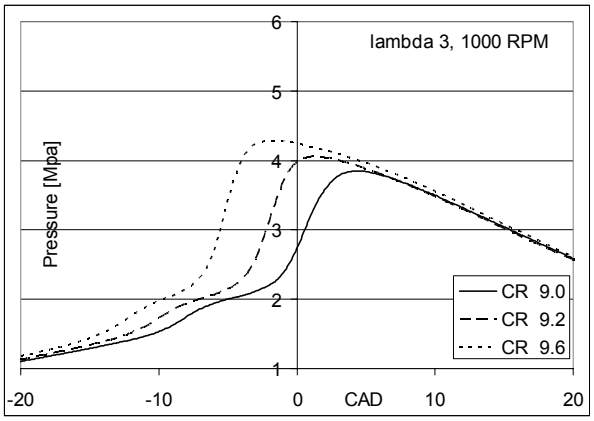

Figure 12: Cylinder pressure curves for CR 9.0, 9.2 and 9.6

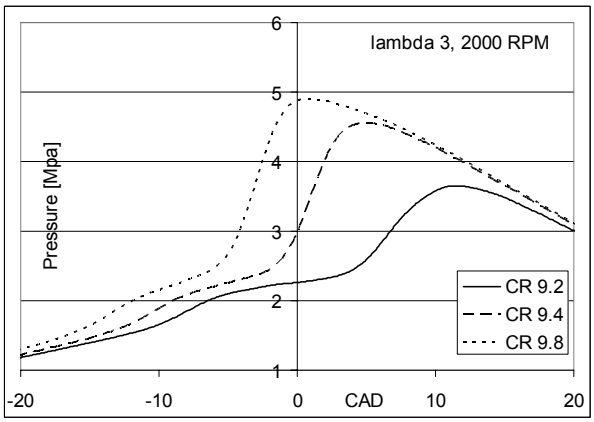

Figure 13: Cylinder pressure curves for CR 9.2, 9.4 and 9.8

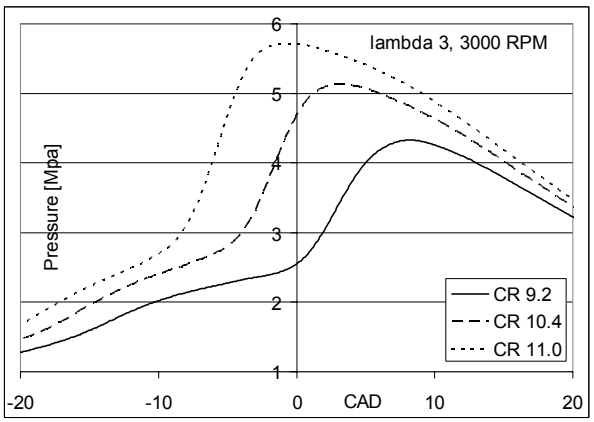

Figure 14: Cylinder pressure curves for CR 9.2, 10.4 and 11.0

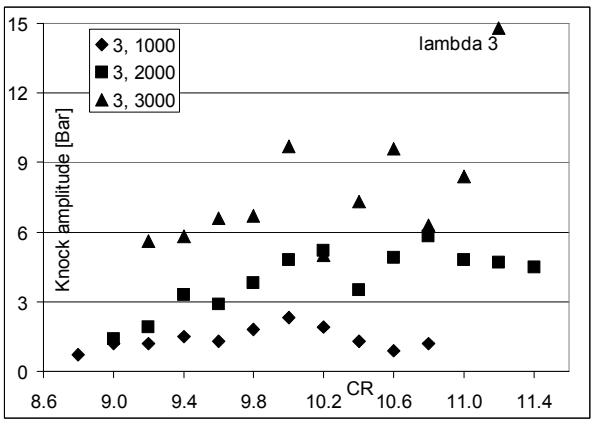

Figure 15: Knock amplitude for lambda 3

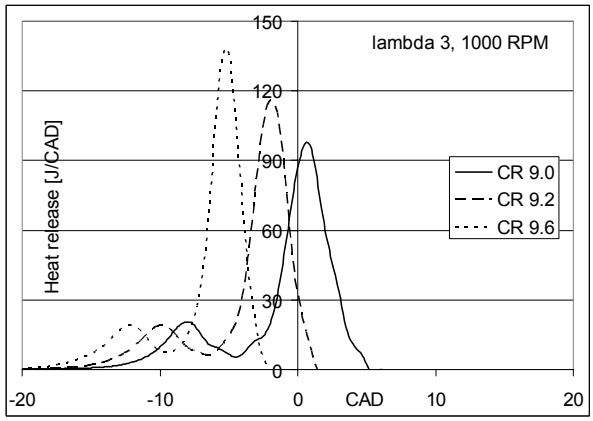

Figure 16: Equivalent heat release for CR 9.0, 9.2 and 9.6

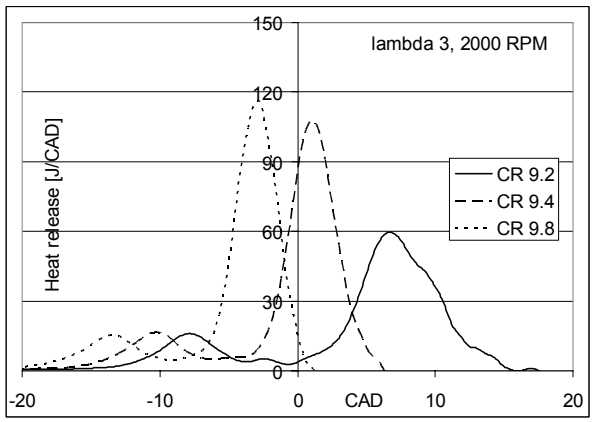

Figure 17: Equivalent heat release for CR 9.2, 9.4 and 9.8

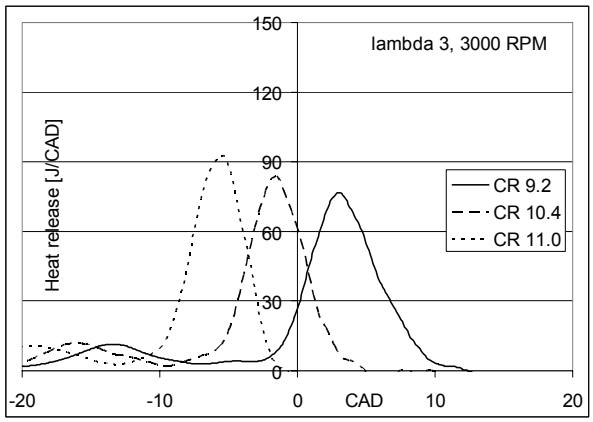

Figure 18: Equivalent heat release for CR 9.2, 10.4 and 11.0

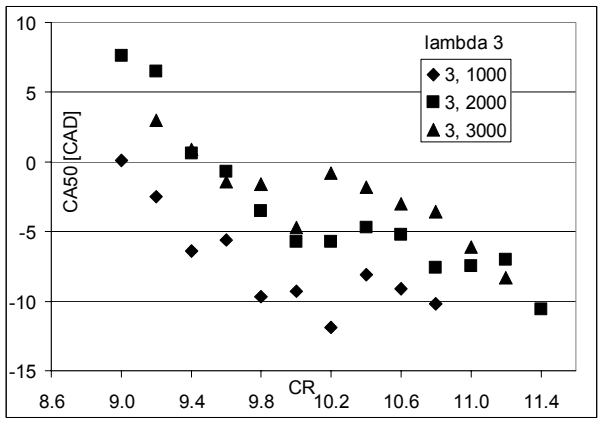

Figure 19: CA50 for lambda 3

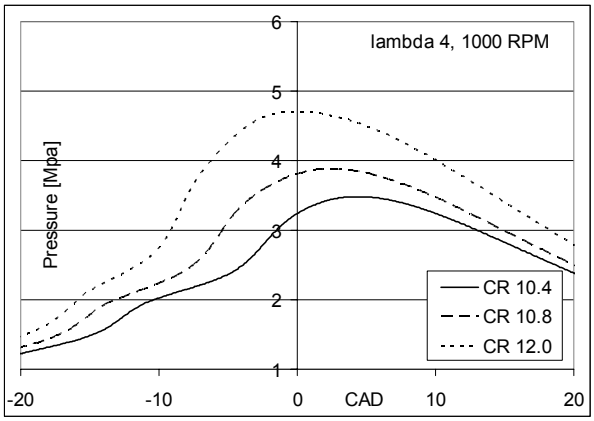

Figure 20: Cylinder pressure curves for CR 10.4, 10.8 and 12.0

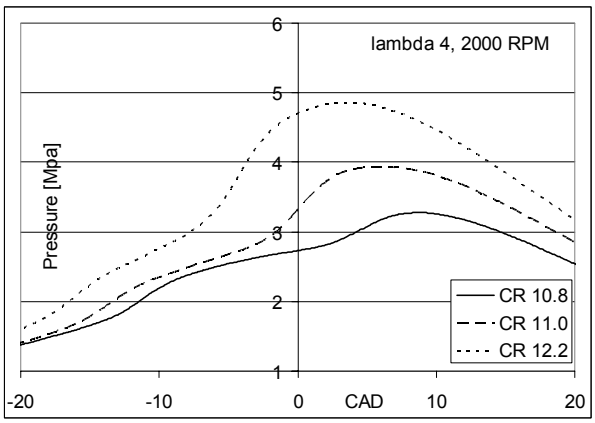

Figure 21: Cylinder pressure curves for CR 10.8, 11.0 and 12.2

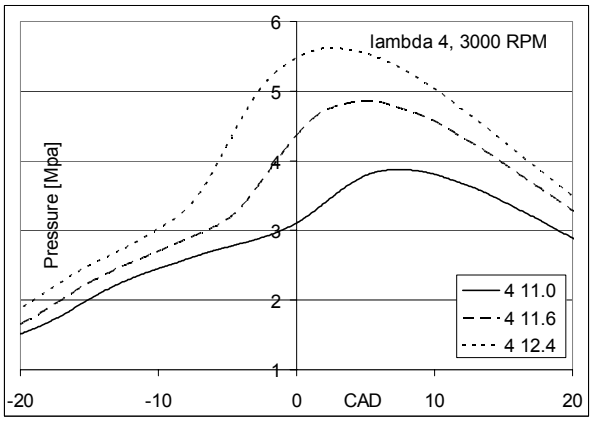

Figure 22: Cylinder pressure curves for CR 11.0, 11.6 and 12.4

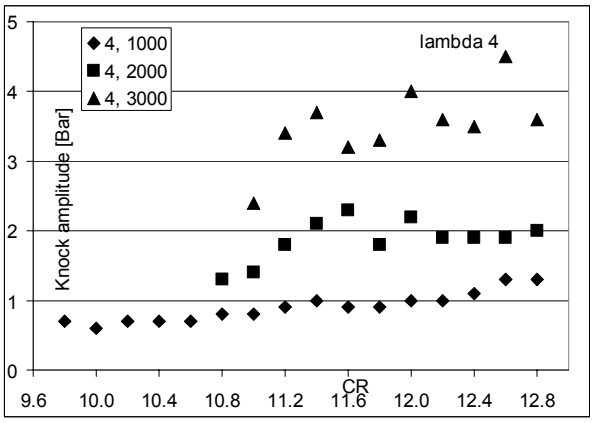

Figure 23: Knock amplitude for lambda 4

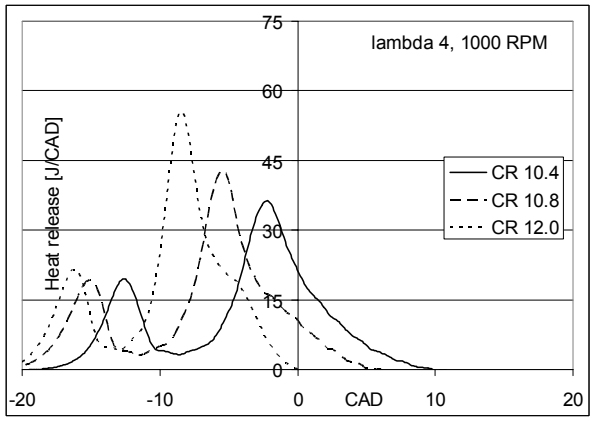

Figure 24: Equivalent heat release for CR 10.4, 10.8 and 12.0

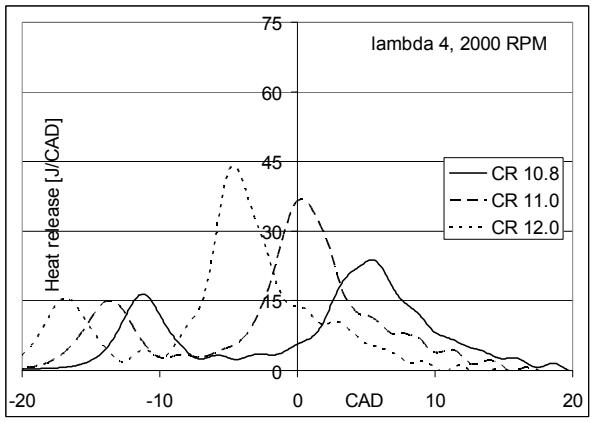

Figure 25: Equivalent heat release for CR 10.8, 11.0 and 12.2

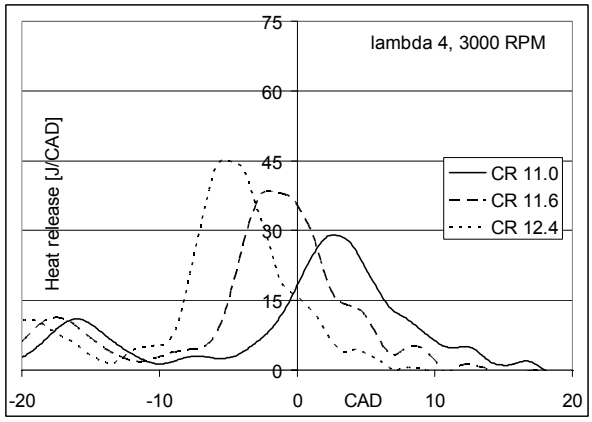

Figure 26: Equivalent heat release for CR 11.0, 11.6 and 12.4

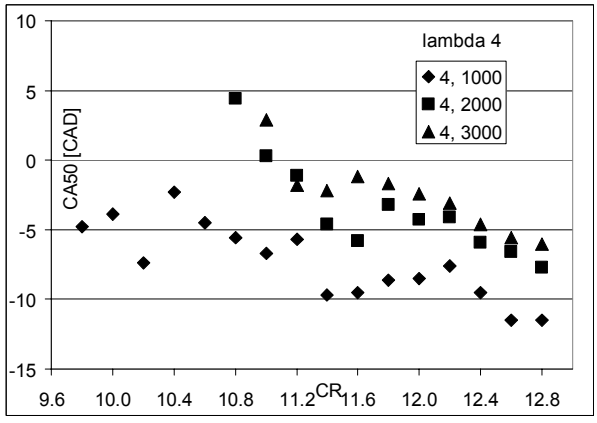

Figure 27: CA50 for lambda 4

Notes on pressure and heat release curves

The cylinder pressure curves illustrated are drawn from data which has been smoothed by moving average as described on the previous page. The cylinder pressure data recorded would otherwise have displayed super imposed pressure oscillations of varying amplitudes, ranging from merely visible at low loads to amplitudes of more than 20 Bars.

The quantity of heat release is not very precise, as the derivation of the heat release is based on a moving average of the cylinder pressure. The peaks of heat release are therefore also lower than if untreated data was used. This damping effect is highest at curves for 3000 RPM, where the average of 30 values has been used. By comparison with untreated data it is found that peaks are lowered about 30-40 percent at 3000 RPM.

Observed effects of engine speed

In general, increasing the engine speed seems to lower the rate of heat release significantly. But taking into account the effect of the data treatment that was necessary to produce the curves in the first place, the decrease in reaction rate may in fact be more modest.

It is observed that CA 50 at lambda 2.5 is slightly advanced with engine speed, which may be a result of higher compression pressure and higher in-cylinder temperatures. This seemingly counteracts the decrease in time for the reactions effectively at this equivalence ratio. At the leaner mixtures however, CA50 is delayed with higher engine speeds, indicating that the increased compression pressure and heat flux resulting from the higher engine speeds do not adequately compensate for the reduced time for reactions to finish.

Another observation is that knocking amplitude is strongly enlarged with higher engine speeds at lambda 2.5. Running with lambda 2.5 at engine speeds of 2000 and 3000 RPM produces unacceptable levels of knock with any compression ratio other than the lowest possible. Thus, operation with lambda 2.5 requires the lowest possible compression ratio and a low engine speed to avoid knock.

At lambda 3 and 4, knocking amplitude is also higher with the higher speeds, but the amplitude is closer to being acceptable especially near the lower limit of usable compression ratio. The values for lambda 3 at 3000 RPM are however beyond acceptable limits.

The LTR is not affected in a negative way by engine speed. On the contrary it is seen that LTR occurs earlier with higher engine speed.

Higher engine speeds made it generally more difficult to initiate self-sustaining combustion. This may be the result of inadequate cylinder temperatures and inadequate time for the reaction to initiate.

Observed effects of compression ratio

As expected, LTR, HTR and therefore also CA50 was generally advanced with increase in compression ratio.

At 1000 RPM for all equivalence ratios, knocking amplitude seems largely unaffected by changes to the compression ratio even though CA50 is advanced. At 3000 RPM, knocking amplitude is however increased with compression ratio. It is therefore obvious that the lowest possible compression ratio should be used if heavy knock is to be avoided at these speeds.

It should be expected that the best performance is achieved with the lowest possible CR that could sustain the combustion, as the major part of the combustion would then be positioned after TDC. However, it was found that increasing the CR beyond the point where the combustion of a given amount of fuel is self sustaining does not consistently reduce the IMEP. This may be the results of a more complete combustion, e.g. a higher conversion of CO to CO_2 and a better penetration of the thermal boundary layer that quenches the combustion.

Observed limitations of the used equivalence ratios

Lambda 2.5 will operate at all speeds with reasonable levels of knock with a compression ratio of 9.0. Operating at 3000 RPM produces excessive knock in any case and operation at 3000 RPM is therefore not an option with this equivalence ratio.

Lambda 3 requires a compression ratio of at least 9.2 to initiate combustion at all engine speeds. Operating at 3000 RPM is however not recommended, as knock exceeds 5 bars disregarding the compression ratio.

Lambda 4 requires a compression ratio higher than 11.0 to initiate combustion at all engine speeds. Knock is very limited except at 3000 RPM where knock approaches 5 bars of amplitude. The general impression was however that knock is acceptable under all conditions at lambda 4.

IMEP

Figures 28-30 display the calculated IMEP for all points of operation.

The values of IMEP achieved with lambda 2.5 show that the highest output should be expected with a compression ratio around 9. Higher compression ratios will only lower the performance, as combustion is advanced and engine knock becomes unacceptable.

For lambda 3, peak values of IMEP are found at a compression ratio of 9.2, except at 1000 RPM where peak IMEP is found at a compression ratio of 8.8. As compression ratio is increased, IMEP is lowered but remains high throughout the tested interval.

At lambda 4, IMEP peaks at a compression ratio of 10.2 for 1000 RPM, while at 2000 and 3000 RPM a much higher compression ratio of 11.4 must be used. At this point IMEP at 1000 RPM is still close to the peak value, which makes 11.4 the best solution for all speeds.

For all equivalence ratios and compression ratios it is found that increasing engine speed from 1000 RPM to 2000 RPM significantly increases IMEP The benefit of further increasing to 3000 RPM is less, probably because engine knock is higher at this speed.

Whereas the optimal compression ratio should ideally be that which results in a combustion phasing slightly after TDC, it is found that at over advanced combustion phasing does not have a very large effect on the IMEP. It may be explained by better combustion efficiency when higher compression ratios are applied.

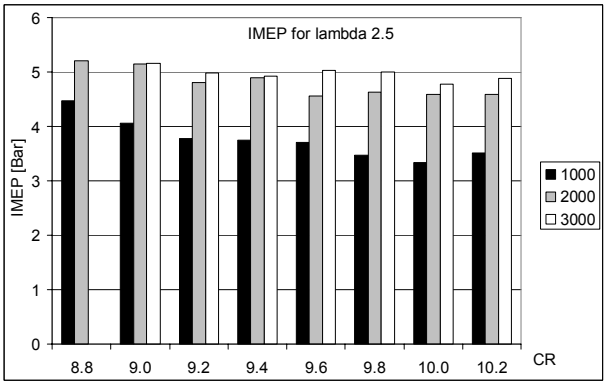

Figure 28: IMEP for lambda 2.5

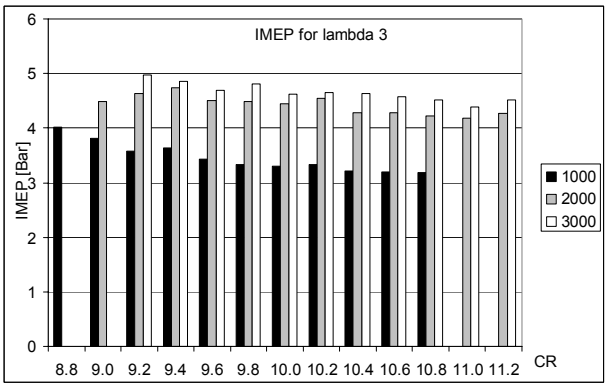

Figure 29: IMEP for lambda 3

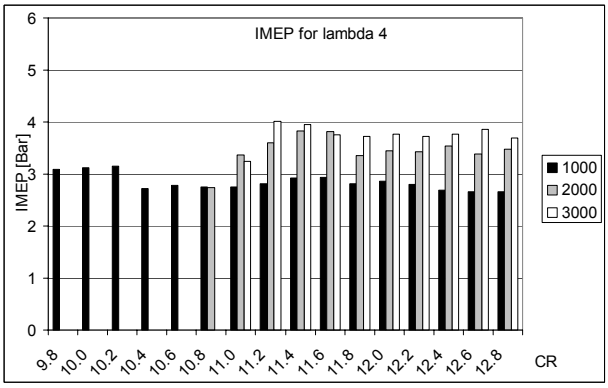

Figure 30: IMEP for lambda 4

Indicated efficiencies

Figures 31-33 contain the calculated values of indicated efficiencies. As the amount of fuel per cycle was kept constant for each lambda, the graphical representation is also the same as that for IMEP. The effects of engine speed and compression ratio on the indicated efficiencies are of course the same as are observed for IMEP.

High indicated efficiencies of 40-45 percent are observed at lambda 3 and 4 at engine speeds of 2000 and 3000 RPM. This is believed to be a result of both a higher compression ratio and less heat loss due to engine speed.

The indicated efficiency at lambda 2.5 is more modest, around 30-35 percent. This is most likely due to the lower compression ratio and higher heat losses due to higher temperatures.

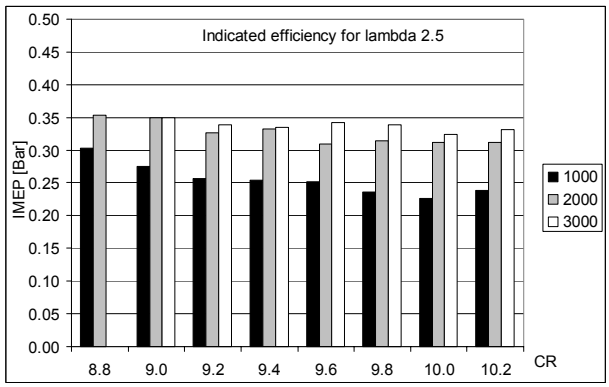

Figure 31: Indicated efficiency for lambda 2.5

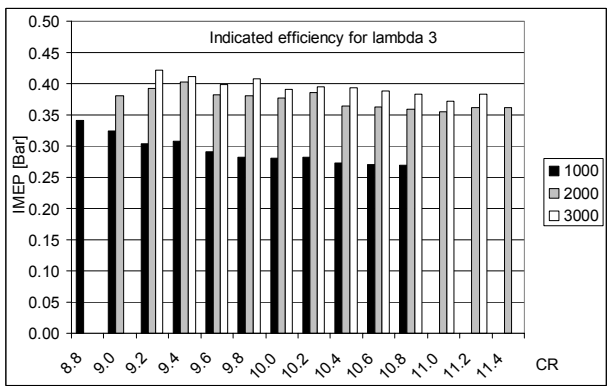

Figure 32: Indicated efficiency for lambda 3

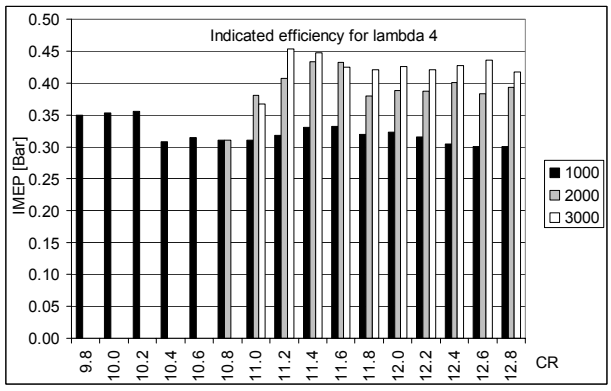

Figure 33: Indicated efficiency for lambda 4

Emissions

The emissions were used during the experiment to judge if combustion had stabilized after changing the operating point. With a stable and effective combustion, only small levels of CO were measured, indicating high combustion efficiency.

The emission levels can also be used to judge the quality of the experiment. A few outliers of higher CO are found in figure 35 at the lower compression ratios with lambda 2.5 and 3, which together with corresponding lower values of CO_2 in figure 34 indicate that fuel supply has been below target. Values of CO_2 are altogether not as constant as desired, indicating that fuel supply has not been absolutely constant.

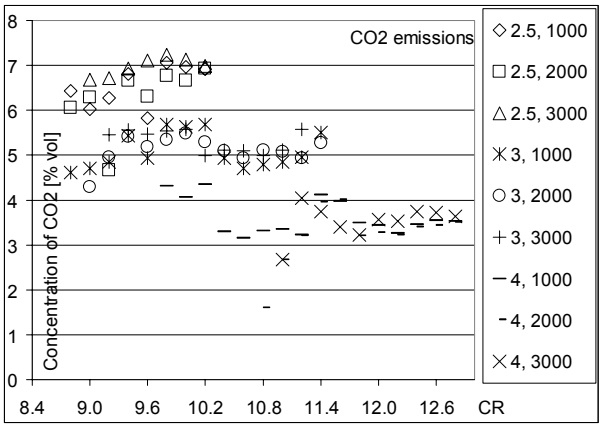

Figure 34: Measured emissions of CO2

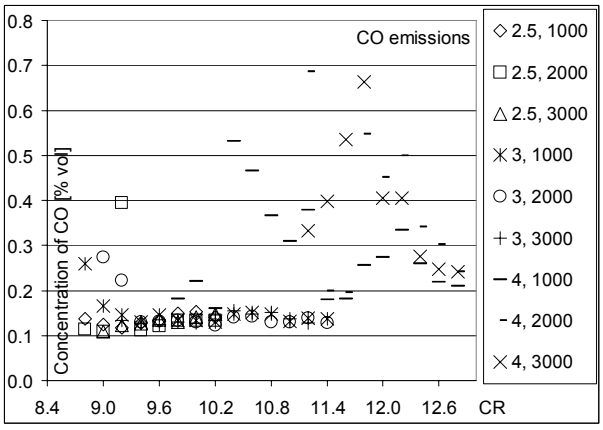

Figure 35: Measured emissions of CO

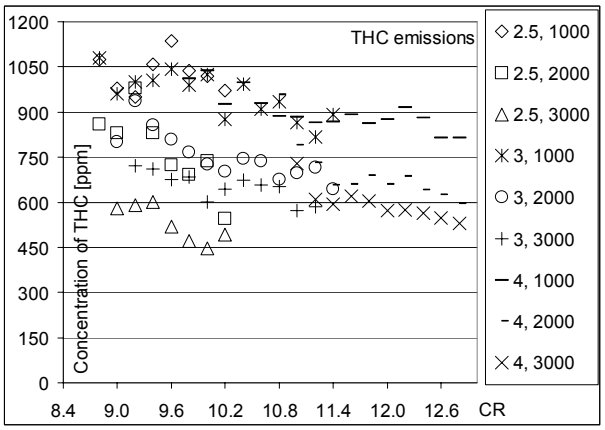

Figure 36: Measured emissions of THC

The values of CO at lambda 4 indicate that combustion efficiency is not as high as for lambda 2.5 and 3. Values are somewhat scattered, but it seems that combustion efficiency improves at the higher compression ratios, thereby resulting in less CO.

Emissions of THC are generally at levels that may be expected to be caused by the crevice volume between the cylinder liner and piston [16]. Levels are decreased with engine speed, presumably due to higher in-cylinder temperatures and more post-oxidation.

Emission of unburned DME does not pose a health risk with at concentrations, as DME is non-toxic at low concentrations. DME is also short-lived in the atmosphere where it is degraded in a photochemical process to produce CO_2 and water. Therefore emission unburned of DME is not a concern. It is however unknown to which extend DME is partially combusted, and therefore the composition of exhaust gases is unknown. But as cheap catalytic converters can be used to reduce hydrocarbons in the exhaust, emissions of hydrocarbons are not really an issue with these levels.

Comments on the uncertainties of the experiment

The compression ratio and engine speed are only some of the parameters that influence the combustion process. Other parameters are important too, but they may be more difficult to control. Some of those are:

- Temperature of cylinder wall, piston and valves
- Temperature of cooling water
- Initial cylinder pressure and temperature
- Amount of residual gas
- Volumetric efficiency
- Engine geometry

The influence of these variables means that it is difficult to isolate the effect of changing just the compression ratio or engine speed, as conditions in the cylinder changes as well. It also makes it difficult to make consistent results without careful consideration to these issues.

In a parameter study on HCCI [17] focused on temperature influence it was found that the limits of operation were highly dependant on coolant temperature. It was also experienced in this study that cooling water temperature could have significant influence on the combustion timing. Therefore cooling water temperature was monitored and cooling water flow carefully adjusted to maintain a constant temperature of the coolant at the outlet.

The temperature of piston and cylinder liner was also noticed to be of great importance. When changing from lambda 2.5 or 3 to lambda 4, it was observed that combustion was slowly retarded as piston and liner cooled under the reduced thermal load.

CONCLUSION

- It was possible to achieve values 4.5 to 5 Bars of IMEP both lambda 2.5 and 3, and around 3.5 Bars of IMEP for lambda 4.
- Indicated efficiencies of up to 40 and 45 percent could be achieved with lambda 3 and 4 respectively, whereas lambda 2.5 resulted in indicated efficiencies up to 35 percent
- The best engine performance with acceptable amplitude of knock was achieved with the leanest charge at 3000 RPM. The combustion delay and low pressure rise rates resulted in a high efficiency, low noise and high IMEP
- It was found that the different equivalence ratios used required that the compression ratio was within narrow limits to avoid knock and achieve optimum performance. A compression ratio of approx. 9.2 was found suitable for both lambda 2.5 and lambda 3, while a compression ratio of approx. 11 was required to operate with lambda 4.
- Increasing engine speed generally increases the engine knock. The amplitude of knock was generally unacceptable at 3000 RPM with lambda 2.5
- Emissions of CO and THC are generally low, except for lambda 4 which produced relatively large emission levels of CO compared to the richer mixtures.

REFERENCES

1. Zunqing Zheng, Chuntao Shi, Mingfa Yao. Experimental study on Dimethyl Ether Combustion Process in Homogeneous Charge Compression Ignition Mode. Transactions of Tianjin University, Vol. 10, No. 4, Dec. 2004
2. Hu Tiegang, Liu Shenghua, Zhou Longbao, Zhu Chi. Combustion and emission characteristics of a homogeneous charge compression ignition engine. Proceedings of the Institution of Mechanical Engineers, journal of Automobile engineering, Vol. 219, p. 1133-1139. 2005
3. Hu Tiegang, Liu Shenghua, Zhou Longbao, Li Wei. Effects of compression ratio on performance, combustion, and emission characteristics on an HCCI engine. Proceedings of the Institution of Mechanical Engineers, Journal of Automobile engineering, Vol. 220, p. 637-645. 2006
4. Keisuke Hamada, Shun Niijima, Kazunori Yoshida, Koji Yoshida, Hideo Shoji, Kazuto Shimada, Kenji Shibano. The effects of the Compression Ratio, Equivalence Ratio, And Intake Air Temperature on Ignition Timing in an HCCI Engine using DME Fuel. SAE paper 2005-32-002.
5. Masato Ikemoto, Yuichiro Kojima, Norimasa Lida. Development of the Control System using EGR for the HCCI Engine running on DME. SAE paper 2005-32-0062.
6. Tetsuo Ohmura, Masato Ikemoto, Norimasa Lida. A Study on Combustion Control by using Internal and External EGR for HCCI Engines Fuelled with DME. SAE paper 2006-32-0045
7. Hiroyuki Yamada, Masataka Yoshii, Atsumu Tezaki. Chemical mechanistic analysis of additive effects in homogeneous charge compression ignition of dimethyl ether. Proceedings of the Combustion Institute, Vol. 30, no. 2, pp. 2773-2780. 2004
8. Hideyuki Ogawa, Noboru Miyamoto, Naoya Kaneko, Hirokazu Ando. Combustion Control and Operating Range Expansion with Direct Injection of Reaction Suppressors in a Premixed DME HCCI Engine. SAE paper 2003-01-0746.
9. Zunqing Zheng, Mingfa Yao, Zheng Chen, Bo Zhang. Experimental Study on HCCI Combustion of Dimethyl Ether (DME) /Methanol Dual Fuel. SAE paper 2004-01-2993
10. Mingfa Yao, Zunqing Zheng, Jin Qin. Experimental Study on Homogeneous Charge Compression Ignition Combustion With Fuel of Dimethyl Ether and Natural Gas. Transactions of ASME, Vol. 128, p.414-420, 2006.
11. Susumu Sato, Daesu Jun, Soonpyo Kweon, Daisuke Yamashita, Norimasa Lida. Basic Research on the Suitable Fuel for HCCI Engine from the Viewpoint of Chemical Reaction. SAE paper 2005-01-0149.
12. T. Shudo, Y. Ono, T. Takahashi. Ignition Control by DME-Reformed Gas in HCCI combustion of DME. SAE paper 2003-01-1824
13. Mingfa Yao, Jin Qin, Zunqing Zheng. Numerical study of the combustion mechanism of a homogenous charge compression ignition engine fuelled with dimethyl ether and methane, with a detailed kinetics model. Part 1: the raction kinetics of dimethyl ether. Proceedings of the Institution of Mechanical Engineers, journal of Automobile engineering, Vol. 219, p. 1213-1223. 2005
14. Andreas Vressner, Andreas Lundin, Magnus Christensen, Per Tunestal, Bengt Johansen. Pressure Oscillations During Rapid Hcci Combustion. SAE paper 2003-01-3217
15. Tadashi Tsurushima, Yasuo Asaumi, Yuzo Aoyagi: The Effect of Knock on Heat Loss in Homogeneous Charge Compression Ignition Engines. SAE paper 2002-01-0108
16. Jesper Schramm, Spencer C. Sorensen. A Model for Hydrocarbon Emissions from SI Engines. SAE paper 902169.
17. M. Lida, T. Aroonsrisopon, M. Hayashi, D. Foster, J. Martin. The Effect of Intake Air Temperature, Compression Ratio and Coolant Temperature on the Start of Heat Release in An HCCI (Homogeneous Charge Compression Ignition) Engine. SAE paper 2001-01-1880

CONTACT

Troels Dyhr Pedersen
Nils Koppels Alle, Building 402, 1.st floor
Technical University of Denmark
2800 Kgs. Lyngby, Denmark
Email: tdp@mek.dtu.dk

2010-01-1489

Controlling the heat release in HCCI combustion of DME with methanol and EGR

Troels Dyhr Pedersen, Jesper Schramm
Technical University of Denmark

Tadanori Yanai, Yoshio Sato
National Traffic Safety and Environment Laboratories, Japan

ABSTRACT

The effects of methanol and EGR on HCCI combustion of dimethyl ether have been tested separately in a diesel engine. The engine was equipped with a common rail injection system which allowed for random injection of DME. The engine could therefore be operated either as a normal DI CI engine or, by advancing the injection timing 360 CAD, as an HCCI engine. The compression ratio of the engine was reduced to 14.5 by enlarging the piston bowls.

The engine was operated in HCCI mode with DME at an equivalence ratio of 0.25. To retard the combustion timing, methanol was port fuel injected and the optimum quantity required was determined. The added methanol increased the BMEP by increasing the total heat release and retarding the combustion to after TDC. Engine knock was reduced with increasing quantities of methanol. The highest BMEP was achieved when the equivalence ratio of methanol was around 0.12 at 1000 RPM, and around 0.76 at 1800 RPM.

EGR was also used to retarding the timing. With a moderate amount of EGR the effect on the combustion was not notable, but as the equivalence ratio approached unity the combustion was increasingly delayed and the rate of reaction reduced. Engine knock seized entirely as the EGR ratio was increased above 60 %. The BMEP gain was however moderate, since lower cylinder pressures at higher EGR quantities counteracted the positive effects of combustion timing.

INTRODUCTION

HCCI combustion is considered to be an efficient alternative to part load SI and CI operation. The main advantage of HCCI combustion is a high efficiency compared to SI part load, and much lower emissions of NO_x and PM than DI.

The efficiency of part load HCCI combustion is usually higher than SI part load since there are no throttling losses. The part load efficiency of HCCI can be comparable to DI CI engines, which has the advantage of a higher compression ratio but also the disadvantage of a slow combustion.

Very low emission levels of NO_x and negligible amounts of particulate matter are inherent effects of the lean and premixed combustion. NO_x formation is kept low due to a uniform low combustion temperature and PM formation is avoided due to absence of fuel rich zones.

CO and HC levels are high and comparable to untreated emissions from SI operation. CO is believed to originate from flame quenching near the combustion chamber walls, and from running the combustion very

close to the lean limit. HC is composed of both unburned fuel from the crevice volumes and partially burnt fuel from wall quenching. HC avoids post oxidation due to the lower temperatures in the cylinder and exhaust system. HC and CO emissions are however efficiently reduced in a DOC with surplus amounts of oxygen.

The lowest equivalence ratio that may be applied in HCCI combustion is determined by the minimum temperature, which must be reached to ensure rapid oxidization of CO to CO_2. This temperature is approximately 1500 K, which means that for the typical range of compression ratios in internal combustion engines the equivalence ratio cannot be less than 0.15 to 0.2. This corresponds approximately to idle condition.

The highest applicable equivalence ratio is usually limited by engine knock which may not surpass a specified tolerance limit. An equivalence ratio of 0.3 to 0.4 is commonly the limit with DME as fuel, depending on the magnitude of knock and pressure rise rates that are tolerated.

An important feature of HCCI combustion is that it relies on auto-ignition. This means that combustion timing depends on both fuel and engine properties, and a proper timing requires that fuel and engine is matched properly. In reality, changing operating conditions and demands for a large operating range mean that either engine or combustion chemistry must be manipulated to maintain an optimal operation at all times [1]. For engines, this usually means changing the effective compression ratio through variable valve timing or similar, whereas combustion chemistry may be changed by mixing fuels with different properties.

DME is an interesting fuel due to its auto ignition characteristics. It has a low temperature of auto ignition and a short ignition delay. The cetane ranking of DME is 55-60, which makes the fuel an excellent alternative to standard diesel fuel which has a cetane ranking of 45-50. The disadvantage of DME is that it has a very low lubricity. This requires that the fuel system components are designed to handle a fuel with no lubrication. In the current study a test engine with a common rail system specifically made for DME is used [18], and the lubricity is increased with Lubrizol.

DME is also suitable for HCCI operation in engines with a compression ratio is around 10. If a higher compression ratio is used, some means of delaying the combustion onset must be used to ensure optimal position of the heat release.

In this paper, methanol addition has been used to control the combustion timing in HCCI combustion of DME. The use of methanol in combination with DME has previously been demonstrated by other authors [2, 3, 4]. The common observation is that up to 30 % of methanol by mass is possible before combustion becomes retarded to the point where it fails to complete. The exact amount does however depend on the compression ratio of the engine.

Exhaust gas recirculation can also be used to delay the combustion timing. Some authors [5, 6] have looked into the subject. The use of EGR is however a challenge, since it requires a high ratio of EGR to inlet air to achieve the desired effect, as demonstrated in this paper. EGR works mainly by increasing the concentration of CO_2 and H2O, which increases the specific heat capacity and decreases the specific heat ratio. This reduces the temperature increase during compression and combustion. Secondly, it reduces the amount of oxygen which is normally not desired in diesel engines, meaning they are usually not capable of operating with more than 30 % EGR. In HCCI combustion however, it is possible to operate with much lower oxygen concentrations. It is only required that the concentration of oxygen is sufficient to complete the combustion.

The compression ratio used here (14.5) is much higher than comparable studies with pure DME [7, 8]. The high compression ratio was selected since it is suitable both for normal DI CI operation and for HCCI operation. This is considered a requirement, since HCCI operation cannot operate at higher loads.

LOW TEMPERATURE REACTIONS

Methanol affects the combustion timing by consuming OH radicals [9, 10]. The balance between OH production and consumption plays a crucial role in the low temperature reaction paths. By suppressing the low temperature reactions, the high temperature reactions which constitute the major part of the heat release are consequently delayed.

HCCI combustion of DME is always initiated by a series of low temperature reactions, also known as cool flames. These are characterized by producing up to 20 % of the heat release in a rapid, self terminating reaction. The reactions are self terminating due to an alternative reaction path that becomes dominating as the temperature rises, thereby consuming the important OH radicals faster than they are produced in the chain branching reactions. As the branching reactions cannot continue without the OH radicals the low temperature reactions are deactivated as temperature increases.

Curran et al developed the mechanism DME 2000 [11], from which the key reactions were found in a CHEMKIN II simulation. The initial low temperature reaction path looks as follows:

$$CH_3OCH_3 + OH \rightarrow CH_3OCH_2 + H_2O$$
$$CH_3OCH_2 + O_2 \rightarrow CH_3OCH_2O_2$$
$$CH_3OCH_2O_2 \rightarrow CH_2OCH_2O_2H$$
$$CH_2OCH_2O_2H + O_2 \rightarrow O_2CH_2OCH_2O_2H$$
$$O_2CH_2OCH_2O_2H \rightarrow HO_2CH_2OCHO + OH$$
$$HO_2CH_2OCHO \rightarrow OCH_2OCHO + OH$$

A few more steps lead to the formation of formic acid which is a stabile intermediate species in the low temperature reaction scheme. These reactions do not form or consume any OH radicals. The net production rate of OH is therefore positive.

As the temperature increases, the reaction path changes to formation of formaldehyde which reacts with OH in two reactions:

$$CH_2OCH_2O_2H \rightarrow 2 \cdot CH_2O + OH$$
$$CH_2O + OH \rightarrow HOCH_2O$$
$$CH_2O + OH \rightarrow HCO + H_2O$$

The HOCH2O radical reacts further to formic acid without OH radical intervention, while HCO is a stabile intermediate in the low temperature reaction scheme and does not react further. Since two CH2O radicals are formed for each fuel molecule, the net production rate of OH is negative for this reaction path. This causes the concentration of OH radicals to decrease swiftly. As reactions proceed slowly without the OH radical, the heat release ceases while the temperature increases.

Reactions do however not stop entirely. The methoxy-methyl radical is split into formic acid and a methyl radical in the time between the low and high temperature reaction events:

$$CH_3OCH_2 \rightarrow CH_3 + CH_2O$$

This reaction creates radicals continuously and increases the temperature further along with the adiabatic temperature increase from compression. The radicals formed require additional OH radicals to be further oxidized. Therefore, consumption of OH radicals by other reactions, such as those with methanol, will further delay the formation of the stabile intermediates.

Methanol is an efficient consumer of OH radicals. It reacts mainly with OH in two chain terminating reactions:

$$CH_3OH + OH \rightarrow CH_2OH + H_2O$$
$$CH_3OH + OH \rightarrow CH_3O + H_2O$$

Both of these radicals react again to form formaldehyde without OH interaction. The reactions with methanol are therefore using OH radicals that would otherwise be used in the low temperature reaction paths of DME. By varying the concentration of methanol the OH radical concentration is therefore suppressed. This also suppresses the heat release and the buildup of intermediate species in the low temperature reactions. The lower temperature decreases the thermal cracking of the methoxy-methyl radical, while the reduced production of intermediate species reduces the overall reactivity of the gas.

The suppressing effect of methanol is strong enough to stop the low temperature reactions entirely when the concentration reaches a certain level.

The motivation for controlling the cool flame region is that it produces a large amount of heat and radicals (mainly formaldehyde, formic acid and hydrogen peroxide) that are important for the high temperature reactions, which produce the majority of the heat release. By lowering the temperature increase and the amount of radicals, the onset of high temperature heat release is delayed consequently. This makes it possible to position the major part of heat release close to or after TDC as desired, in order to improve the thermal efficiency.

The high temperature reactions of DME follow the normal mechanisms as other hydrocarbons. The details of the full high temperature mechanism are given in [12].

EXPERIMENTAL SETUP

A four cylinder, 4.6 L ISUZU truck engine was used. The engine and the development of the common rail system are further described in earlier papers [13, 14 and 18]. Table 1 shows the data for this engine

This engine was already modified to run on DME, with the major modification being a common-rail injection system specifically designed for DME. Another important modification was the addition of an EGR cooler which proved capable of allowing a large flow of EGR gas in the second part of the experiment.

The engine was equipped with a turbocharger and intercooler. These could have been dismounted to avoid changes to the cylinder filling and hence the equivalence ratio during the tests. It was decided however to leave the turbocharger on since exhaust temperatures would be quite low, which would mean that the turbocharger

would not be increasing the pressure. Additionally it was argued that it would make more sense to compare HCCI data with DI CI data on the same engine if the setup was identical. The turbocharger did however increase the absolute pressure up to 1.2 bars at 1800 RPM as the total equivalence ratio was increased with methanol, which meant that the equivalence ratio for DME became lower than the target.

Engine	ISUZU 4HG1T
No. of cylinders	4
Bore x Stroke	115 mm x 110 mm
Connecting rod length	250 mm
Displacement	4.57 L
Compression ratio	14.5 (19.0 original)
Injection system	DME Common rail
Rated power	88 kW @ 3000 RPM
Rated torque	322 Nm @ 1800 RPM

Table 1: Engine specifications

The engine was coupled with a speed regulated motor-generator equipped with a load cell for measuring torque, which was used for calculating BMEP. The cylinder pressure was measured on all 4 cylinders with piezoelectric pressure pickups and logged in intervals of 1 CAD.

The geometric compression ratio was reduced from 18 to 14.5 by enlarging the piston bowls. The bowl geometry was maintained to enable normal DI CI operation.

Changing the engine to HCCI operation required that the electrical connections for the common rail injector were switched pair wise, due to a limited advance setting in the injector driver software. The injectors were then set to inject at the beginning of the intake stroke, since this should result in good mixing. The emission values did not indicate leakage of DME through the exhaust valves when this injection timing was used.

METHANOL INJECTION SYSTEM

Four low pressure gasoline injectors were installed in a custom inlet manifold. The methanol was supplied from a tank that was pressurized to three Bar. Injector drivers enabled accurate control of the injection duration and timing. The injection was adjusted to begin at inlet valve opening. Varying the timing showed no significant change to the heat release or emissions, so it was kept at this position throughout the test.

TEST CONDITIONS

Prior to all tests the engine was heated in normal DI CI operation with DME. After 30 minutes of preheating the engine was stopped and the injector leads were switched to inject at 360 BTDC for HCCI operation.

The tests were performed at engine speeds of 1000 and 1800 RPM. These two engine speeds used were chosen since part load operation usually implies running at lower engine speeds. It is however fully possible to operate with DME HCCI combustion at higher engine speeds, such as 3000 RPM.

METHANOL TEST PROCEDURE

In the first part of the experiment the amount of DME injected was kept constant. Methanol was then added to the intake manifold in increasing amounts. The injector opening time was increased in steps of 1 millisecond and the equivalence ratio of methanol to air calculated subsequently. The increased amount of methanol retarded the combustion as expected. Ultimately partial combustion and misfire was observed. This was indicated by increasing levels of CO and THC in the exhaust, as well as unsteady operation and decreasing torque. This meant that the optimum amount of methanol had been passed, which concluded the test.

The equivalence ratio of DME was kept at approximately 0.25. This equivalence ratio results in moderate engine knock in the given engine, particularly when combustion timing is advanced as was the case before methanol or EGR was applied. By adding a sufficient amount of methanol the experience was however that combustion noise was reduced, despite the increase in total fuel amount.

A major problem with port fuel injection of methanol is that it is difficult to obtain a good vaporization into the air stream. A part of the methanol will enter the engine as droplets rather than as a gas. These droplets are likely to dissolve into the lubricating oil when they come into contact with the cylinder wall.

During the experiment it was observed that methanol was evaporating from the crankcase ventilation, which had been disconnected from the inlet manifold. This meant that the amount taking part in the reaction could only be calculated by an exhaust carbon balance. The equivalence ratio of methanol in the combustion was therefore calculated from the carbon balance, with the equivalence ratio of DME being determined without injection of methanol. The method given by Heywood [15] for determining equivalence ratio from exhaust gas composition of fuels containing oxygen was used. The carbon and hydrogen numbers (m, n and o) in the calculation were adjusted from the mole fraction determined. The mole fractions of the calculated species differed from the measured species by less than 2 %.

EGR TEST PROCEDURE

The test with EGR was also conducted with an equivalence ratio of approximately 0.25 for DME. The equivalence ratio was measured without EGR. The amount of DME injected was then kept constant by maintaining the injection duration.

EGR was gradually increased in steps of 10 percent. The exhaust back pressure sufficed to ensure that the EGR was guided back to the inlet manifold up to about 60 % EGR. Hereafter the inlet air was throttled slightly to force additional EGR uptake. The amount of EGR was calculated from accurate inlet air flow measurements while assuming a constant volumetric efficiency. This was justified by the inlet temperature being constant due to the efficient water cooled EGR cooler.

At very low concentrations of remaining oxygen in the exhaust gas the combustion efficiency started to drop with increasing emissions of CO and HC, at which point the test was ended. The effect of increasing the EGR is observed from figures 5-8.

EMISSIONS MEASUREMENT

All emissions were measured with a Horiba MEXA 7500 DEGR. This analyzer has two direct lines. The gas was collected before and after the DOC in the exhaust pipe. The measured gases, detection technology and range are found in table 2.

	Technology	State	Range
CO_2	NDIR	Dry	0-20%
CO	NDIR	Dry	0-12 %
CO	NDIR	Dry	0-5000 ppm
O2	MPD	Dry	0-25 %
THC	FID	Wet	0-5000 ppm
CH4	NMC-FIC	Wet	0-5000 ppm
NMH	Calculated	Wet	0-5000 ppm
NO_x	CLD	Dry	0-500 ppm

Table 2: Measured species

RESULTS

CYLINDER PRESSURE AND HEAT RELEASE

The net heat release was calculated without compensation for heat loss and with a constant specific heat ratio of 1.37, since only position and duration were of interest. The magnitude of the peaks is also reduced due to the filtering necessary to remove noise from the signal.

THE EFFECT OF METHANOL ON THE COMBUSTION

Figures 8 and 9 show how the rate of heat release in the low temperature reactions is both delayed and reduced with an increasing equivalence ratio of methanol. The time between end of low temperature reactions and high temperature reactions is also extended. The high temperature heat release is delayed but increased in magnitude. The increase in HTR heat release is due both to the additional amount of fuel and the heat that was not preserved due to the absence of LTR heat release.

The delays in heat release are seen to be somewhat proportional to the amount of methanol added initially. The delay caused by going from equivalence ratio 0.117 to 0.12 is however much stronger in the 1000 rpm case, and also when moving from 0.07 to 0.076 in the 1800 RPM case. The combustion process is thus much more sensitive to a marginal increase in this region. This suggests that accurate control of fuel composition is required for successful operation with this dual fuel combination.

Less methanol is required for the same delay in terms of CAD at 1800 RPM compared to 1000 CAD. The delay measured in time is however roughly equivalent to the 1000 RPM case. But since less delay in time is required for the same delay in CAD at the higher engine speed, a smaller quantity of methanol can be added before the combustion is retarded so much that it fails to ignite.

HEAT OF VAPORIZATION

Another effect of port fuel injection of methanol is that it has a cooling effect on the inlet air, which further delays the combustion. The heat of vaporization for methanol is approximately 1200 kJ/kg and the heat capacity of air approximately 1 kJ/kg-K at 298 K. For small amounts of methanol evaporating into air, the temperature decrease will therefore be around 1.2 K per gram of methanol evaporating into 1 kg of air. Figure 1 shows the expected temperature decrease for the range of amounts used in the experiment. It should be noted that this is only valid if the methanol evaporates adiabatically. The actual decrease will be less due to wall heat transfer.

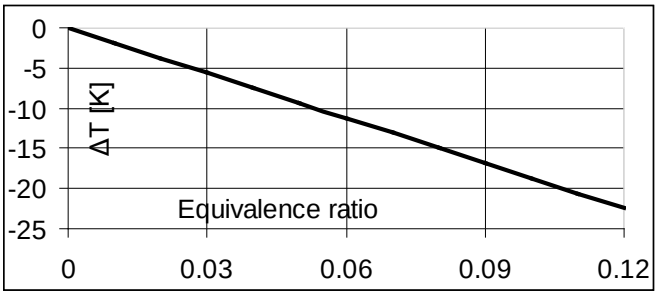

Figure 1: Cooling effect of methanol on inlet air

ENGINE KNOCK REDUCTION WITH METHANOL

HCCI combustion of DME creates a very hard sound, though it is not harmful to the engine in the same way as SI engine knock. The temperature and pressure is not high enough to damage the engine at lean conditions. The sound is however undesired and sometimes unacceptably high. Reduction of the knock is therefore a high priority.

The rate of reaction for the high temperature reaction increased to more than twice the initial value as the equivalence ratio of methanol was increased to 0.12 in the 1000 RPM test. The pressure rise rate increased up to about 10 Bar/CAD with the highest amount of methanol. The sharp knocking sound observed with pure DME combustion was however reduced with increasing amounts of methanol. There was no equipment available to verify this tendency, so no data can be presented. A possible explanation is however that methanol not only increases ignition delay, but also the octane rating of the fuel [16, 17]. As the octane rating is increased, so is the fuels ability to resist detonation which is the primary cause of knock. The increased pressure rise rate is thus not a problem, since it is more uniform and hence does not cause any transmission of noise through the engine.

BMEP

The increase in BMEP (figure 2) is caused both by the increase in total fuel amount and the retarded combustion. The increases are very linear in both cases and follow the same line.

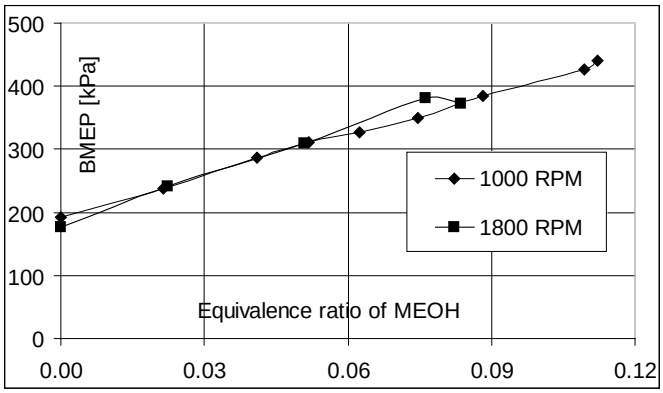

Figure 2: BMEP vs. MEOH equivalence ratio

Since the total equivalence ratio did not reach the same level at 1800 RPM as the 1000 RPM case, the BMEP did not reach the same level either. To increase the torque it would be required to increase the amount of DME and balance the combustion timing with methanol.

THE EFFECT OF EGR ON COMBUSTION TIMING

Figures 10 and 11 shows that the combustion timing was retarded approximately 12 CAD when the EGR ratio was increased from 0 to 65 % for both 1000 and 1800 RPM.

There was no notable effect on the heat release rate within this interval. The peak pressure was however reduced 8 bar in the 1000 RPM case and 13 bar in the 1800 RPM case. At 1000 RPM the turbocharger is not active, and hence the pressure reduction is due both to the increase in specific heat capacity resulting from increasing concentrations of water and carbon dioxide, as well as the inlet throttling required to force additional EGR back to the inlet manifold. At 1800 RPM the pressure increase from the turbocharger is reduced when EGR is increased, so the pressure reduction is also due to a decrease in inlet manifold pressure.

BMEP is increased with increasing amounts of EGR (figure 3), despite the decrease in peak pressure. This is due to lower heat losses and increased expansion work which are the consequences of later combustion. The BMEP is only slightly higher at 1800 RPM, despite a notable increase in compression pressure at this speed due to the turbocharger.

It was not possible to retard the combustion as much as desired. The optimum timing would have been somewhere around 10 CAD after TDC, but the latest timing achieved was a few CAD before TDC.

It was noted that the combustion timing became very sensitive to changes in the EGR at the highest ratios used, where the exhaust gas oxygen concentrations were low. Changing the EGR rate from 65 to 70 % caused a delay of 5 CAD, the same result as changing from 0 to 60 %. It is most likely due to the fact that the oxygen concentration is more important for the reaction rate when it is closer to the stoichiometric limit.

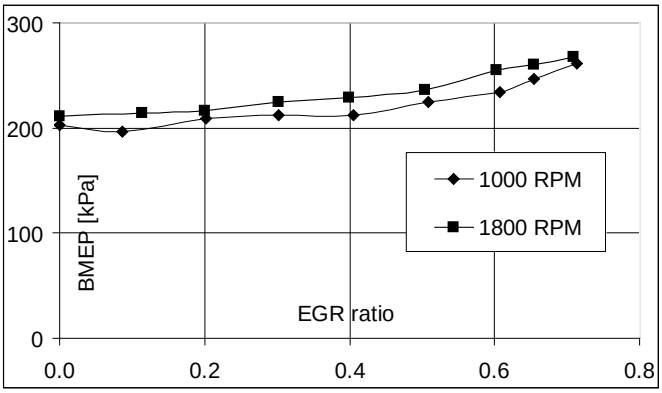

Figure 3: BMEP vs. EGR ratio

It is also observed that the peak pressure is greatly reduced as the amount of EGR increases. This does however not mean that the power is reduced. Both torque and IMEP increases with increasing EGR percentage. The reason is that the compression work is reduced at a greater rate than the expansion work. A secondary effect is that friction work is also reduced slightly as the cylinder pressure decreases.

With EGR there was a notable change in the engine sound as the exhaust oxygen concentration reached 3-5 %. The engine sound changed to become very quiet, which must be a result of a decreased rate of reaction.

As the combustion becomes increasingly sensitive to exhaust gas concentration of oxygen, the EGR valves should possibly be controlled using feedback from an exhaust gas measurement with a broadband lambda sensor. This would ensure that the optimum concentration of oxygen is maintained.

PERFORMANCE RELATIVE TO DI CI

Table 3 shows the performance at each operating condition, at the highest brake efficiency obtained. The BSFC is given as diesel fuel equivalent.

Table 4 shows the performance at similar loads previously recorded for the same engine operating in DI CI mode. The engine was fitted with a jerk-type pump and injection system made for DME and operating at the standard compression ratio of 19 [13]. The data are those achieved at optimum BSFC. It is worth noticing that the BSFC achieved in HCCI operation with methanol is not much higher than those of the same engine in DI CI part load, despite the difference in the compression ratio.

Mode	HCCI DME+ MEOH	HCCI DME+ MEOH	HCCI DME+ EGR	HCCI DME+ EGR
Speed	1000	1800	1000	1800
Torque [Nm]	160	138	95	97
Power [kW]	16.8	26.1	9.9	18.3
BMEP [kPa]	441	380	261	267
η_e	0.35	0.31	0.29	0.26
Bsfc [g/kWh]	236	266	287	320

Table 3: Performance at highest brake efficiency

Mode	HCCI DME+ MEOH	HCCI DME+ MEOH	HCCI DME+ EGR	HCCI DME+ EGR
Speed	1000	1800	1000	1800
Torque [Nm]	150	161	75	81
Power [kW]	15.7	30.3	7.9	15.3
BMEP [kPa]	412	443	206	223
η_e	0.36	0.37	0.33	0.29
Bsfc [g/kWh]	235	230	260	290

Table 4: Performance of the engine in DI CI mode

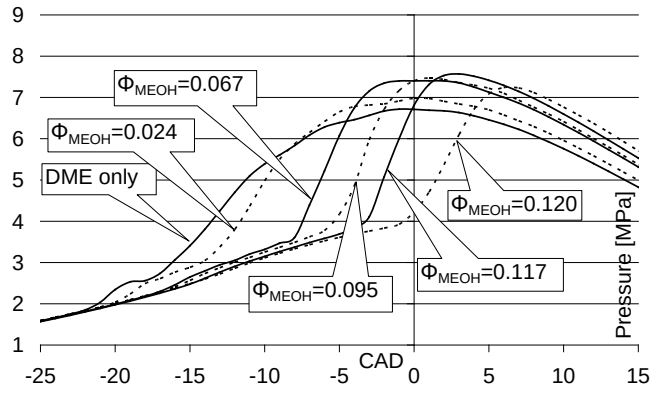

Figure 4: Cyl. pressure, DME + MEOH at 1000 RPM

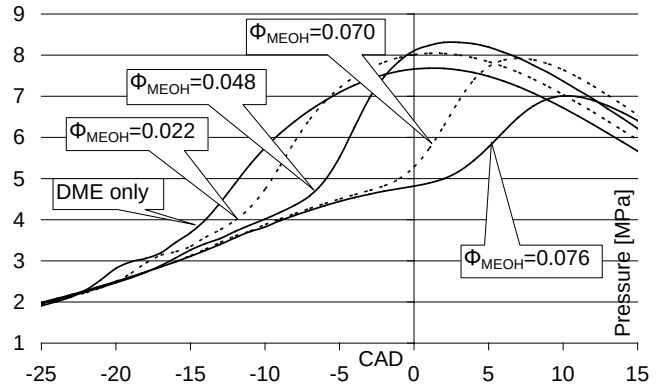

Figure 5: Cyl. pressure, DME + MEOH at 1800 RPM

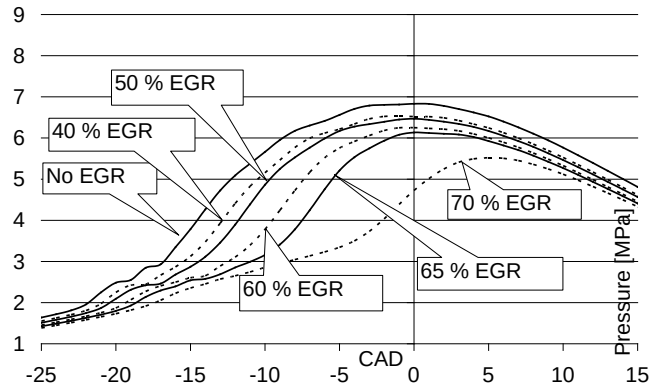

Figure 6: Cyl. pressure, DME + EGR at 1000 RPM

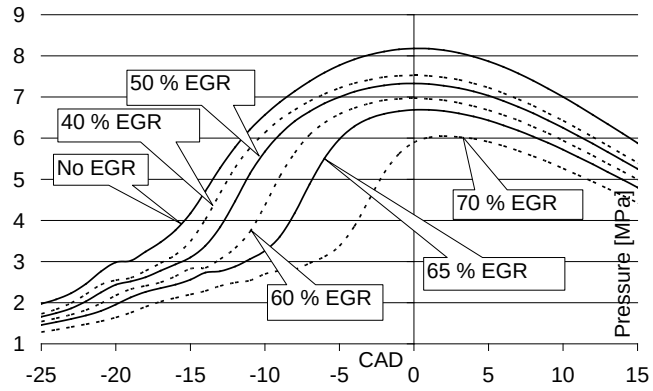

Figure 7: Cyl. pressure, DME + EGR at 1800 RPM

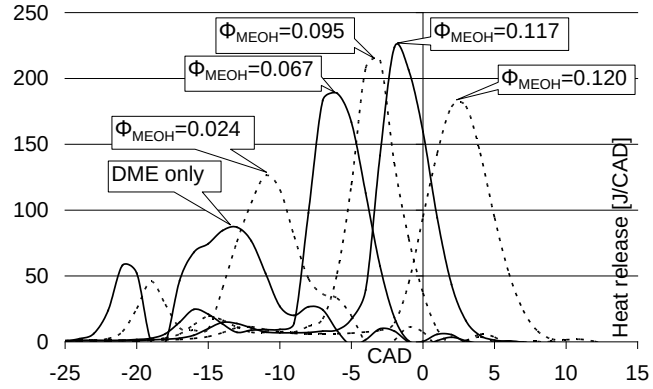

Figure 8: Heat release, DME + MEOH at 1000 RPM

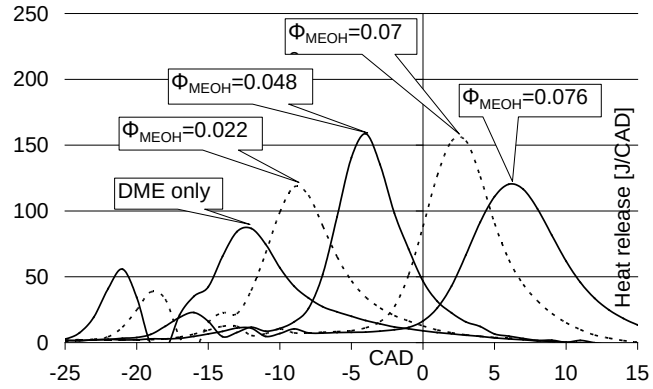

Figure 9: Heat release, DME + MEOH at 1800 RPM

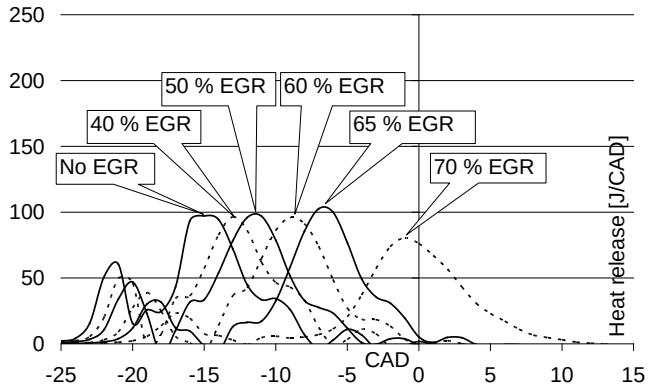

Figure 10: Heat release, DME + EGR at 1000 RPM

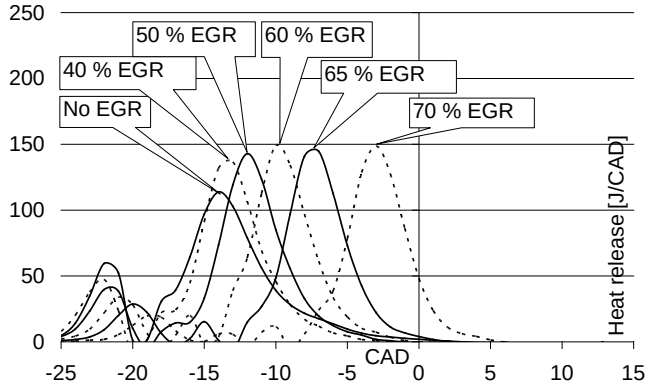

Figure 11: Heat release, DME + EGR at 1800 RPM

COMPARISON WITH SIMULATIONS

A 0-D CHEMKIN II simulation was made for the 1000 RPM tests. The CHEMKIN model used was the 0-D closed homogeneous IC engine reactor. The model was setup with the same parameters as the engine tested. Heat transfer was modeled with the built-in Woschni correlation.

For the experiment with methanol, mole fractions of methanol and DME identical to those used in the test were implemented in a parameter study. The reactor initial temperature was decreased with increasing equivalence ratio of methanol according to figure 1. The result of the simulation has been plotted in figure 12.

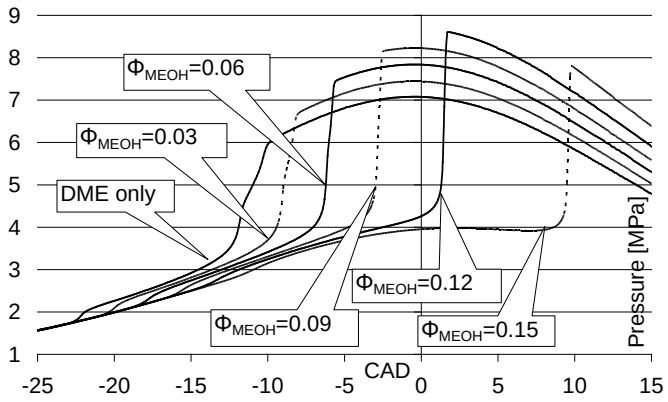

Figure 12: Simulated effect of methanol, 1000 RPM

The delay caused by increased quantities of methanol in figure 12 is quite similar to the observed delay. The simulation does allow for a slightly higher equivalence ratio of methanol before misfire, which occurs at an equivalence ratio around 0.16. The pressure rise rate in the simulation is not comparable to the experiment since the simulation is 0-dimensional only.

In the EGR case, a simple model of the inlet gas composition assuming complete combustion was made and the composition entered in the parameter study. The inlet conditions were kept constant. The result of this simulation is shown in figure 13.

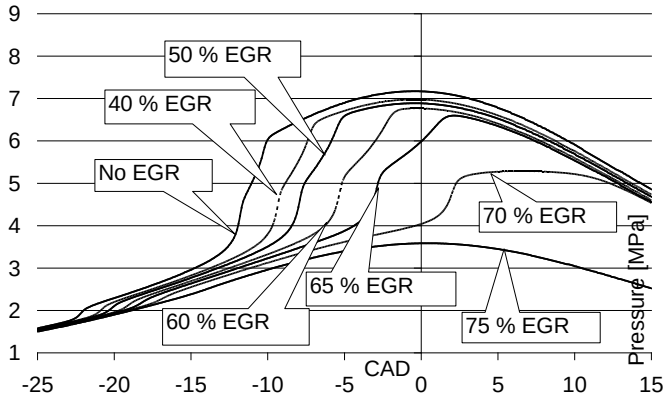

Figure 13: Simulated effect of EGR, 1000 RPM

The simulation of the EGR case shows largely the same delay as the experiment. A case with 75 % EGR is included in the simulation, which interestingly seems to result in lack of both low and high temperature reactions. In the experiment, the combustion timing was very sensitive to changes as 75 % EGR was approached. At 70 %, the reactions take much longer to complete, which is also visible in the figure. This indicates that chemical kinetics is indeed affected, as the observed effects appear both in the experiment and the simulation. It is likely a combination of a reduced concentration of oxygen that affects the low temperature reactions, as well as the increased heat capacity of the inlet gas.

EMISSIONS

The emissions in table 6 are those obtained at the best brake efficiency. The specific emissions are calculated both before and after the DOC. The DOC efficiently converts HC and CO even at the relatively low exhaust temperatures resulting from lean HCCI combustion.

The conversion efficiency of CO to CO_2 in the DOC was close to 100 % at all times, whereas HC was reduced with a factor of 10 most of the time.

The specific emissions shown in figures 14-16 are those measured during the experiments. They are plotted against the engine power, which in all cases increased with either increasing amounts of methanol or EGR.

Since fuel flow could not be measured, a carbon balance based on the exhaust emissions and air flow measurements were used to calculate the specific emissions. The CO_2, CO and THC emissions after the DOC were used for making the carbon balance. The calculations take into account humidity (0.13 kg/kg dry air) and CO_2 (380 ppm) in the inlet air.

RPM	1000	1800	1000	1800
	DME + MEOH	DME + MEOH	DME + EGR	DME + EGR
Specific emissions before DOC [g/kWh]				
CO_2	680	710	930	1075
CO	13	42	49	13
THC	22	25	13	11
NO_x	0.14	0.04	0.03	0.08
Specific emissions after DOC [g/kWh]				
CO_2	733	810	1059	1108
CO	0.02	0.67	0.88	0.01
THC	2.7	7.5	2.8	1.1
NO_x	0.12	0.05	0.16	0.07

Table 5: Specific emissions before and after DOC

<u>NO_x</u>

The specific emissions of NO_x before the DOC are plotted in figure 14. The range was generally from 2-30 ppm, with the majority being less than 20 ppm. Accuracy is still good in this region, since the MEXA measures NO_x from 1 ppm with +/- 2 % point accuracy.

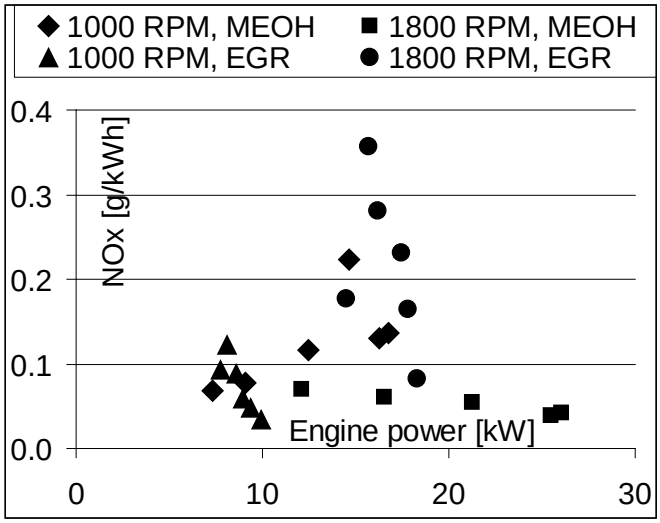

Figure 14: Specific NO_x emissions during testing

The instrument does however not allow for separate determination of NO and NO_2. The majority of nitric oxide is therefore considered to be NO. Specific emissions are therefore calculated from a molar mass of 30 g/mol.

The DOC is known to convert NO to NO_2 to some degree, depending on the catalyst temperature. Since NO_2 is generally considered more harmful than NO, it may be argued that using a DOC to convert HC and CO is having a negative side-effect by forming NO_2. With HCCI combustion this negative effect is however negligible given the very low NO concentration compared to HC and CO levels.

THC

The specific emissions of THC before the DOC are plotted in figure 15. Methane concentrations before the DOC made up 10-20 % of the THC, which is possibly due to the lack of post-oxidation and the fact that methane is a stabile molecule.

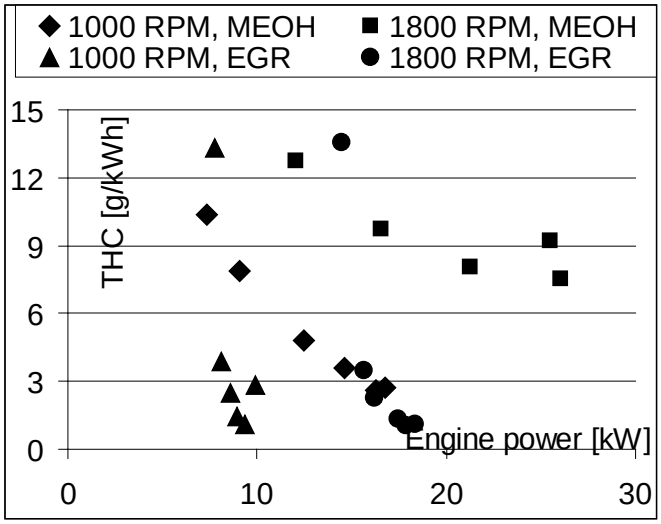

Figure 15: Specific HC emissions

The DOC reduced the concentrations to a much lower level, although the conversion efficiency dropped with high EGR levels where oxygen concentrations were lowered. Methane conversion was not good at low exhaust temperatures, but improved at loads as temperature increased.

CO

Carbon monoxide was measured both on a low scale (0-5000 ppm) and on a high scale (0-20 vol. %). The low scale was used up to the limit when possible for best accuracy. The emissions are plotted in figure 16.

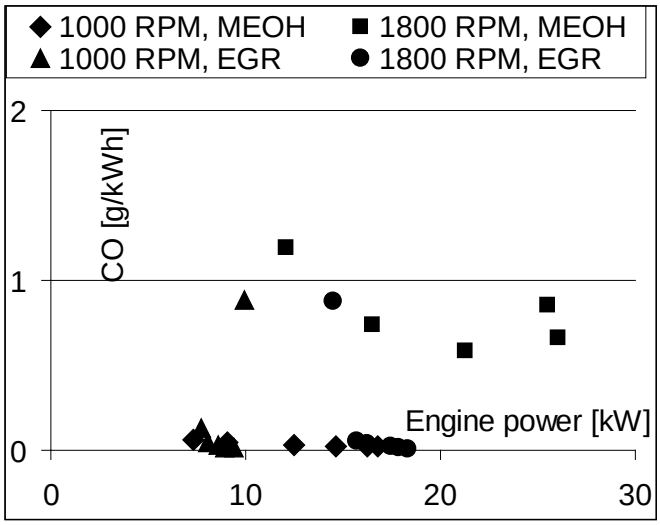

Figure 16: Specific CO emissions

In general, CO emissions are both due to wall quenching and crevice effects, which give low amounts of CO. In case of incomplete combustion however, CO levels will increase dramatically. This is seen in figure 16 in some cases. At 1000 RPM with EGR the combustion efficiency is deteriorated at the highest EGR setting. At 1800

RPM with EGR, the combustion appears to be incomplete before EGR is applied. Apart from these two cases, all EGR experiments resulted in low CO levels.

Using methanol at 1800 RPM seemed to cause high levels of CO regardless of engine load. The reason for this effect is unknown.

The DOC effectively converts CO when the exhaust gas temperature is above 200° C. Since the DOC will usually be hotter than this, the emission of CO is believed to be reduced permanently and is thus of minor importance to the impact on air quality.

CONCLUSION

It has been demonstrated that a diesel engine with a compression ratio of 14.5 and a DI common rail system is suitable for dual fuel HCCI combustion. DME was injected directly through the common rail injectors and the methanol was port injected. The effect of high quantities of EGR was also demonstrated.

Combustion timing control was first demonstrated with methanol. The best result was achieved when the equivalence ratio of methanol reached 0.120 at 1000 RPM and 0.076 at 1800 RPM. These quantities ensured complete combustion about 5 CAD ATDC at the respective engine speeds. Increasing the quantity further caused partial combustion and misfire at both engine speeds.

A BMEP of 440 kPa was achieved at 1000 RPM and 380 kPa was reached at 1800 RPM with the optimum quantity of methanol. The corresponding brake efficiencies were 0.35 and 0.31 respectively, which is close to the performance of the original engine.

Methanol proved to reduce engine knock to a very low level despite the increased equivalence ratio. It may therefore be used to increase the engine power by enabling higher equivalence ratios.

A disadvantage of the port injection was that a large quantity of the injected methanol was diluted into the lubrication oil. This problem could possibly be avoided by mixing the methanol with the DME at a fixed ratio and injecting the mixture as a whole through the common rail injectors.

EGR was also used to retard combustion timing for a fixed quantity of DME. For EGR percentages up to 65, the delay in CAD was proportional to the EGR percentage. At an EGR percentage of 70 % the rate of reaction was reduced and the heat release appeared around 2-3 CAD BTDC.

BMEP increased with increasing amounts of EGR due decreased heat losses and less compression work. The highest BMEP obtained was around 260 kPa at both 1000 and 1800 RPM.

Engine knock was virtually eliminated when the EGR level increased the equivalence ratio close to 1, as the rate of reaction was lowered.

Combustion control of DME HCCI through simultaneous use of methanol and EGR may possibly enable the use of even higher compression ratios than 14.5. This could allow for standard diesel engines to utilize the HCCI combustion process in part load situations.

In general, NO_x emissions were in the 0-30 ppm range. At the operating points with the best thermal efficiencies, the calculated specific emissions of NO_x were close to or less 0.1 g/kWh.

REFERENCES

1. Mingfa Yao: An Investigation on the Effects of Fuel Chemistry and Engine Operating Conditions on HCCI Combustion. SAE 2008-01-1660. 2008
2. Zunqing Zheng, Mingfa Yao, Zheng Chen, Bo Zhang: Experimental Study on HCCI Combustion of Dimethyl Ether (DME)/Methanol Dual Fuel. SAE paper 2004-01-2993
3. Mingfa Yao, Zheng Chen, Zunqing Zheng, Bo Zhang, Yuan Xing: Study on the controlling strategies of homogeneous charge compression ignition combustion with fuel of dimethyl ether and methanol. FUEL 85, p. 2046-2056. Elsevier 2006
4. Hideyuki Ogawa, Noboru Miyamoto, Naoya Kaneko, Hirokazu Ando: Combustion Control and Operating Range Expansion With Direct Injection of Reaction Suppressors in a Premixed Dme Hccl Engine. SAE 2003-01-0746. 2003
5. Yoshihiko Kanoto, Tetsuo Ohmura, Norimasa Iida: An Investigation of Combustion Control Using EGR for Small and Light HCCI Engine Fuelled With DME. 2007-01-1876. 2007
6. Mingfa Yao, Zheng Chen, Zun-qing Zheng, Bo Zhang, Yuan Xing: Effects of EGR on HCCI Combustion Fuelled with Dimethyl Ether (DME) and Methanol Dual-Fuels. 2005-01-3730. 2005
7. S. Katijani; Z. Chen; M. Oguma; M. Konno: A study of low-compression-ratio dimethyl ether diesel engines. Internal Journal of Engine Research, Volume 3: Number 1: ISSN 1468-0874
8. Troels Dyhr Pedersen, Jesper Schramm: A Study on the Effects of Compression Ratio, Engine Speed and Equivalence Ratio on HCCI Combustion of DME. SAE 2007-01-1860. 2007
9. Ming-fa Yao, Zhao-Lei Zheng, Xia Liang: Numerical Study on the Chemical Reaction Kinetics of DME/Methanol HCCI Combustion Process. SAE 2006-01-1521. 2006
10. Atsumu Tezaki, Hiroyuki Yamada, Mitsuaki Ohtomo: Mechanism Controlling Autoignition Derived From Transient Chemical Composition Analysis in HCCI. SAE 2007-01-1882. 2007
11. Curran, H. J., S. L. Fischer, F. L. Dryer: The Reaction Kinetics of Dimethyl Ether. II: Low-Temperature Pyrolysis and Oxidation in Flow Reactors. Int. J. Chem. Kinet. 32: 741–759, 2000. Lawrence Livermore National Laboratory, Livermore, CA, UCRL-JC-239496. 2000
12. Fischer, S. L., F. L. Dryer, H. J. Curran: The Reaction Kinetics of Dimethyl Ether. I: High-Temperature Pyrolysis and Oxidation in Flow Reactors. Int. J. Chem. Kinet. 32: 713–740, 2000. Lawrence Livermore National Laboratory, Livermore, CA, UCRL-JC-239461. 2000
13. Sato, Yoshio; Nozaki, Shinya; Noda, Toshifumi: The Performance of a Diesel Engine for Light Duty Truck Using a Jerk Type In-Line DME Injection System. SAE paper 2004-01-1862
14. Takayugi Tsuchiya, Yoshio Sato: Development of DME Engine for Heavy-duty Truck. SAE paper 2006-01-0052. 2006
15. Heywood, John B. : Internal Combustion Engine Fundamentals, McGraw-Hill ISBN 0-07-100499-8
16. Hiroyuki Yamada, Masataka Yoshii, Atsumu Tezaki: Chemical mechanistic analysis of additive effects in homogeneous charge compression ignition of dimethyl ether. Proceedings of the Combustion Institute 30, p. 2773.2780. Elsevier 2004.
17. Hiroyuki Yamada, M Ohtomo, M Yoshii, A Tezaki: Controlling mechanism of ignition enhancing and suppressing additives in premixed compression ignition. Internal Journal on Engine Research Vol. 6, IMechE. 2005
18. Tadanori Yanai, Yoshio Sato, Atsuhiro Kawamura, Hiroshi Oikawa, Shinya Nozaki, Toshifumi Noda, Teruaki Ishikawa: Development and Engine Bench Testing of a Common Rail Type DME Injection System. SAE 2008-08-0501. 2008

CONTACT INFORMATION

Troels Dyhr Pedersen. Ph.D. student

tdp@mek.dtu.dk

Technical University of Denmark

Nils Koppels Alle, Building 403, room 111

2800 Kgs. Lyngby, Denmark

DEFINITIONS/ABBREVIATIONS

Definitions, Acronyms, Abbreviations

BMEP: Brake mean effective pressure

BSFC: Brake specific fuel consumption

CAD: Crank angle degree

CH4: Methane

CLD: Chemi-luminescence detection

DME: Dimethyl ether

DOC: Diesel oxidation catalyst

EGR: Exhaust gas recirculation

FID: Flame Ionization detection

HCCI: Homogeneous charge compression ignition

HTR: High temperature reactions

LTR: Low temperature reactions

MEOH: Methanol

NDIR: Non-dispersive infrared

NMHC: Non-methane Hydrocarbons

NO: Nitric Oxide

NO2: Nitric Dioxide

PM: Particulate matter

THC: Total Hydrocarbon

2010-01-1487

Reduction of HCCI combustion noise through piston crown design

Troels Dyhr Pedersen, Jesper Schramm
Technical University of Denmark

ABSTRACT

Seven shapes of piston crowns have been evaluated for their ability to reduce HCCI knock and transmission of combustion noise to the engine. The performance of each piston crown was evaluated with measurements of cylinder pressure, engine vibration and acoustic sound pressure measured one meter away from the engine. The experiments were conducted in a diesel engine that was run in HCCI combustion mode with a fixed quantity of DME as fuel.

The results show that combustion knock is effectively suppressed by limiting the size of the volume in which the combustion occurs. Splitting the compression volume into four smaller volumes placed between the perimeter of the piston and the cylinder liner increased the noise to a higher level than that generated with a flat piston crown. This was due to resonance between the four volumes. Using eight volumes instead decreased the noise. The noise was further reduced with another piston crown where eight cylindrical volumes were drilled into the piston crown, so that the cylinder liner was not exposed directly to the combustion. A configuration with seven hemispherical volumes was less silent in operation, but still better than the flat piston crown. The largest and most consistent reduction in noise level was however achieved with a diesel bowl type piston.

The increased surface area as well as the larger crevice volumes of the experimental piston crowns generally resulted in lower IMEP than the flat piston. While the crevice volumes can be reduced, increased heat transfer can not be avoided. Thus, the use of alternative piston crown geometries designed to split the combustion may not be viable means of avoiding HCCI engine knock. The traditional diesel bowl type piston is therefore possibly the best alternative to the flat piston in terms of noise reduction as well as heat losses.

INTRODUCTION

Homogeneous charge compression ignition (HCCI) combustion has a number of advantages such as very low emissions of NOx and particulate matter, high indicated efficiency and the ability to use a wide range of fuels.

HCCI combustion may be used as a part load option in normal SI and DI engines where low emissions are important. The combustion process is limited to part load primarily due to the reaction rate becoming excessively high when load is increased. As the reaction rate and hence the pressure rise rate increases, the noise level from the engine also increases.

The noise from the engine is caused by large amplitude resonance patterns in the chamber, when reflections of powerful pressure waves transfer energy to the cylinder liner. The energy is transmitted through the engine structure and a small fraction is dissipated as noise, while the rest is dissipated as heat in the structure.

Coupling of pressure waves and reaction kinetics is a common cause for amplification of pressure waves in the combustion chamber. One approach to reducing the noise is therefore to design pistons that prevent this phenomenon.

In this study, DME was used as a fuel. It is used due to its excellent auto ignition properties which makes the fuel usable in engines with compression ratios around 10. DME is a gas with a vapor pressure of approx. 6 bars at 25 °C. It evaporates instantly when injected as a liquid in the inlet manifold, thereby creating a premixed charge. The charge is furthermore homogenized during the intake process and thus the homogeneous charge condition is reached. Since the charge burns homogeneously it does not produce soot. As the charge is furthermore lean, formation of nitric oxides is very low. HCCI combustion of DME is therefore a clean alternative to DI CI combustion as well as an inexpensive option due to a low pressure fuel system. The main challenge is to avoid knocking combustion, which is the subject of this study.

THEORY

There are at least three possible mechanisms which are responsible for creating pressure waves in the chamber. These are local explosions, pressure wave amplification and detonations.

Local explosions may occur when part of the gas in the chamber has a higher fuel concentration and/or temperature. The explosion will cause a pressure wave to propagate through the remaining charge, thereby compressing it. Pressure wave amplification may then occur as the temperature is increased by the adiabatic compression. The phenomenon is described by [1] and [2]. When a pressure wave approaches a solid wall, e.g. the cylinder liner, the pressure difference increases to twice the magnitude of the traveling wave close to the wall. The corresponding rise in temperature will lead to an increase the reaction rate in the charge locally and hence cause the pressure to increase further. The pressure wave is therefore amplified upon reflection on the wall. This phenomenon can result in engine knock with moderate amplitudes.

Detonation is known to cause severe cases of engine knock in SI engines [3, 4, and 12]. Heat transfer is enhanced when knock occurs due to disturbance of the thermal boundary layer [5]. This may result in melting of the piston due to excessive thermal load. The destructive nature of the detonation on SI engines is due to the excessive pressure and temperature in the shock front. Detonations can however not reach a fully developed state in engines due to the small distance available for the detonation to grow in amplitude. The term “developing detonation” is therefore more appropriate when referring to detonation in engines. Pressure waves from developing detonations are however still clearly recognizable since they create a rapid and discontinuous pressure wave, while explosions cause a slower rise in pressure and hence a more harmonic pressure wave.

The distance in which a detonation can develop is larger when the engine is operated with HCCI combustion. In the SI engine the detonation can only develop within the end gas pocket, while in an HCCI engine the whole combustion chamber is filled with partly reacted gas in which the detonation can increase its magnitude. Therefore a logic approach to reducing pressure waves from developing detonations would be to reduce the dimensions of the combustion chamber. This can be done by splitting the compression volume into smaller volumes.

In this study, splitting the combustion chamber into smaller volumes proved successful in reducing the noise to very low levels compared to the flat piston geometry. It was observed that the cylinder pressure fluctuations were reduced. The engine vibration level and the sound pressure level of the impulse emitted from the engine were reduced as well.

The frequency content of the acoustic noise generated in the cylinder is important since these frequencies are transmitted directly to the surroundings but with different efficiency due to the frequency response of the engine. The nature of in-cylinder oscillations in cylindrical chambers were investigated by [6], [7] and [8]. These studies showed that the resonance frequencies in a cylindrical combustion chamber follow acoustic theory for closed cylindrical chambers.

The lowest resonance mode in a cylindrical chamber is a transverse wave with a single node through the center of the cylinder as shown to the left in figure 1. This mode usually has the highest amplitude. In the figure, dark represents high and low pressure zones and bright shows the node between them. The pressure zones shift from high to low and back again at the given frequencies. The frequency of the modes in figure 1 are calculated at a temperature of 1900 K in a chamber with a diameter of 85 mm.

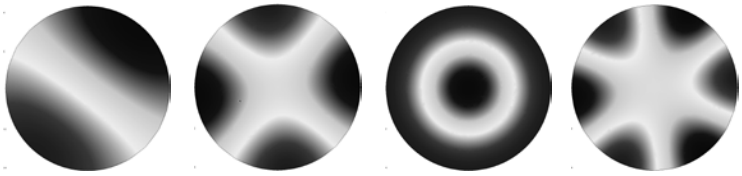

Figure 1: Illustration of resonance modes in a cylindrical chamber. From the left, the modes and corresponding frequencies are: (1, 0): 5.9 kHz; (2, 0): 9.7 kHz, (0, 1): 12.2 kHz and (3, 0) 15.5 kHz

The index (a, b) refers to circumferential and radial modes of vibration. There is also a third mode which is the axial modes, but due to the limited distance between piston and cylinder head the axial modes have very high frequencies and are rarely exited at magnitudes of importance. In experiments the first circumferential mode (1, 0) is most often dominating, while the first radial mode (0, 1) and the second circumferential mode (2, 0) are present at lower amplitudes. Higher modes can be present, but their amplitudes are generally much lower than the first circumferential mode.

When looking at the chamber geometries which are presented on the next pages, the theory for cylindrical cavities does no longer support accurate calculations of the frequencies. In general however, similar patterns will be established in the chamber while the differences in piston geometry will alter the frequencies and possibly reduce the amplitudes.

EXPERIMENTAL SETUP

PISTON CROWNS

Being the focus of this study, these piston crowns are presented first. Seven different types were designed for the study. All piston crowns were designed to a compression ratio of 10. In all cases, except for the flat piston crown, the distance from piston top to cylinder head was 1 mm, which was the minimum requirement for avoiding valve contact.

The purpose was first of all to test different geometries that could possibly reduce the interaction between pressure and reaction rate, in order to avoid the larger pressure oscillations found in the typical cylindrical chamber.

The cylindrical chamber is formed by a flat piston crown (fig. 2) which has a compression height (distance to the cylinder head) of eight millimeters. The acoustic behavior of the flat piston is relevant in SI type combustion

chambers which often have this flat structure. The advantage of this structure is that the crevice volume is low and that the flame (in SI engines) is not quenched due to narrow gaps such as with diesel pistons. In HCCI engines this piston is however less advantageous, since the large open chamber is ideal for pressure waves and resonance.

Figure 2: Flat piston crown

The diesel bowl type piston (fig. 3) is relevant to DI CI engines which can operate in HCCI mode as well. The advantage of this piston is a low heat loss, while the disadvantage is a large volume which is quenched between cylinder head and piston.

Figure 3: Diesel bowl piston crown

The diesel bowl type piston tested here has a larger combustion bowl than normal to obtain a compression ratio of 10. The chamber diameter is smaller than the flat piston which gives a higher frequency at the first circumferential mode. The frequency will decrease as the piston moves down after TDC and the full diameter of the cylinder becomes dominating, thus shifting the frequency towards that of the flat piston. The acoustic properties of the bowl type piston has been studied by Broatch et al. [9] who made a numerical study on the subject.

The piston crown with the ring shaped (fig. 4) was based on the idea that directing the pressure waves around the chamber in a circular motion could reduce the momentum transfer from wave reflections and hence reduce the transmitted sound energy. This was however not the case, possibly because the cylinder liner was fully exposed to the pressure waves.

Figure 4: Piston crown with ring shaped chamber

Although not very successful in reducing the noise, the ring shaped chamber however turned out to be interesting from an acoustic point of view. In this study it was found to develop both the first and second circumferential modes at large amplitudes, with frequencies of 4 and 8 kHz respectively. The higher modes appear as multiples of the first mode, but at lower amplitudes.

The idea of dividing the combustion chamber into smaller sub chambers (fig. 5 and 6) was to split the combustion to limit development of detonations as well as possible interaction of pressure waves and combustion. It was believed that the piston crowns would then reduce the pressure oscillations.

The piston crown with four side chambers (fig. 5) turned out to produce strong oscillations at 3-4 kHz, due to Helmholtz resonance between the chambers.

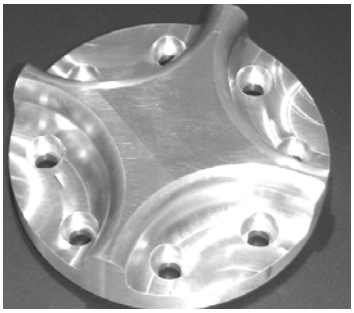

Figure 5: Piston crown with four side chambers

To see if the resonance could be avoided a version with eight side chambers (fig. 6) was made. It was more silent in operation, but the increased surface area also increased the heat transfer and hence reduced the IMEP.

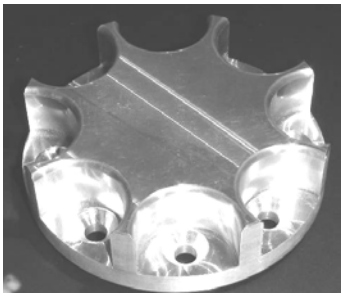

Figure 6: Piston crown with eight side chambers

The two piston crowns with chambers in their perimeter exhibit Helmholtz resonance since the chambers are connected across the top of the piston. The resonance will appear at a lower frequency than the first circumferential mode of the flat piston crown. With a clearance of one millimeter to the cylinder head the frequency of the Helmholtz resonance will be around 3.5-4 kHz at TDC and increase slightly as the piston moves down.

Finally it was decided to test a piston with chambers inside the piston (fig. 7 and 8), rather than on its perimeter. The main disadvantage of the first piston crown with eight cylindrical chambers (fig. 7) is the increased surface area. The piston was silent in operation, but the IMEP was reduced due to heat losses.

Figure 7: Piston crown with eight cylindrical chambers

A piston crown with seven hemispherical chambers (fig. 8) was made to reduce the large heat transfer area with the eight cylindrical chambers. The larger open surface towards the cylinder head should also reduce turbulence and hence heat transfer. The piston crown was less silent in operation than the first while IMEP was improved slightly.

Figure 8: Piston crown with seven hemispherical chambers

PISTON MODIFICATION

To allow for the various changes in piston crown geometry, the pistons were modified so that the top of the piston could be replaced. The top of the piston was cut off above the top piston ring, and eight holes with six millimeter tread were made in the piston. The piston crowns were attached to the pistons with six millimeter bolts to keep the crown firmly attached to the piston. An annealed copper disc was inserted between piston and crown to ensure a high thermal conductivity as well as an airtight seal. Figure 9 shows the piston in the cylinder.

ENGINE MODIFICATION

To increase the room for the various geometries, the engine block and cylinder head were separated by a ten millimeter thick steel plate. The cylinder liners were kept in their original position. Apart from longer pushrods, no further modifications were necessary. Figure 9 shows the assembly.

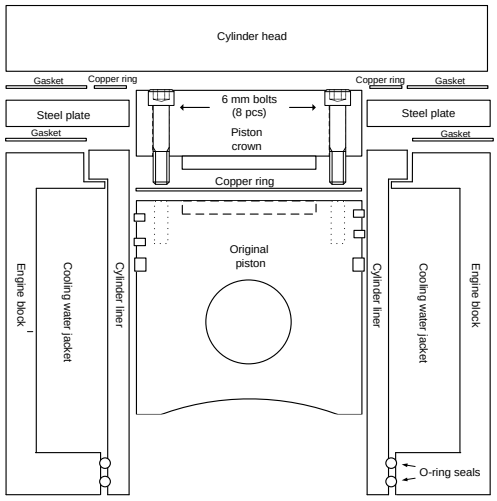

Figure 9: Modification of engine block and piston

Gaskets were used on both sides of the steel plate. The surface against the cylinder head was furthermore sealed with a copper ring resting in a groove in the plate. The alignment of the plates 85 mm holes is accurate enough for the pistons to pass, but piston rings cannot move across the gap.

The cylinder liner is made of cast iron. The liner is inserted from the top of the engine and is surrounded completely by the cooling water. It rests on a shoulder on top of the engine. The bottom seal is provided by two o- rings. Therefore only the top end of the cylinder liner is capable of transferring high frequency vibrations directly to the engine block. Vibrations transferred to the water will however also transfer sound efficiently to the engine block due to the incompressibility of water.

The cylinder in which the piston crowns were tested was equipped with a cylinder pressure transducer positioned in the steel plate as shown on figure 10. The steel plate can be seen in position on figure 11.

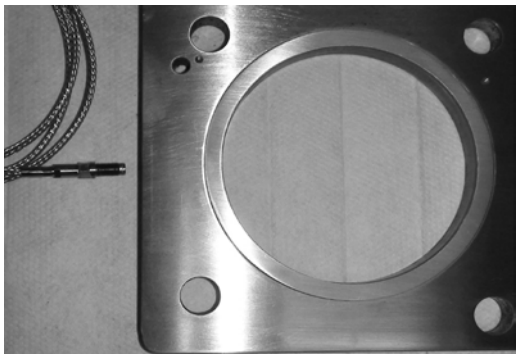

Figure 10: Steel plate with pressure transducer

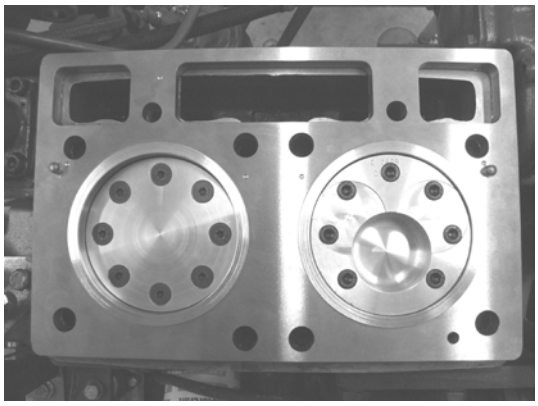

Figure 11: HCCI cylinder to the left, DI CI cylinder to the right

The engine construction is possibly one of the most important factors in determining the transfer of sound from the combustion to the surroundings. Therefore the results obtained with this engine are of course not directly applicable to any other engine. The effect of the various piston crowns on the in-cylinder pressure effects and hence their noise reducing capabilities does however not depend on the engine surrounding it. The difference in noise reducing capability as an effect of the piston crown geometry will therefore most likely apply to any engine of similar size.

CREVICE VOLUMES

The volumes between piston and cylinder were of varying size in this experiment. This influences the combustion efficiencies and hence the IMEP. Table 2 holds the calculated values of the crevice volumes. These calculations are based on the piston crown measures at 25 °C. The actual volumes will decrease as the piston crown heats up.

The crevice volumes of the piston crowns with 27 mm crevice height is very large because it was necessary to increase the radial clearance to avoid contact with the steel plate, and because piston rings could not be used on the crown since the gap between the steel plate and the cylinder liner did not allow for piston ring passage. If the piston crowns were to be used in a normal engine the crevice volumes could be reduced to the same size as a normal diesel piston.

Piston crown design	Crevice height [mm]	Radial clearance [mm]	Crevice volume [mm^3]	Amount of total volume [%]
Flat chamber	19	0.35	1768	3.4
Bowl type chamber	27	0.5	3584	6.9
Ring shaped chamber	13.4	0.35	1247	2.4
Four side chambers	12.5	0.35	1163	2.2
Eight side chambers	10	0.35	931	1.8
Eight cylindrical chambers	27	0.5	3584	6.9
Seven hemispherical chambers	27	0.5	3584	6.9

Table 1: Clearance and crevice volumes of the piston crowns

ENGINE

The engine used for the experiment is a two cylinder, four stroke DI CI engine. Data for the engine in DI CI operation is given in table 2.

Bore	85 mm
Stroke	85 mm
Connecting rod length	160 mm
Geometric compression ratio	18.5
Compression pressure	47 bar
Inlet valve opens	32 BTDC
Inlet valve closes	64 ABDC
Exhaust valve opens	64 BBDC
Exhaust valve closes	32 ATDC
Power output	11.8 kW @ 2000 rpm

	16.7 kW @ 3000 rpm
	17.9 kW @ 3600 rpm
Maximum torque	55 Nm @ 2000 rpm

Table 2: Engine data and performance

An eddy-current dynamometer was used as engine load. Since the dynamometer did not have motoring capability, the cylinder on the engine not used in the test was run in normal diesel operating mode to keep the engine at operating temperature and at a constant speed.

CYLINDER PRESSURE MEASUREMENTS

An optical pickup was used to measure the cylinder pressure. The sensor measures the diaphragm deflection with light and outputs the reading in a voltage between 0.5 and 5 volts.

The pickup is designed for peak pressures of 350 Bar, which is necessary for long life in knocking conditions. Sensitivity is however adjusted so that the highest output corresponds to 70 Bar, to obtain the best accuracy. The stiffness of the diaphragm provides a high resonance frequency of 120 kHz. The transducer is designed to detect frequencies up to 25 kHz.

It is critical that the resonance frequency is not exited even under strong knocking conditions, as the sampling frequency is insufficient to avoid aliasing at frequencies above 36 kHz. It was verified that the sensor resonance frequency is not present, by sampling the sensor output at 400 kHz at higher amplitudes of knock than used in the tests.

It was chosen to treat the cylinder pressure oscillations as sound pressure. This simple approach means that the sound pressure in the cylinder can be compared directly to the sound pressure of the radiated noise. The difference may then be expressed as attenuation.

VIBRATION MEASUREMENTS

The engine surface acceleration is measured by a ceramic axial shear accelerometer mounted in the top corner of the engine block, on the HCCI cylinder side. This position is favorable for measuring the frequencies transmitted from the chamber, but less favorable for measuring the engines lower resonant frequencies which are strongest in the middle of the large unsupported engine surfaces. The position was chosen since the direct transmission of sound from the cylinder was considered most relevant.

SOUND MEASUREMENTS

The instantaneous sound pressure was recorded with a sound level meter. The microphone was placed 1 meter away from the engine, perpendicular to the crank shaft and at the same elevation as the top of the cylinders.

The walls and the floor in the test cell were partly covered with 50 mm insulation materiel to reduce the sound reverberation. With this material thickness and some distance to the wall it is possible to eliminate reflection of frequencies higher than approximately 1 kHz. Lower frequency noise could not be reduced much under the given circumstances. The noise of interest was however that which was generated by engine vibration, which

from the engine vibration measurements was significantly above 1 kHz. Therefore the low frequency noise was removed from the measurement with a digital high pass filter in the subsequent analysis.

The noise from the diesel combustion event 360 CAD before the HCCI combustion did not influence the acoustic SPL measured outside the engine since all high frequency noise was efficiently attenuated in the test cell. The acoustic SPL for one complete cycle is found in figure 23, from which it can be seen that the acoustic SPL has decreased to around 70 dB before the HCCI cylinder combustion event. Since the acoustic SPL from HCCI combustion increases the

DATA SAMPLING

The amplified signal from the cylinder pressure transducer was measured simultaneously with the engine vibration and sound pressure. The sampling clock was supplied by the engines crank angle encoder which supplies 10 pulses per CAD. At 1200 rpm this results in a sample frequency of 72 kHz which is sufficient to detect frequencies up to 36 kHz. This range fully satisfies the need, since frequencies above 15-20 kHz only appear at very weak amplitudes.

TEST PROCEDURE

The engine was preheated while running on the diesel cylinder alone. HCCI combustion was initiated on the other cylinder with a fixed quantity of DME per cycle, which was maintained during the test.

The quantity of DME was controlled by having a fixed injector opening time of 4.5 ms per cycle, which results in 20.4 mg of DME per injection. The resulting equivalence ratio was calculated to be 0.35, corresponding to an excess air ratio of 2.85. The engine can tolerate higher fuelling rates and hence higher pressures than this. The service life of the pressure transducer is however severely shortened when very strong knock occurs, which is the case at higher fuelling rates. With an injection time of 5.5 ms per cycle the amount of fuel per cycle increases to 24.0 mg and the equivalence ratio becomes 0.41. At this point, pressure pulsations with peak amplitudes of more than 10 bars are observed. At higher fuelling rates there are indications of developing detonations, such as extremely rapid pressure rise rates which can only be associated with shock waves. These can rapidly destroy the pressure transducer and are therefore avoided.

After HCCI combustion was established, the inlet air manifold was coupled to an air cooler which supplied air at approx. -13 °C. The inlet air temperature was measured at the inlet manifold, before the injector position. The engine was then allowed five minutes to adjust to the new inlet condition. When the HCCI combustion was stabilized in its retarded position, the cooling unit compressor was switched off to allow a slow increase in inlet air temperature. Due to the large thermal mass of cooling liquid and heat exchanger, the temperature increment was in the order of 1 °C per two minutes. This allowed ample time for the engine to adjust thermally, as well as measurements to be made at near steady conditions.

The first measurement was made at -10°C and the subsequent in 5°C intervals. The last measurement was made at +15°C. The cylinder pressure sensor, accelerometer and microphone output were sampled simultaneously in 0.1 CAD intervals for 20 consecutive cycles in each recording.

The equivalence ratio is slightly affected by the reduction in inlet temperature. Table 3 shows the calculated equivalence ratio as function of inlet temperature. It has been assumed that the volumetric efficiency relates to inlet temperature as:

$$\eta_v = \eta_{v,ref}\sqrt{\frac{T}{T_{ref}}}$$

with T and T_{ref} being the inlet and reference temperatures in Kelvin, while η_{ref} is the reference volumetric efficiency, which is 0.91 for this engine speed.

Temperature [C]	Density [kg/m3]	Equivalence ratio	Excess air ratio
25	1.17	0.372	2.68
20	1.19	0.369	2.71
15	1.21	0.366	2.73
10	1.23	0.363	2.75
5	1.25	0.360	2.78
0	1.28	0.357	2.80
-5	1.30	0.353	2.83
-10	1.32	0.350	2.86

Table 3: Equivalence and excess air ratio dependence on inlet temperature

The inlet manifold pressure was atmospheric. The engine is naturally aspirated and pressure drop in the heat exchanger and connecting tube are negligible.

DEFINITIONS

Sound pressure

The sound pressure (SP) is defined as the RMS value of the pressure variation. It is measured in Pascal.

Sound pressure level

The sound pressure level (SPL) in decibel (dB) is defined as:

$$SPL = 20\log\left(\frac{p_{rms}}{p_{ref}}\right)$$

where p_{ref} is a reference pressure. This definition is used for both the cylinder pressure and the acoustic sound pressure measured one meter away from the engine.

The reference sound pressure is 20 μPa for the exterior sound. The reference for the SPL of the cylinder pressure was set to 1 Pa The reference for the in-cylinder SPL was chosen because it turned out that this made the in-cylinder and the external SPL approximately equal. The ratio between the two references corresponds to 94 dB. No frequency weighting has been used since the noise measured is in the 1 - 5 kHz region where the sensitivity of the ear is quite linear.

The acceleration level is defined by the same formula as the SPL:

$$AL = 20\log\left(\frac{a_{rms}}{a_{ref}}\right)$$

where a_{ref} is the reference acceleration level which is set to 1 μm/s^2.

RESULTS

Sound pressure level

There is a linear relationship between the SPL measured in the cylinder and the SPL measured 1 meter away from the engine. This is seen in figure 12, where the acoustic SPL is plotted against the cylinder SPL. It is obvious that reducing the SPL in the cylinder results in a reduction in the acoustic SPL as well.

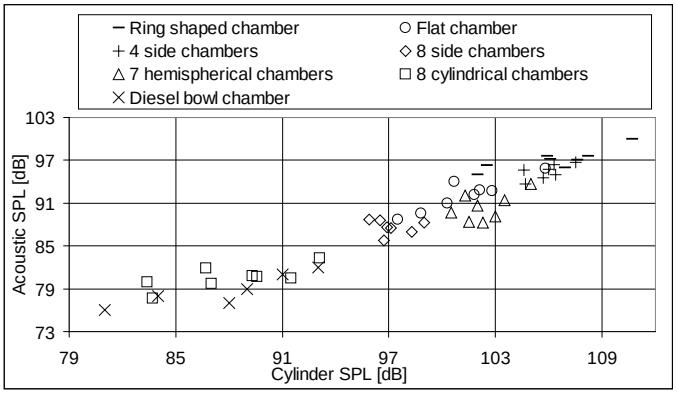

Figure 12: Cylinder vs. acoustic SPL obtained with the piston crowns

The lowest acoustic SPL were obtained with the eight cylindrical chamber and the diesel bowl piston crowns. These were both very silent in operation. The subjective evaluation of the sound emitted from the HCCI combustion was that it was considerably more silent than the DI CI combustion occurring in the other cylinder at approximately the same load.

The highest acoustic SPL was reached with the ring shaped chamber. The shape of this piston crown is ideal for the circumferential modes, which results in frequencies of 4 and 8 kHz at high amplitudes. In addition, these frequencies are transmitted efficiently to the cylinder liner which is exposed the most with this piston crown. The same problem is apparent with the 4 side-chamber piston crown which also has strong oscillation at 3-4 kHz and an exposed cylinder liner. The SPL of the eight side-chamber piston crown is about 10 dB lower. The piston crown with seven hemispherical chambers has a SPL which is 3-6 dB lower than the flat piston, but 8-12

dB higher than the 8 cylindrical chambers. This indicates that the acoustic modes are not suppressed very efficiently with the 7 hemispherical chambers.

Figure 13 shows the SPL as a function of combustion phasing. In general, the acoustic SPL decreases slightly as combustion phasing is delayed. The piston crown which is least successful in reducing noise is the ring shaped chamber, which increases the SPL considerably above that of the flat piston. The crown with four side chambers also increases the noise level higher than the flat piston. The crown with seven hemispherical chambers reduces the noise level with 3-6 dB. The piston with eight side chambers provides a similar reduction. The best results are obtained with the diesel piston and the eight cylindrical chambers. These two are equally silent in operation, as they provide a reduction of 10-15 dB over the flat piston.

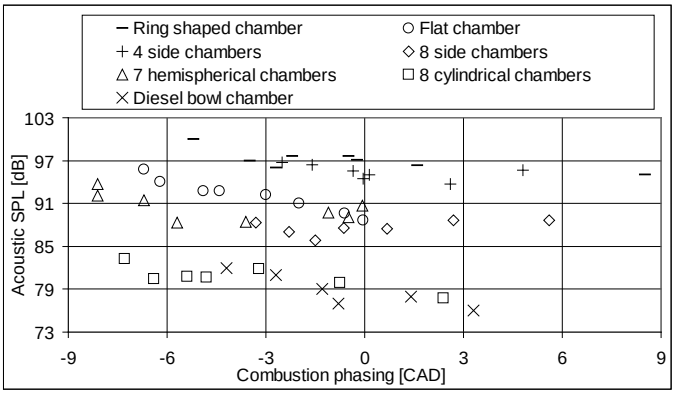

Figure 13: Acoustic SPL as function of combustion phasing

IMEP

In figure 14 the IMEP is plotted against the combustion phasing. The spread in combustion phasing shows the effect of the inlet cooling, as the leftmost point in each series is obtained at +15 °C and the rightmost at -10 °C. The inlet cooling was however insufficient to reach the best possible combustion phasing which would be around 10 CAD ATDC.

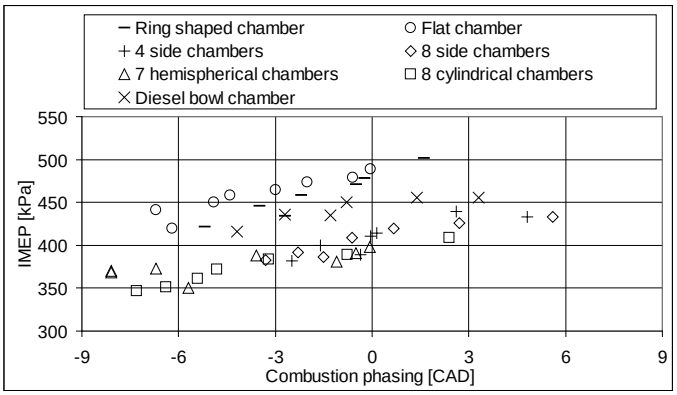

Figure 14: IMEP plotted against combustion phasing

The highest IMEP measured (approx. 500 kPa) is obtained with the ring shaped piston crown at 2 CAD ATDC. It appears that this piston crown can result in a higher IMEP than the flat piston crown at a later combustion phasing than TDC, although the ring shape results in more noise.

The flat piston crown has an advantage by having the smallest surface area and a small crevice volume as well. The result is the highest IMEP at any given combustion phasing.

The diesel bowl piston crown has a large crevice volume of 7 % of the total compression volume. In addition, a large part of the unburned charge on top of the piston will also be compressed into the crevice volume during combustion in the bowl which will further decrease combustion efficiency. The IMEP of this piston crown type is therefore lower than the flat and ring shaped piston crowns.

The remaining 4 piston crowns have equally poor performances in terms of IMEP. The primary reason for the lower IMEP of these piston crowns may be attributed to increased heat losses, as well as the large crevice volumes with the internal cavity piston crowns.

Since heat transfer may be expected to be considerably higher when surface area is increased, the temperature of the piston crown can be expected to be increase as well. No problems related to advanced ignition or thermal damage was however detected in this experiment. Hot spots occurring at sharp edges could function as local ignition points, but there is no indication that such ignition affects the overall reaction timing.

Frequency distribution

Figures 15-21 show the Fast Fourier Transform (FFT) analysis of the external peak sound pressure. The peak sound pressure is computed as an average of the peaks in 20 consecutive cycles, since some variation does occur in the sound pressure level. The peak pressure has been chosen since this was considered most relevant in terms of annoyance from transient acoustic noise. A short term average (5 ms) will typically be 5-6 dB lower than the peak SPL. The SP value on the y-axis is 1 Pa in all graphs, corresponding to a SPL of 94 dB.

It was found that the damping of the emitted noise after the combustion was quite similar with all piston crowns. The high frequency noise from directly transmitted frequencies disappeared within 10 ms, while the engine resonance would be more slowly attenuated.

The three lines present in each graph below were obtained at three different inlet temperatures of 10, 0 and -10 C. The different temperatures result in different timing and inlet density, but as can be seen from the figures, the effect of temperature on sound pressure level is not very strong.

Figure 14 reveals that the heat losses and increased crevice volumes caused by the alternative piston crown shapes reduce IMEP significantly.

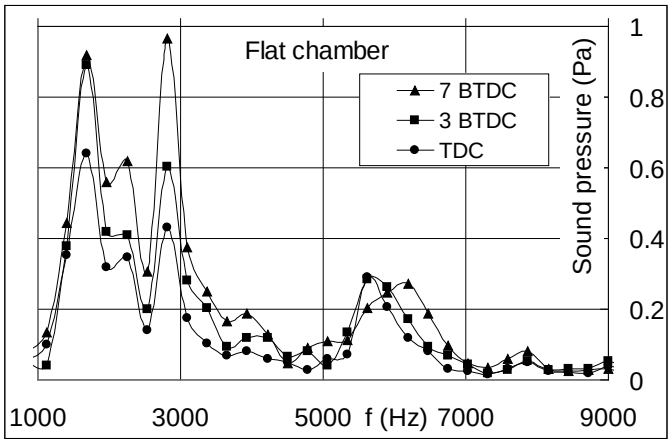

Figure 15: Frequency distribution with the flat chamber

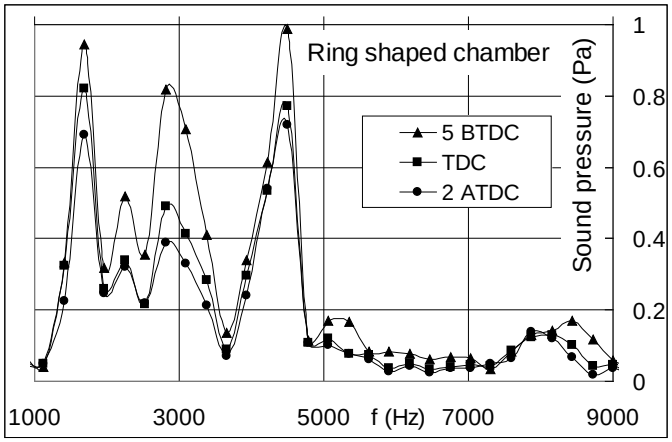

Figure 16: Frequency distribution with the ring shaped chamber

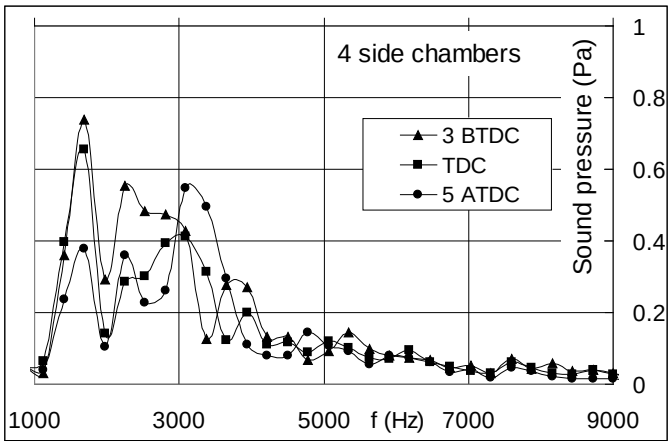

Figure 17: Frequency distribution with the four side chamber piston

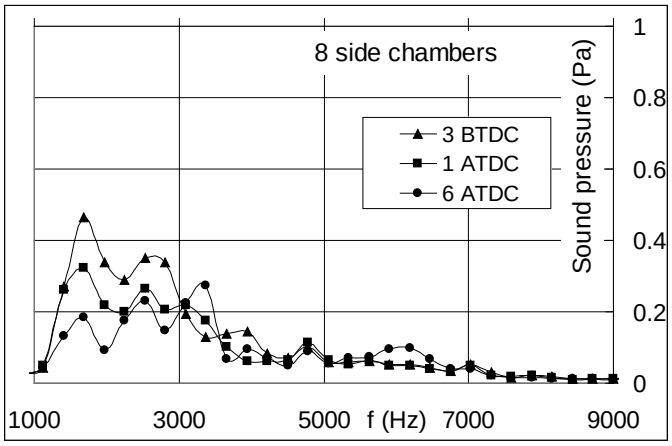

Figure 18: Frequency distribution with the eight side chamber piston

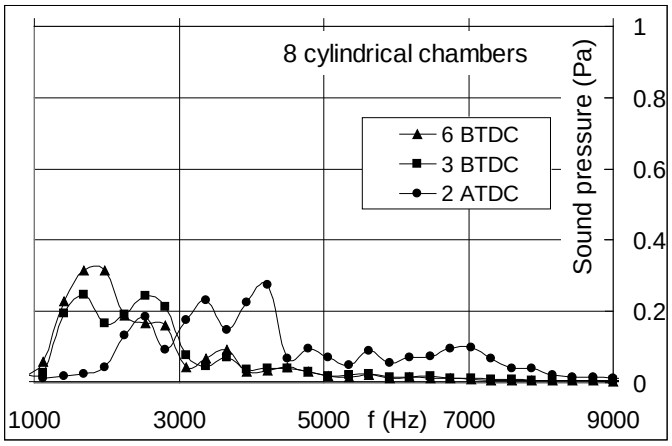

Figure 19: Frequency distribution with the eight cylindrical chamber piston

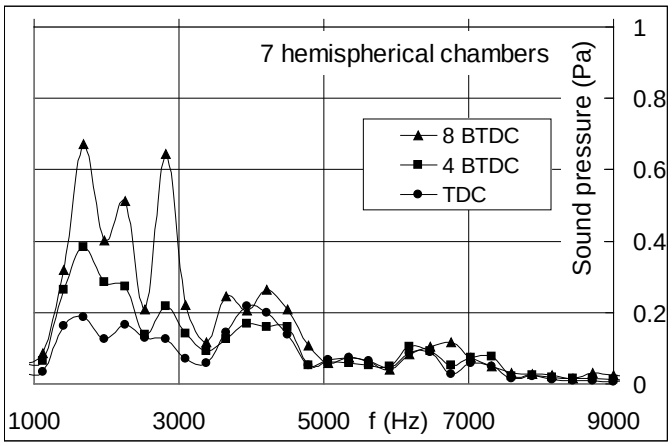

Figure 20: Frequency distribution with the seven hemispherical chambers

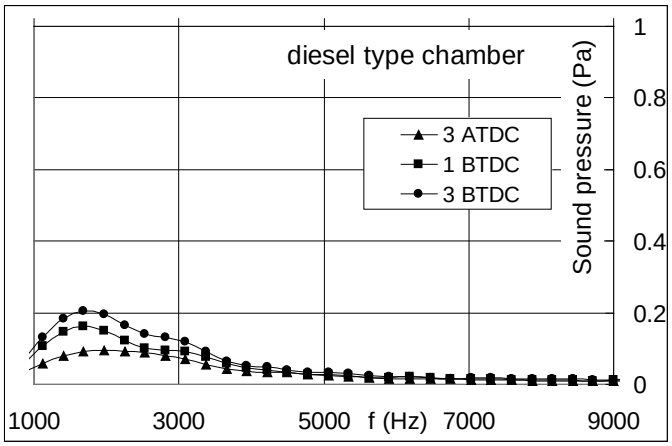

Figure 21: Frequency distribution with the diesel bowl chamber piston

The common feature of all the FFT analysis result is that the largest contribution to the total SPL is found in the lower part of the frequency band from 1-3 kHz. These frequencies cannot exist inside the cylinder, since the lowest resonance frequency is 5-6 kHz in all cases except for the ring shaped geometry, which has its primary resonance frequency at 4 kHz. The 4 kHz frequency is clearly present in the analysis for this piston crown (fig. 16).

Engine block resonance will however occur as a result of higher frequencies being transmitted through the structure. The connection between structure born noise and emitted noise was investigated by Andreae et al [10]. It was found that the general source of noise was not that which was directly transmitted, but that of engine structure resonance being exited by the transmitted noise.

A great reduction in the noise level was achieved by moving the chambers away from the cylinder walls and into the piston. The total surface area and therefore heat transfer was however increased. The crevice volume with this and the following pistons was very large since it was not possible to fit piston rings. This resulted in a reduction of combustion efficiency. In terms of noise reduction the performance was similar. The crevice volume was however unchanged, so the combustion efficiency was still reduced

Frequency response

The frequency response of the engine is here defined by the ratio of the sound pressure measured outside the engine to the sound pressure generated in the cylinder. The response is calculated for the range of frequencies in the FFT. A short term average of 5 ms following the peak heat release was used to allow all established modes of vibration to be included.

The response is converted to dB. Since -100 dB corresponds to an attenuation of 100,000, a SP of 100 kPa in the cylinder will result in a SP of 1 Pa outside the engine.

Figure 22 is an example of the frequency response of the flat chamber. The response of the other piston crowns was found to follow this pattern. The response of the flat chamber was selected because it produces a wide range of frequencies in the cylinder and thus provides a good signal-to-noise ratio for the response curve.

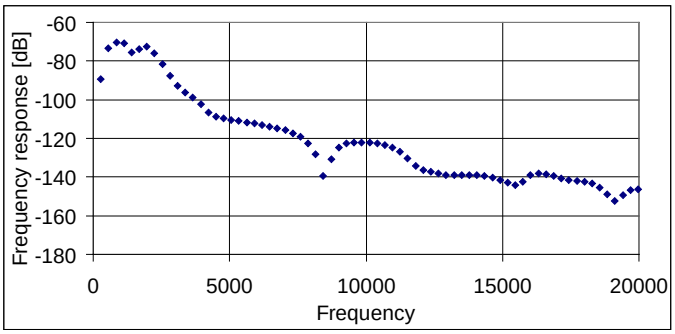

Figure 22: Frequency response of engine to internal sound pressure

As indicated by the figure, lower frequencies are more efficiently transmitted to the surroundings. This may be part of the explanation why the diesel chamber is very silent compared to the other geometries. The diesel chamber resonance frequency was measured to be approx. 10 kHz, and this frequency is attenuated 10 dB more than frequencies around 5 kHz. The piston crowns producing lower frequencies than 5 kHz were also found to result in more noise, which is also part due to the frequency response of the engine.

In figure 22, the rise in frequency response from 0-3 kHz is primarily due to this region being the engine's resonance frequency. This frequency band is exited shortly after the combustion although the cylinder does not emit any vibrations at frequencies lower than the first mode, which is approx. 5.8 kHz. The frequency band from 3 kHz and above indicates a somewhat linear decrease in response at increasing frequencies.

Engine acceleration level

The coherence between the cylinder SPL and the engine acceleration level is illustrated in figure 23. The figure is a plot of the acceleration level and the acoustic and cylinder SPL for one complete cycle of the engine in knocking combustion with the ring shaped chamber. The increased acoustic SPL and acceleration levels after -360 CAD are caused by the diesel combustion event. The HCCI combustion occurs at -10 CAD and causes a rapid increase in cylinder and acoustic SPL as well as the acceleration level. This is due to acoustic energy from the cylinder being transmitted directly to the surface during combustion [11]. The SPL and the AL decrease at the same rate, while the acoustic SPL decreases at a slower rate due to the engine resonance which is not measured by the accelerometer.

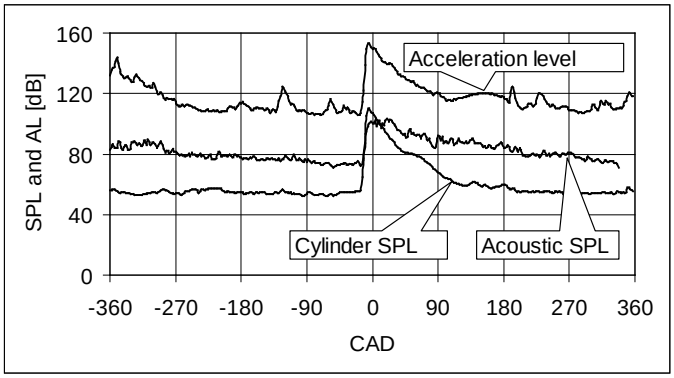

Figure 23: Cylinder SPL, acoustic SPL and acceleration level

CONCLUSION

HCCI combustion generated noise is primarily reduced by limiting exposure of the cylinder liner to the combustion. A diesel type piston is most effective in achieving this reduction.

A flat piston type, as commonly used in SI combustion, results in large amplitude pressure waves in the combustion chamber. The exterior noise level is therefore high with this kind of chamber.

A diesel type piston provided the largest reduction in the combustion noise of all tested piston crown geometries. It is believed that the smaller diameter of the bowl in which the combustion takes place is the reason that the combustion does not generate strong pressure waves. The exposure of the cylinder liner is also minimized with this kind of piston, which helps to reduce the noise further.

Two pistons with the compression volume split into 4 and 8 volumes respectively placed in their perimeter were tested. The latter was found capable of reducing the noise, but not the indicated efficiency which suffered from increased heat losses to piston and cylinder liner. The first piston crown increased combustion noise due to Helmholtz resonance between the volumes.

Two pistons with combustion chambers placed as cavities in the top of the piston were tested. One of them had 8 cylindrical cavities and was found capable of similar noise reduction capability as the diesel type piston. The large surface area, crevice volume and possibly the squish region as well however resulted in a lower indicated efficiency. The second piston had hemispherical chambers in order to reduce the heat transfer and the squish region, but as a result of a more open geometry, combustion noise increased to a level comparable to the flat piston.

The diesel type piston is possibly the best option for obtaining a silent combustion. It may however not be the best option with respect to indicated efficiency, in which case the flat piston design is the best solution.

REFERENCES

1. Chris Morley, Derek Bradley, X. J. Gu, D. R. Emerson: Amplified Pressure Waves During Auto Ignition: Relevance to Cai Engines. SAE 2002-01-2868. 2002
2. Ge-Qun Shu, Jingsi Wei, Hai-qiao Wei, Xinwei Chen. Research on Couple Mechanism of Heat Release and Acoustic Characteristics during Combustion of Butane in Close Chamber. SAE 2007-01-2175. 2007
3. B. Stiebels, M. Schreiber and A. Sadat Sakak. Development of a New Measurement Technique for the Investigation of End-Gas Auto Ignition and Engine Knock. SAE 960827. 1996
4. J. Pan and C.G.W. Sheppard. A Theoretical and Experimental Study of the Modes of End Gas Auto Ignition Leading to Knock in S.I. Engines. SAE 942060. 1994
5. Tadashi Tsurushima, Yasuo Asaumi, Yuzo Aoyagi: The Effect of Knock on Heat Loss in Homogeneous Charge Compression Ignition Engines. SAE 2002-01-0108. 2002
6. David Scholl, Craig Davis, Stephen Russ, Terry Barash. The Volume Acoustic Modes of Spark-ignited Internal Combustion Chambers. SAE 980893. 1998.
7. Eng, J.A.; Characterization of Pressure Waves in HCCI combustion. SAE 2002-01-2859. 2002
8. Andreas Vressner; Andreas Lundin; Magnus Christensen; Per Tunestål; Bengt Johansson. Pressure Oscillations During Rapid HCCI Combustion. SAE 2003-01-3217. 2003
9. A. Broatch, X. Margot, A. Gil, J. C. Donayre: A CFD Approach to Diesel Engine Combustion Chamber Resonance. SAE 2007-24-0043. 2007

10. Morgan M. Andreae, Wai K. Cheng , Thomas Kenney, Jialin Yang. On HCCI Engine Knock. SAE 2007-01-1858- 2007
11. Scott Eaton, Robert Wagner, James Drallmeier. Influence of the Combustion Energy Release on Surface Accelerations of an HCCI Engine. SAE 2009-01-2741. 2009
12. Blunsdon, C.A; Dent, J.C.; The simulation of Auto Ignition and Knock in a Spark Ignition Engine with Disc Geometry. SAE 940524. 1994

CONTACT INFORMATION

Troels Dyhr Pedersen. Ph.D. student

tdp@mek.dtu.dk

Technical University of Denmark

Nils Koppels Alle, Building 403, room 111

2800 Kgs. Lyngby, Denmark

DEFINITIONS/ABBREVIATIONS

AL: Acceleration level

CAD: Crank Angle Degree

CI: Compression Ignition

dB: Decibel

DI: Direct Injection

DME: Dimethyl Ether

FFT: Fast Fourier Transform

HC: Hydrocarbons

HCCI: Homogeneous Charge Compression Ignition

RMS: Root Mean Square

SI: Spark Ignition

SP: Sound Pressure

SPL: Sound Pressure Level